Development and application of analytical methods based on enhanced Raman gas spectroscopy for biogeochemical process monitoring

Dissertation

(kumulativ)

zur Erlangung des akademischen Grades *doctor rerum naturalium (Dr. rer. nat.)*

vorgelegt dem Rat der Chemisch - Geowissenschaftlichen Fakultät der Friedrich Schiller Universität Jena

Von M. Sc. Tobias Jochum

Gutachter:

1. Prof. Dr. Jürgen Popp, Leibniz Institut für Photonische Technologien, Institut für Physikalische Chemie und Abbe School of Photonics, Friedrich Schiller Universität Jena

2. Prof. Dr. Susan E. Trumbore, Max Planck Institut für Biogeochemie, Jena

Tag der Verteidigung: 29.08.2017

Abstract

The present work reports on novel analytical approaches and instrumentation for several biogeochemical gas monitoring applications. Exploiting Raman gas spectroscopy in combination with two signal enhancement techniques – either fiber or cavity enhancement – we developed quantitative methods for estimating the gas composition and exchange during soil biodegradation, biological nitrogen fixation, fruit ripening and physical leakage processes in environmental chambers. The first part of this thesis describes the fruit ripening analysis and the developed gas sensor based on fiber enhanced Raman spectroscopy for fast and non-destructive gas monitoring throughout the complete postharvest production chain of tropical produce. Analytical solutions for the other applications rely on the use of a cavity enhanced Raman gas analyzer. Linking gas diffusion theory, the tracer sulfur hexafluoride and a developed experimental protocol, we demonstrate the influence of physical gas leakage on determined gross exchange rates of biological systems and provide an analytical correction method to quantify the underlying biological signal. Within the scope of a soil biodegradation study, we developed an analytical method to follow the fate of xenobiotics after a contamination. The non-invasive gas monitoring solution we present is capable of quantifying the fraction of degraded hydrocarbons as contaminants, as well as identifying changes in respiration. Our Raman spectroscopic approach indicates the potential to elucidate the dynamics of specific enzymatic reactions and the occurrence of concomitant processes such as changes in the substrate for soil bacterial metabolism. In the last part of this thesis, we report on a novel analytical approach, which enables determination of biological nitrogen fixation rates without requiring a proxy, isotopes or an exchange of the natural ecosystem atmosphere. Common standard techniques do not support such a simple and most natural experimental design and we report on the first biological nitrogen fixation rate estimates derived by optical spectroscopy of N_2. Our proposed method indicates the potential to reduce existing uncertainties in nitrogen fixation measurements and might open up a new avenue of biological nitrogen fixation research.

Keywords: Raman, gas analysis, biological nitrogen fixation, biodegradation, respiration, gas diffusion, fruit monitoring

In dieser Arbeit werden neuartige analytische Methoden und zugehörige Technik vorgestellt, die im Rahmen verschiedener biogeochemischer Anwendungen entwickelt wurden. Diese quantitativen Methoden basieren auf Raman Gas-Spektroskopie kombiniert mit Signalverstärkungstechniken wie der Faser- oder Kavitätsverstärkung. So war es möglich Zusammensetzung und Austauschraten von Prozessgasen im Bereich Bodenbiodegradation, biologischer Stickstofffixierung, Fruchtreife und Leckage-Fluss Bewertung zu bestimmen. Im ersten Teil der Arbeit wird auf die Fruchtreife-Analytik eingegangen und der hierzu entwickelte Faser Raman Gassensor charakterisiert. Dieser erlaubt die schnelle und nichtinvasive Analyse aller eingesetzten Prozessgase in der kompletten Nachernte-Produktionskette. Die Analytik der weiteren Anwendungen beruht auf kavitätsverstärkten Raman Gassensoren. Durch Verknüpfung der thermodynamischen Gasdiffusionstheorie, dem Indikatorgas Schwefelhexafluorid und einem eigens entwickelten experimentellen Protokoll konnten wir den Einfluss physikalischer Leckage in ökologischen Kammersystemen ermitteln. Eine analytische Methode zur Korrektur gemessener Brutto-Gasströme und zur Identifizierung des biologischen Signals wurde entwickelt. Im Rahmen einer Bodenbiodegradationsstudie entwarfen wir ein analytisches Verfahren zur Überwachung von Fremdstoffen, hier Kohlenwasserstoffe, im Boden und deren Abbaudynamiken. Die verwendete nichtinvasive Methode quantifiziert den Anteil der abgebauten Stoffmenge gemessen an der Gesamtmenge des Schadstoffes. Da zudem simultan die Bodenatmung bestimmt werden kann, besitzt unser analytischer Ansatz das Potential die Dynamik spezifischer enzymatischer Reaktionen während der Biodegradation sowie deren Begleitprozesse aufzuzeigen. Im letzten Teil der Arbeit wird ein neuartiges analytisches Verfahren präsentiert, das erstmalig eine direkte Bestimmung biologischer Stickstofffixierungsraten ohne Indikatorgase, Isotopenmarkierung oder Austausch der natürlichen Atmosphäre ermöglicht. Solch simples und vollkommen natürliches Experimentdesign ist mit derzeitigen Standardmethoden nicht möglich. Wir zeigen erstmalig direkte quantitative Messungen von Stickstofffixierungsraten mittels optischer Spektroskopie von N_2. Der von uns vorgestellte analytische Ansatz besitzt das Potential bestehende Messunsicherheiten von Stickstofffixierungsraten zu reduzieren und neue Forschungsrichtungen im Bereich biologischer Stickstofffixierung zu eröffnen.

Schlüsselwörter: Raman, Gasanalytik, biologische Stickstofffixierung, Biodegradation, Atmung, Gasdiffusion, Fruchtreife-Überwachung

Table of contents

1. Motivation

In the year 2001, the president of the Geological Society of America, Mary Lou Zoback, identified grand challenges in earth and environmental sciences for the beginning twenty-first century.[1] Each of these challenges, e.g. recognizing the signal within the natural variability, defining mass fluxes in natural ecosystems or quantifying impacts and effects, will require creative interdisciplinary approaches. To meet these grand challenges, "we need to aggressively exploit technological advances in the area of monitoring active processes, both in situ and remotely".[1] This thesis addresses that request by discussing newly developed monitoring methods for several biogeochemical processes and specifically designed Raman gas sensors and analyses.

Gases are part of various global biogeochemical cycles such as the carbon cycle, e.g. in form of the greenhouse gas carbon dioxide (CO_2),[2] and the nitrogen cycle, e.g. as dinitrogen (N_2) or nitrous oxide (N_2O).[3] Gas monitoring can yield important information on not only active microbial processes, but also at which times these processes occur and at which efficiency. Thus, advanced gas sensors play a crucial role in many environmental studies, e.g. in climate research,[4] investigations of the earth's critical zone,[5] environmental pollution studies[6] or global nutrient cycling.[7] The requirements a gas sensor should meet, depend on the specific application, of course. In general, a gas sensor should provide a decent repetition rate to trace fast exchange processes; be sensitive to detect small amounts of a substance; be selective to separate different gas species present in a sample; measure non-destructively to allow for repeated measurements of small sample volumes; be portable for on-site operation; and measure several gas species simultaneously. No gas sensor can bring all of these requirements to perfection and, despite of recent technological advances in absorption spectroscopy and mass spectrometry (see section 2.2) major challenges remain. This is especially the simple and simultaneous detection of oxygen (O_2) along with a manifold of other gas species, the gas leakage assessment of environmental chambers without specialized equipment and the quantification of N_2 at natural concentration levels without the need of an artificial proxy.

O_2 is still widely neglected in soil respiration measurements, most likely because additional sensors are needed to quantify it together with CO_2, which is commonly detected with gas sensors based on absorption spectroscopy. It is usually assumed that the CO_2 efflux equals soil respiration. That assumption was recently challenged by evidence of a large temporal decoupling between soil gas exchange fluxes (CO_2 and O_2) and biological soil respiration.[8] This finding, based on the determination of respiration quotients (RQ) as the ratio between CO_2 efflux and O_2 influx, might result in an adjustment of the contribution of soil respiration as major flux in the global carbon cycle (approx. 100 Pg C yr^{-1} to the atmosphere[9]). Measuring O_2 simultaneously with CO_2 and calculating the RQ can also be a valuable tool to identify specific chemical classes as potential carbon sources.[10,11] In a model experiment on soil biodegradation of pathogenic benzene, we demonstrated a novel analytical approach on quantifying time-resolved respiration quotients and the evaporated fraction of the contaminant with just a single Raman gas sensor (section 4.3). The developed methods and instrumentation indicate the potential to simplify soil biodegradation assessments while the high temporal resolution of the acquired data allows a deeper understanding of active microbial processes.

Accurately determining gas leakage rates is vital to reliably quantify gas fluxes during environmental chamber experiments.[12] A purely anthropogenic and one of the most inert and least soluble tracer gases is sulfur hexafluoride (SF_6).[13,14] Standard sensing techniques for SF_6 mostly lack short detection and analysis times which yield more medium-term, general gas leakage trends. Thus, we developed an analytical approach using SF_6 injections, gas diffusion theory and cavity enhanced Raman gas spectroscopy to quantify gas leakage simultaneously with biological respiration and photosynthesis processes (section 4.2). This method could improve the analysis of chamber gas dynamics and help to avoid under- or overestimation of biological process rates.

Another major challenge is the direct detection and quantification of N_2 at natural levels such as the current dry air concentration of 78.084 per cent. Although nitrogen is abundantly available in the atmosphere and essential for the synthesis of nucleic acids and proteins,[7] most organisms cannot use N_2.[15] Instead, prokaryotic diazotrophs take up N_2 via biological nitrogen fixation (BNF) and represent a crucial factor facilitating agricultural productivity. Despite its importance, physiological control of biological nitrogen fixation is not completely understood,[16] also because quantification of N_2 fixation rates at the field level or in real-time is difficult,[17] especially because of the high natural background of N_2.[18] In this thesis, a novel analytical approach based on Raman gas spectroscopy is presented, enabling the determination of biological nitrogen fixation rates without requiring a proxy or an exchange of the natural ecosystem atmosphere (section 4.4). Given its simplicity, the proposed method indicates the potential to open up a new avenue of nitrogen fixation research.

2. Current state of research

This chapter opens with a description of the kinetic theory of gases, relevant quantities and fundamental laws relating them to each other. Established analytical methods and techniques to derive these quantities, e.g. the mixing ratio, the amount of substance or the gas flux, are discussed in the second part.

2.1 Kinetic theory of gases and fundamental laws

The kinetic theory of gases explains macroscopic properties such as pressure, temperature and volume by considering a gas as a large number of submicroscopic particles (atoms and molecules), which move constantly and randomly. Based on relatively simple assumptions, the theory predicts the physical state of gas with remarkable accuracy. Besides the random movement, these basic assumptions include that (1) the particle volume is negligible; (2) the particles have the same mass *m*; (3) a large particle number justifies a statistical treatment and (4) the particles do not interact except in elastic collisions.[19]

The pressure *p*, which is defined as the force exerted by particles when hitting the container walls, can be related to the kinetic energy E_{kin} by

$$p = \frac{2}{3}\frac{N}{V}E_{kin} \tag{2.1.1}$$

Here, *N* represents the number of particles and *V* the volume. The absolute temperature *T* is given by the average particle velocity $\bar{v}$ and the Boltzmann constant $k_B (= 1.381 * 10^{-23}\ J\ K^{-1})$ as

$$T = \frac{m\bar{v}^2}{3k_B} \tag{2.1.2}$$

By combining these equations, the ideal gas law can be derived

$$p\,V = N\,k_B\,T = n\,R\,T \tag{2.1.3}$$

The amount of substance *n* is defined as the ratio of particles *N* and the Avogadro constant N_A $(= 6.022 * 10^{23}\ mol^{-1})$. *R* represents the universal gas constant $(= 8.314\ J\ mol^{-1}\ K^{-1})$ and is determined as the product of k_B and N_A.

In a mixture of different gas species i, which don't react chemically, each component acts independently and exerts an individual partial pressure p_i. These partial pressures add up to the total gas pressure (Dalton's law)

$$p = \sum_i p_i \tag{2.1.4}$$

Like the Raman gas analyzers used in this thesis, gas sensors typically provide measurement data as volume mixing ratios χ_i in units of ppm (v/v) or ppb (v/v). But for the calculation of biochemical gas

exchange rates, it is necessary to quantify absolute quantities such as the amount of substance *n* (in mol).[20] Following equations 2.1.3 and 2.1.4, the amount of substance n_i of an individual gas species can be determined by

$$n_i = \frac{p_i\, V}{R\, T} = \frac{\chi_i\, P\, V}{R\, T} \tag{2.1.5}$$

Using absolute quantities instead of volume mixing ratios is of particular importance in experiments with varying water vapor levels which might cause a significant dilution of the other gases.

The derived relations for ideal gases usually agree well with the behavior of real gases for ambient conditions, i.e. pressures of approx. 1 atm and room temperature. However, at very low temperatures or high pressures, real gases deviate significantly from ideal gases. This happens because basic assumptions of the kinetic theory of gases do not hold for these conditions. At high pressures, the gas gets compressed and the volume the gas particles occupy isn't a negligible fraction of the total volume anymore. Further, it does exist an attractive force between the gas particles, which eventually results in gas condensation at low temperatures. The van der Waals equation

$$\left(p + \frac{an^2}{V^2}\right)(V - nb) = n\, R\, T \tag{2.1.6}$$

accounts for these deviations by introducing correction terms for pressure and temperature. The constants *a* and *b* stand for the particle attraction and volume, respectively, and vary among different gas species. However, for normal pressure and temperature conditions, e.g. at approx. 1 atm and 20°C, the ideal gas law and the van der Waals equation yield essentially the same results and typically differ by not more than 1 per cent. Because all experiments described in this thesis were done under close to ambient conditions, ideal gas behavior was assumed for all analytical calculations.

An important transport process is diffusion, governing e.g. the gas flux from soils to the atmosphere (and vice versa, see 4.3) or the leakage flux out of an environmental chamber (see 4.2). Diffusion refers to the process of equalizing concentration differences by molecular movement. It is based on the statistical particle movement described by the kinetic theory of gases. The random movement of a gas species is superimposed by a diffusion flux *J* pointing towards regions with lower concentration. This diffusion flux is proportional to the concentration difference $\frac{\partial C}{\partial x}$ (one-dimensional) and can be described by Fick's first law

$$J = -\, D\, \frac{\partial C}{\partial x} \tag{2.1.7}$$

The gas diffusion coefficient *D* depends on the gas species. Small molecules such as helium or hydrogen have higher diffusion coefficients than bigger and heavier molecules such as sulfur hexafluoride or benzene.[21] If two gas species (A and B) diffuse through air, the diffusion constants are related to their reduced masses according to[22]

$$\frac{D_A}{D_B} = \frac{\sqrt{\frac{M_{air} + M_A}{M_{air} M_A}}}{\sqrt{\frac{M_{air} + M_B}{M_{air} M_B}}} \tag{2.1.8}$$

However, this dependence on the reduced mass is not regular and diffusion constant should be determined empirically.[23] One of these exceptions is the common tracer gas sulfur hexafluoride. Experimental diffusion constants compared to SF_6 differ significantly from theoretical values[24,25] and careful analysis is needed when calculating experimental gas fluxes based on SF_6 fluxes. An analytical solution, optimized for gas measurements in static environmental chambers, is discussed in section 4.2.

In some cases, a substance's volatility, i.e. its tendency to vaporize, needs to be considered for an exact quantification of gaseous partial pressures. The Clausius-Clapeyron relation describes phase transitions of a substance between the gaseous phase and a condensed phase (liquid or solid). For temperatures much lower than the critical temperature and at common pressures, two phases α (p_1, T_1) and β (p_2, T_2) are related by

$$\ln\left(\frac{p_1}{p_2}\right) = -\frac{L}{R}\left(\frac{1}{T_1} - \frac{1}{T_2}\right) \tag{2.1.9}$$

Here, L denotes the latent heat of vaporization, which is commonly assumed to be constant for specific temperature ranges.[26] For volatile substances such as benzene, the gaseous partial pressure at a specific temperature can then be calculated using boiling point temperature and pressure. Following this approach, benzene calibration spectra were created for the Raman gas measurements within the scope of soil biodegradation monitoring (see section 4.3).

2.2 Established analytical techniques

Most common gas analyzers can be assigned to one of the following techniques: electrochemical detection, mass spectrometry or absorption spectroscopy. In this section, these gas sensing techniques including their individual characteristics are briefly discussed.

Electrochemical gas sensors detect gases by oxidizing or reducing them at an electrode and measure the resulting electrical signal. Typically, the gases pass a capillary-type opening and diffuse through a membrane before reaching the sensing electrode.[27] Various sensor types and geometries exist which deploy different electrode materials and electrolytes optimized for specific gas species.[28,29] The output signal of the electrochemical cell is directly related to the partial pressure of the gaseous species. Depending on the signal type, an electromotive force or an electrical current, electrochemical gas sensors can be classified in potentiometric or amperometric. Electrochemical sensors are currently the most used gas sensor types for oxygen, carbon monoxide, hydrocarbons and nitrogen oxides in exhaust emission measurements.[30] They indicate huge potential as relatively inexpensive and miniaturized gas sensors, especially if integrated on silicon chips.[31] However, electrochemical sensors typically suffer degradation which renders calibration data inapplicable.[32] Additionally, these sensors measure destructively and often experience strong cross-sensitivities[33] which significantly limits the range of possible process monitoring applications.

In mass spectrometry, gases or other chemicals get ionized and separated by their mass to charge ratio, typically by exposing them to an electric or magnetic field. The unimolecular decomposition of ions in the mass spectrometer is described by the quasi-equilibrium theory, which delivers the theoretical background to interpret mass spectra.[34] Mass spectrometry is often used in tandem with chromatographic or other separation techniques to enhance mass resolution and specificity. Particular attention is attracted by isotope ratio mass spectrometry (IRMS) which allows determination of abundance ratios of stable isotopes such as $^{13}C/^{12}C$ or $^{15}N/^{14}N$.[35] This technique provides excellent precision and is generally used to define and evaluate the isotopic composition of international reference materials.[36,37] IRMS stimulated research in environmental science and added new analytical tools to biologists, ecologists and geoscientists.[38] However, some analytical challenges still remain. For instance, samples are measured destructively and in most process monitoring applications N_2 cannot be quantified because of too high natural N_2 background concentrations.[39]

Gas detection via infrared (IR) absorption spectroscopy is based on the Lambert-Beer law

$$I = I_0 \, e^{-\alpha L} \tag{2.2.1}$$

where the transmitted light intensity I equals the product of the incident light intensity I_0 and the absorption term $e^{-\alpha L}$ with the absorption coefficient α and the optical path length L.[40] Here, the absorption strength is proportional to the dipole strength of the investigated molecule.[41] Most common absorption spectroscopy principles are non-dispersive infrared (NDIR), spectrophotometry and tunable diode laser absorption spectroscopy (TDLAS).

Broadband, non-dispersive gas sensors are compact and relatively easy to construct and have great commercial significance.[42] Typically, emission from a broadband light source passes two adjacent filters, one covering the absorption features of the target gas species (measurement channel) and the other a non-absorbing spectral region (reference channel). Standard NDIR sensors rely on mid IR absorption strength, which can be several orders of magnitude higher than that in the near-IR absorption region. Thus, even with relatively unsophisticated sensor design, e.g. uncooled detectors, weak light sources and short optical path lengths, remarkable performance and low detection limits can be reached already.[43] Fourier transform infrared (FTIR) spectroscopy is also a non-dispersive technique as it uses an interferometer to measure many IR frequencies simultaneously and with high speed. The resulting interferogram is decoded via a mathematical Fourier transformation.[44]

In contrast to NDIR, spectrophotometric approaches use a dispersive element, e.g. a grating, to split light from a broadband source. The advantage is that multiple gas species can be detected simultaneously while regions with no absorption serve as reference. This fast screening of a large number of unknown gases is of particular importance in first responder operations and security applications.[45]

In TDLAS, the emission of a narrow linewidth laser diode is scanned across an individual absorption feature of a gas species at very high resolution. The measurement is effectively self-referenced by comparing the major peak absorption to the zero level on either side of the line.[42] One approach to further enhance the detectability of a TDLAS gas sensor is to increase the optical path length by using different optical cavity designs, either on-axis or off-axis. Here, prominent techniques are cavity ring-down spectrometry[46] (CRDS, on-axis) and off-axis integrated cavity output spectroscopy[47] (OA-ICOS, off-axis). Because of the high speed and sensitivity of TDLAS, it is successfully applied in atmospheric

trace gas monitoring and isotope quantification measurements.[48] However, absorption spectroscopy is insensitive towards molecules which do not change their dipole moment upon excitation such as O_2, H_2 or N_2. These gases make up most of the earth's atmosphere and take part in various biogeochemical processes, which creates the need for different gas sensing techniques. Raman spectroscopy as a possible approach to overcome some of the remaining gas-analytical challenges is discussed in the following section.

3 Raman gas spectroscopy

In contrast to previously discussed techniques, Raman spectroscopy relies on the inelastic scattering of photons, typically from a laser, by the investigated molecules. Because of the crucial role of Raman spectroscopy for the presented analytical approaches in this thesis, the theory of Raman scattering and applied enhancement techniques are discussed in this chapter.

3.1 Raman scattering

The actual scattering process of photons by molecules, Raman scattering, can be readily illustrated on the basis of classical physics.[49,50] The incoming electromagnetic wave

$$\vec{E} = \vec{E}_0 \cos(2\pi\nu_0 t) \tag{3.1.1}$$

with an electric field vector $\vec{E}$, oscillating at frequency ν_0, induces a dipole in the molecule

$$\vec{\mu}_{ind} = \tilde{\alpha}(\nu)\,\vec{E} \tag{3.1.2}$$

Here, $\tilde{\alpha}(\nu)$represents the polarizability tensor. This quantity varies with time as it describes the electron response to the movements of the nuclei, which oscillate with normal mode frequency ν_n. The displacement of the nuclei is typically very small, such that a Taylor expansion with the normal coordinates q_n of the molecule can be applied (equilibrium position at q_n = 0).

$$\tilde{\alpha}(\nu) = \tilde{\alpha}_0(\nu_0) + \sum_{n=1}^{3Q-f} \left(\frac{\partial\tilde{\alpha}}{\partial q_n}\right)_0 \cos(2\pi\nu_n t) \tag{3.1.3}$$

The number of normal modes is given by 3Q-f with the number of nuclei *Q* and degrees of freedom *f* (*f* = 5 for linear and *f* = 6 for non-linear molecules). This yields the time dependent induced dipole moment

$$\begin{aligned}\vec{\mu}_{ind} = \tilde{\alpha}_0\,\vec{E}_0 \cos(2\pi\nu_0 t) + \vec{E}_0 \sum_n \left(\frac{\partial\tilde{\alpha}}{\partial q_n}\right)_0 q_n \cos(2\pi[\nu_0+\nu_n]t) \\ + \vec{E}_0 \sum_n \left(\frac{\partial\tilde{\alpha}}{\partial q_n}\right)_0 q_n \cos(2\pi[\nu_0-\nu_n]t)\end{aligned} \tag{3.1.4}$$

As an oscillating dipole moment creates new electromagnetic waves, the molecule contributes to elastic scattering (Rayleigh) at the incident frequency ν_0 and to inelastic scattering (Raman) at the frequencies $\nu_0 \pm \nu_n$. If the molecule was in an excited state before the scattering took place, it can transfer energy to the photon and the scattered wave oscillates at the frequency $\nu_0 + \nu_n$ (Anti-Stokes scattering). When the frequency of the scattered light is lower than that of the incident wave, i.e $\nu_0 - \nu_n$, the molecule remains in an higher excited state (Stokes scattering) after its interaction with the photon. At ambient temperature, thermal energy is lower than the energies of most normal modes, such that molecules predominantly exist in the vibrational ground state and Stokes scattering

represents the most important case of Raman scattering.[49] The developed spectroscopic methods and experimental setups in this thesis rely on Stokes scattering, too.

Although the frequencies of Raman scattered light can be predicted on the basis of classical physics, quantum mechanics is necessary to describe its intensities.[51] The polarizability tensor $\tilde{\alpha}$, with components defined by the molecule coordinates, determines the probability of a molecular transition from a vibrational state $|i\rangle$ to $|f\rangle$

$$\vec{\mu}_{ind} = \begin{bmatrix} \alpha_{xx} & \alpha_{xy} & \alpha_{xz} \\ \alpha_{yx} & \alpha_{yy} & \alpha_{yz} \\ \alpha_{zx} & \alpha_{zy} & \alpha_{zz} \end{bmatrix} \vec{E} \tag{3.1.5}$$

It is useful to define the Raman cross-section σ_{if} for the transition $i \rightarrow f$ by

$$I_{if} = \sigma_{if} I_0 \tag{3.1.6}$$

with the incident and scattered light intensity I_0 and I_{if}, respectively. For a non-oriented sample these intensities integrate over all scattering angles and polarizations. The Stokes Raman cross-section correlates with the polarizability by

$$\sigma_{if} \sim (\nu_0 - \nu_n)^4 \sum_{\rho,\phi} \left|\alpha_{\rho\phi}\right|^2 \tag{3.1.7}$$

The indices ρ and ϕ denote the molecule coordinates.

As spontaneous Raman scattering is a notorious weak process resulting in low scattered light intensities,[52] almost all applications require an enhancement of I_{if}. Eqn. 3.1.6 and 3.1.7 reveal two possible options; using higher incident light intensities I_0 or higher frequencies ν_0. A third option is to analyze not only scattered light from a single molecule, but simply to increase the number *N* of scattering molecules exposed to the incident light intensity I_0. The techniques applied in this thesis, cavity enhanced Raman spectroscopy (CERS) and fiber enhanced Raman spectroscopy (FERS), exploit some of these light enhancement approaches by either increasing the incident light intensity I_0 (CERS) or the number of scattering molecules *N* (FERS).

3.2 Cavity enhanced Raman spectroscopy

An increase of the incident light intensity I_0 by using optical cavities can be achieved in several ways. One approach is to deploy a Raman cell inside a laser resonator with the gain medium and to use the high effective laser intensity within the cavity (intra-cavity laser Raman spectrometer).[53] However, the method used in this thesis takes advantage of the laser power build-up in an external optical cavity. This approach, combined with Raman spectroscopy, was firstly published by King and Pittaro,[54] describing the frequency-locking of an diode laser to a power build-up cavity (PBC). In its simplest form, an optical cavity consists of two parallel, highly-reflective mirrors arranged in a linear geometry.[55] If a laser is tuned to a resonance frequency of the cavity, light can be effectively coupled into the cavity and the initial laser power increased by several orders of magnitude.[56,57]

3.2.1 Experimental setup

The Raman gas sensor used in this thesis (figure 1) is based on the power build-up of an anti-reflection coated laser diode (650 nm, 50 mW). The emitted light passes a gradient-index (GRIN) lens and the input mirror, is focused in the center of the PBC (volume of approx. 4 cm^3) and reflected back by the end mirror. Considering the continuous input by the laser diode and the low intra-cavity losses, the confocal PBC is capable of establishing an internal power of up to 100 Watt. Via the gas inlet port, analyte gases enter the cavity, which acts as sample container. Additional sensors record the gas pressure and temperature inside the cavity. The scattered light leaves the PBC in a 90° angle to the cavity axis, passes aspherical lenses and an edge filter and is diffracted by a planar grating. A linear charge-coupled device (CCD) array with 512 pixel records the scattered light. An exemplary spectrum of a multi-component gas mixture is given in figure 2. Eventually, the gases leave the PBC via the gas outlet port.

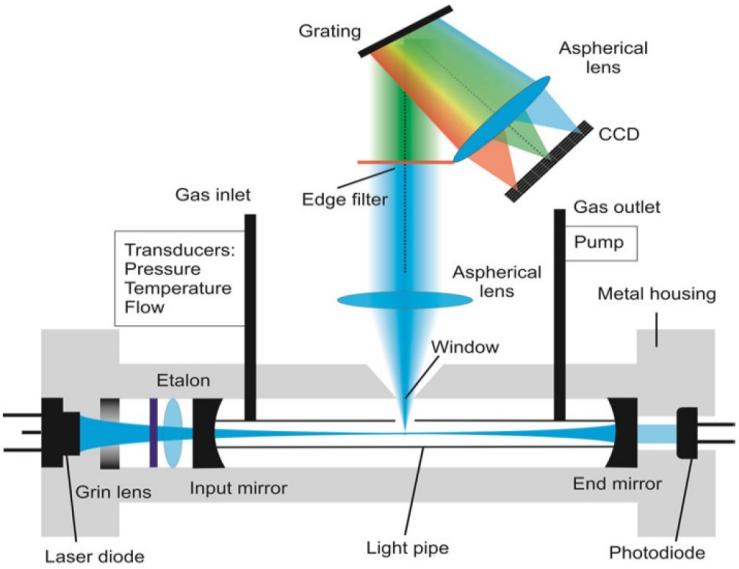

Figure 1: Schematic diagram of the Raman gas sensor.[58] The resonator mode is depicted in blue, the scattered Stokes light after the edge filter in green.

The temporal resolution of the Raman gas setup is approx. 30 milliseconds. Spectra with longer acquisition times are averaged over the respective amount of individual 30 ms spectra. The spectral resolution is about 50 cm^{-1}, which enables simultaneous detection of main atmospheric gases such as N_2, O_2 and CO_2. Depending on the mixing ratios of the investigated gas species, the CERS sensor also provides sufficient selectivity to separate these gases from concurrently present methane, hydrogen, sulfur hexafluoride (see figure 2) or acetone.

For exact quantification of gas composition changes during experimental monitoring of biological or chemical processes, the response time of the CERS sensor is important. From repeated step-wise changes of applied gas mixing ratios, the 98 % response time (τ_{98}) was determined to approx. 2 seconds. Thus, the CERS system has the capability to monitor dynamic and fast gas exchange processes.

Another important issue is the long-term stability of the gas sensor, in temperature as well as in spectral background behavior. For best sensor performance, it is recommended to maintain a constant temperature in the optical cavity. A small fan next to the laser diode stabilizes the internal sensor temperature at about 4 (± 0.3 K) Kelvin above ambient. A warm-up phase of approx. 10 minutes is necessary after turning the power switch. The total level of background noise shows no systematic behavior and is not increasing with time. This indicates a homogeneous cooling of the CCD chip and frequent acquisition of dark spectra to correct for changing background intensities during long measurement campaigns is not necessary.

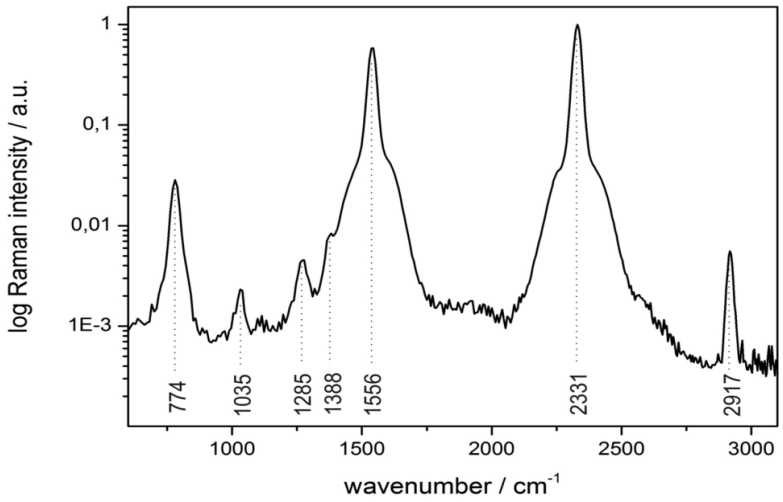

Figure 2: Normalized spectrum of sulfur hexafluoride, hydrogen, carbon dioxide, oxygen, nitrogen and methane.[59] Tagged are the vibrational band ν_1 of methane at 2917 cm^{-1}, the ro-vibrational bands of nitrogen (around 2331 cm^{-1}) and oxygen (around 1556 cm^{-1}), the Fermi dyad of carbon dioxide (1285 and 1388 cm^{-1}), the rotational band S_0 (J = 3) of hydrogen (1035 cm^{-1}) and the fundamental band ν_1 of sulfur hexafluoride at 774 cm^{-1}.

3.2.2 Gas species quantification

For hardware control and processing of the experimentally acquired spectra, a software module based on LabView (National Instruments, USA) was programmed. This module automatically processes the recorded spectra in several steps. First, the beforehand acquired and stored background spectrum, i.e. a spectrum of the Raman-inactive noble gas argon (Ar), is subtracted to compensate for potential systematic errors. Second, the recorded spectrum is normalized by the current laser power and gas pressure to correct for changes in the intra-cavity light intensity or ambient pressure. Beforehand calibrated spectra of pure reference gases (Linde, Germany and Air Liquide, France), which were measured individually, built the basis set for the data analysis. In the third processing step, measured experimental spectra comprising a mixture of spectral features of N_2, O_2 and CO_2 are expressed as a sum of those basis set spectra, where the weighing coefficients of each basis spectrum are proportional to the mixing ratios of that species. For this, the overdetermined linear equation system

$$\left| \sum_{k=1}^{m} I(\tilde{\upsilon}_{kl}^{ref}) * \chi_k = I(\tilde{\upsilon}_l^{mix}) \right|_{l = 1 \ldots n} \tag{3.2.1}$$

is solved, where *m* represents the number of reference gases, $I(\tilde{\upsilon}_{kl}^{ref})$ and $I(\tilde{\upsilon}_l^{mix})$ the intensity at a specific relative wavenumber of a reference gas and the measured gas mixture, respectively, χ_k the mixing ratio (v/v) and *n* the number of CCD pixels. This strategy[60] allows for simultaneous quantification of several constituents in a gas mixture while minimizing cross interferences.[61] Furthermore, deviations between the generated synthetic spectrum from the partial least square fit and the experimental multi-gas spectrum indicate the presence of additional gas species, which could be quantified by extending the amount of pure reference spectra.[62] The robustness of this spectral data analysis can be tested with reference gases comprising the relevant gases and Ar at various mixing ratios close to expected experimental compositions. Those reference gases were typically created using mass flow controllers (model GF80, Brooks Instrument, USA), which were calibrated against primary standard air flow calibrators (model Gilibrator II, Sensidyne, USA and model Definer 220, Brooks Instrument, USA). These test measurements yield a relative accuracy of 1 per cent for measured N_2, O_2 and CO_2 mixing ratios.

The limit of detection (LOD), a measure for the smallest concentration which can be quantified with a specified precision, is of major interest for any instrument operator. Given no spectral interferences with other gases, the limit of detection of the CERS sensor depends on the Raman cross-section σ_{if} and the CCD quantum efficiency. Detection limits were investigated by evaluating the spectral background and its standard deviation (instrument noise) at the respective Raman bands for a blank sample, i.e. pure argon. As a conservative estimation of the LOD, a signal-to noise ratio (SNR) of 3 was taken into account. The intersection of a linear regression onto the mean Raman peak intensities plus three times the SNR yielded 35, 130, 230 and 320 ppm as LOD values for CH_4, CO_2, O_2 and N_2 respectively.

3.3 Fiber enhanced Raman spectroscopy

Besides enhancing the incident laser intensity, low Raman signal intensities can also be overcome by increasing the number *N* auf analyte molecules interacting with a constant laser intensity I_0. The total Stokes Raman intensity I_{if} scales linearly with the number of molecules *N*.[63]

$$I_{if} \sim N \, \sigma_{if} \, I_0 \tag{3.3.1}$$

This effect can be exploited by filling pressurized gas into hollow-core photonic crystal fibers[64] (HC-PCF), which thus act as sample confinement but also as wave guides for incident laser as well as scattered Raman light. Depending on the fiber design, the mechanism of light guiding can be very different; while e.g. Kagome lattice-type fibers[65] rely on a mechanism akin the formation of Von-Neumann-Wigner quasi-bound states in a continuum,[66] the HC-PCF used in this work guides via a photonic bandgap (PBG). The latter provides much lower guiding losses and might be more suited to detect low concentrated gas species.

The HC-PCF traps light in a central defect, i.e. the hollow core, via an out-of-plane PBG created by the microstructure of the photonic crystal cladding. This crystal structure is formed by a periodic pattern of electromagnetic media, in this case a repeating hole geometry, in the scale of the effective optical wavelength. The PBG, which can be theoretically described by Bloch modes similar to electronic wavefunctions in atomic lattices,[67] represents a range of frequencies in which light cannot propagate through the structure. Thus, the HC-PCF forms a kind of optical 'insulator' by confining light in the hollow core.

The FERS sensor repetition time - the time between two consecutive measurements - depends largely on the time needed to fill the hollow core homogeneously with gas. Assuming a laminar flow regime, the filling time t_{fill} is given by[68]

$$t_{fill} = \frac{32}{\Delta p} \left(\frac{L}{D}\right)^2 \mu \tag{3.3.2}$$

with fiber length *L*, diameter *D*, pressure difference Δp and viscosity μ. Given a fiber diameter of 4.8 µm, a pressure difference of approx. 1 bar and a typical fiber length of approx. 30 cm, gas filling times for N_2, O_2, H_2, CO_2 and C_2H_4 lie in the order of several seconds but do not exceed one minute. This was experimentally confirmed in various test measurements. Thus, 2 minutes for gas filling and evacuation between consecutive measurements ensure a homogeneous gas distribution and avoid cross-contamination from one measurement to the next.

4. Research results

Developed analytical methods, instrumentation and major findings resulting from research projects within this thesis are discussed in this chapter. First, a newly designed fiber enhanced Raman gas spectroscopy setup optimized for postharvest fruit monitoring applications is presented. The following sections describe novel analytical approaches to estimate the gas leakage of static environmental chambers and to monitor soil biodegradation and respiration processes simultaneously. Finally, an analytical method to trace biological nitrogen fixation at natural N_2 levels without a proxy is discussed in the last section.

4.1 An universal sensor for postharvest fruit monitoring

In today's fruit conservation rooms, ripening of harvested fruit is deliberately delayed by precise management of the interior O_2 and CO_2 concentration levels. Shortly before entering the final market, the natural plant hormone ethylene (C_2H_4) is commonly used to trigger fruit ripening. Monitoring of these critical process gases is a crucial task in modern postharvest fruit management. Also the increasingly favored cooling agent ammonia (NH_3) requires permanent monitoring as, in the case of leakage, it could cause severe human health risks[69] and spoil delivered fruit[70]. Currently, a variety of different sensing techniques is needed to cover all gas monitoring situations, which leads to high costs, intensive user training and low comparability of measured data. The goal of this work was to develop and characterize a gas sensor setup based on fiber enhanced Raman spectroscopy for fast (time resolution of a few minutes) and non-destructive process gas monitoring throughout the complete postharvest production chain encompassing storage and transport in fruit conservation chambers as well as commercial fruit ripening in industrial ripening rooms.

The developed setup (figure 3) utilizes a HC-PCF as analyte container and light guide. The laser beam from a solid-state laser (excitation wavelength λ_{exc} = 532 nm) is reflected by a dichroic beamsplitter into an objective, where it is focused in a 30 cm hollow core fiber with a bandgap suitable for low-attenuation guiding of Raman Stokes signals up to 3500 cm^{-1}. Custom-made adapters[71] are installed at each fiber end, which provide reproducible laser coupling and Raman light collection as well as fiber filling with analyte gases. After laser-molecule interaction, the redshifted Stokes signal is coupled out of the fiber in a backscattering geometry, passes again the objective and the dichroic beamsplitter. Pinholes of 10 or 15 µm diameter filter out the silica signal originating from the fiber cladding and thus reduce the spectral background. We simulated typical process gas compositions within the fruit ripening product chain by thoroughly mixing of pure gases. Gas preparation, injection and data acquisition is completely automated by a custom-made LabView routine.

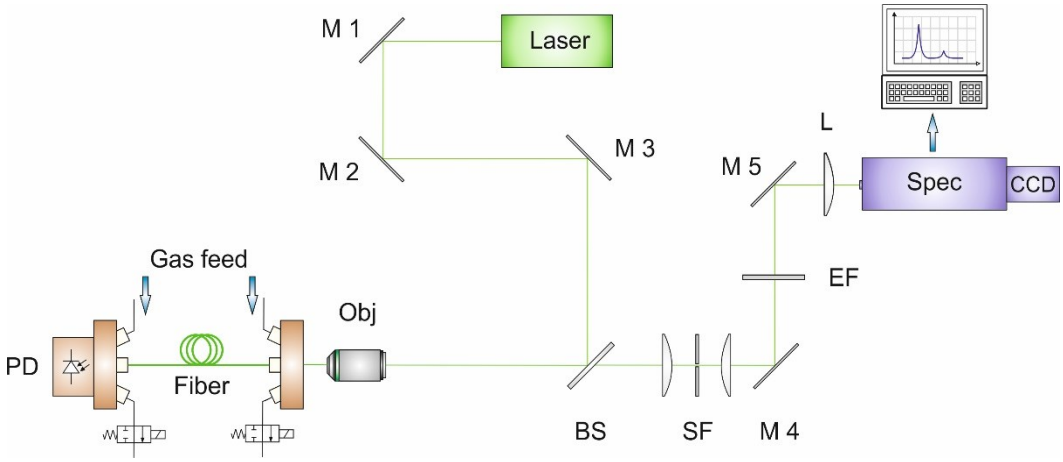

Figure 3: Schematic sketch of the fiber enhanced Raman gas spectroscopy setup.[72] The sensor design and the developed analysis tools facilitate its use in postharvest fruit monitoring.

For the first time, a robust O_2 and CO_2 calibration (R^2 values of more than 0.999) for a fiber enhanced Raman sensor was achieved. For this, Raman peaks had to be integrated and normalized by gas pressure, temperature and current laser power. Here, the vibrational band ν_0 of O_2 (1556 cm^{-1}) and the Fermi dyad of CO_2 (vibrational bands ν_1 at 1285 and 2 ν_2 at 1388 cm^{-1}) were selected for concentration analysis. It was demonstrated that this calibration procedure is capable of determining reference gas mixtures with relative accuracy of 5 percent or better. O_2 and CO_2 concentrations of standard gas atmospheres[73] in fruit conservation chambers were successfully quantified, which demonstrates the potential of the developed system for fruit monitoring in the frame of conservation and storage applications.

Typical ammonia concentrations suited for chemical alarm purposes could be detected with the FERS gas setup. As the vibrational band of NH_3 at 3334 cm^{-1} was evaluated, ammonia monitoring does not interfere with the O_2 and CO_2 calibration and even higher NH_3 levels does not require a sensor re-calibration.

In fruit ripening chambers, ethylene is applied to trigger efficient ripening by coordination of the expression of genes responsible for a variety of processes such as rise in respiration, autocatalytic ethylene production and changes in color, texture, flavor and aroma.[74] We simulated typical atmospheres in fruit ripening chambers including approx. 250 ppm C_2H_4. It could be demonstrated that ethylene can be measured simultaneously with other present gas species due to the sensor's high spectral resolution. By evaluation of ethylene's vibrational band ν_3 at 1342 cm^{-1}, C_2H_4 can be easily distinguished from the ro-vibrational bands of the O branch of O_2 as well as from the vibrational bands of CO_2. In summary, the potential of fiber enhanced Raman systems as universal sensors for postharvest fruit monitoring processes could be demonstrated. Using just one sensor for all relevant process gases - instead of a variety of different techniques - has many benefits; it reduces costs and facilitates user training, improves comparability of measured values and eliminates most systematic errors involved in the analysis.

4.2 Gas leakage assessment of environmental chambers

Accurate gas leakage quantification is essential for the precision of determined gas exchange rates, especially in the case of small net fluxes or accumulation phases. In static environmental chamber experiments, gas leakage fluxes might cause significant over- or underestimation of biological processes such as photosynthesis or respiration.[12] If gas leakage is accounted for, it is commonly estimated by leakage fluxes of a tracer gas such as SF_6 at before or after the experiment. However, leakage fluxes might change during a chamber experiment due to varying gas concentration inside or outside of the chamber. Thus, to improve the precision of biogeochemical gas monitoring, we developed and demonstrated a novel analytical approach for fast on-site determination and correction of gas leakage fluxes.

We selected sulfur hexafluoride as tracer gas as it is a purely anthropogenic gas with extremely low natural background, less than 1 ppb.[75] Furthermore, SF_6 is chemically stable, nontoxic and has only a very low aqueous solubility[14], which facilitates its use in plant or soil related studies. Existing analytical methods to detect SF_6, e.g. gas chromatography,[76] cannot provide sub-minute quantification or cannot be used to measure simultaneously O_2 and CO_2 to determine respiration quotients. Hence, we applied cavity enhanced Raman gas spectroscopy to determine leakage fluxes and biogenic exchange rates simultaneously and in real-time. By measuring SF_6 leakage fluxes and using diffusion theory, the current CO_2 (or any other) leakage fluxes could then be estimated.

An important finding of this work is that theoretically derived diffusion coefficients for SF_6 related fluxes deviate from published experimental data. We surveyed the respective literature and found a general underestimation of SF_6 related reduced mass - free air diffusivity ratios compared to experimental data. Further, gas permeability parameters might differ between static environmental chambers due to different materials used to construct the chambers. Thus, we included experimental determination of “effective” diffusivity ratios as first step in the general analytical protocol to quantify biogenic gas leakage. These effective diffusivity ratios can then be used to estimate non-detectable leakage fluxes of investigated biogenic gases by considering the measured SF_6 leakage fluxes.

We demonstrated the developed gas leakage protocol in a model experiment quantifying the respiration of a plant *(Mirabilis jalapa)* – soil ecosystem. The carbon dioxide exchange rate (CER) as the sum of the measured net CO_2 concentration change and the estimated CO_2 leakage flux was determined under different light regimes. For times of dark respiration or reduced photosynthetic activity, CO_2 leakage was only of minor importance and could be neglected. But for small net CO_2 exchange, e.g. at times of enhanced leaf photosynthesis and concurrent soil respiration, CO_2 leakage was found to be of the same magnitude as the measured CO_2 exchange rate. Thus, leakage correction via the developed analytical protocol could improve assessment of biogeochemical process rates by accounting for non-biological, namely physical, gas loss mechanisms. With elaborate analytical leakage correction methods such as the presented approach, it might be possible to eventually reduce the uncertainties of several gas fluxes and responsible processes within global biogeochemical cycles.

4.3 Monitoring soil biodegradation and respiration

Microbial biodegradation encompasses methods to degrade, transform or accumulate environmental pollutants including hydrocarbons, e.g. oil. Here, only the microorganism's natural capability to metabolize these xenobiotics is exploited to reduce the amount of pollutants. As a low-cost and more sustainable approach compared to more active thermal or other physico-chemical techniques, interest in microbial biodegradation has intensified in recent years.[77,78] However, to test the effectiveness of natural soil biodegradation processes and the underlying mechanisms under varying ambient conditions and indigenous microflora, the contamination and remediation needs to be carefully monitored.[79] Especially short-term responses to contamination 'events' are not fully understood, also because analytical techniques providing on-site gas measurements with high temporal resolution are missing. The goal of this work was to develop an analytical method to follow the fate of soil contaminants as well as to monitor changes in respiration by continuously quantifying the RQ. The latter could elucidate the dynamics of specific enzymatic reactions and the occurrence of concomitant processes such as changes in the substrate for bacterial metabolism.

We demonstrated the developed method by investigating soils from the national park Hainich in Thuringia, central Germany. The clayey-silty top soil, sampled from a grassland plot close to Kammerforst, had in general low pH and high C/N values. To simulate a contamination 'event', the field-fresh soil was spiked with benzene (C_6H_6) as one of the major components of industrial oil. Here, we applied ^{13}C-labeled benzene to distinguish the isotopic heavier $^{13}CO_2$ created by aerobic benzene degradation via

$$^{13}C_6H_6 + 7.5\ O_2 \rightarrow 6\ ^{13}CO_2 + 3\ H_2O \qquad (4.3.1)$$

from CO_2 originating from aerobic respiration. By analyzing the total amount of produced $^{13}CO_2$ with cavity enhanced Raman spectroscopy, we estimated the fraction of degraded benzene as almost 4 %. Due to its high vapor pressure, most of the spiked benzene diffused into the atmosphere and did not undergo any degradation during continuous 12 day experiments.

Using a LabView based software program, we quantified automatically the respiration quotient approx. each 30 minutes by analyzing the chamber headspace concentration change of O_2 and CO_2. This monitoring of soil respiration allowed us to identify different phases during the experiments. In the pre-spiking phase before the addition of benzene, aerobic respiration could be observed. The benzene spiking triggered an immediate microbial response in terms of enhanced respiration, which we refer mainly to metabolization of deceased bacteria due to the application of carcinogenic benzene. Another possible process might be an increased phosphatase, as it was observed in similar scenarios in marine environments.[80] It took about 12 hours to detect the first biodegradation products ($^{13}CO_2$) and the microbial biodegradation peaked approx. 33 hours after the contamination took place. After 12 days, no $^{13}CO_2$ could be detected anymore, which indicates the end of the microbial biodegradation process.

To summarize, with the developed non-invasive analytical method it is possible to identify different phases during a biodegradation process and to monitor short-term changes in the soil microbial

metabolism. This might open the door to a deeper understanding of contributing biological processes to microbial biodegradation and their dynamics.

4.4 Direct biological nitrogen fixation measurements under natural conditions

Biological N_2 fixation is a major ecosystem input of bioavailable nitrogen, which represents the most frequent factor limiting the agricultural production throughout the world. Especially the symbiotic association between legumes and *Rhizobium* bacteria could provide substantial amounts of bioavailable nitrogen and thus reduce the need for industrial fertilizers. But measurements of biological nitrogen fixation prove difficult due to the lack of suitable analytical methods to quantify symbiotic N_2 fixation continuously under natural atmospheric conditions. Hence, we developed a novel analytical approach based on Raman gas spectroscopy, which enables determination of BNF rates without requiring a proxy or an exchange of the natural ecosystem atmosphere. We report on the first biological nitrogen fixation rate estimates derived by optical spectroscopy of N_2 and discuss potential limitations and expansions of the presented method as a prelude to future investigations. Given its simplicity, the proposed method indicates the potential to open up a new avenue of nitrogen fixation research.

When it comes to agricultural nitrogen fixation inputs, most attention is directed towards legumes, because of their proven ability to fix N_2 symbiotically in tropical and temperate environments.[81] Thus, N_2 fixation was measured in a laboratory chamber system housing legume plants, namely alfalfa *(Medicago sativa)*. After introducing the undisturbed plants including roots and nodules into the chamber, the headspace was continuously monitored by cavity enhanced Raman gas spectroscopy. Although gas chromatography coupled to various detector types is a very sensitive technique to quantify N_2,[82] it does not provide a similar temporal resolution as Raman gas spectroscopy. In most applications, N_2 exchange rates cannot be measured by these techniques due to the high natural N_2 background concentration.[39] For N_2 fixation rate calculation, a suitable time interval was determined first. Then, a linear regression (ANOVA) was performed onto the temporal evolution of the amount of N_2 in the chamber. The slope of the linear regression yields the biological N_2 fixation rate, e.g. in µmol N_2 h^{-1}. Finally, the obtained rate was normalized to the nodule dry weight.

Because N_2 fixation requires huge amounts of energy,[83,84] active photosynthesis was found to be necessary for stable N_2 fixation behavior. Thus, in order to improve the comparability of measured N_2 fixation rates, reported N_2 fixation rates were determined only at times of stable and linear photosynthetic CO_2 uptake. We selected the time window from closing the chamber (ambient CO_2 levels) until reaching a CO_2 mixing ratio of approx. 200 ppm (v/v) for the calculation of the CO_2 uptake, O_2 release and N_2 fixation rate. CO_2 uptake rates of the alfalfa plants are strongly correlated with O_2 release rates (correlation coefficient of 0.97), indicating a dominant photosynthesis. However, O_2 release rates are generally lower than CO_2 uptake rates, suggesting that nodule CO_2 fixation contributes significantly to the total CO_2 consumption of the plant.

To test the proposed analytical approach, we measured the biological N_2 fixation rates of 5 individual alfalfa replicates. Measured N_2 fixation rates were normalized to the nodule biomass and ranged from 70 to 85 µmol N_2 (g dry weight nodule)$^{-1}$ h^{-1}, which corresponds to 47 to 57 mg N (g dry weight

nodule)$^{-1}$ d^{-1}. All determined rates are statistically significant ($p < 0.0001$), even the shortest analysis time of approx. half an hour yielded statistically robust data. Thus, the proposed BNF rate quantification is applicable to short-term measurements from 30 min up to several hours without introducing artifacts due to the static environmental chamber design. The mean N_2 fixation rate yielded 78 ± 5 µmol N_2 (g dry weight nodule)$^{-1}$ h^{-1}. This result agrees well with reported values from biological nitrogen fixation studies with alfalfa and other legumes using the $^{15}N_2$ incubation[85,86] or the H_2 evolution[87] technique.

In summary, the proposed method has the potential to simplify and improve biological nitrogen fixation measurements by (1) using ambient N_2 as a direct indicator for BNF, (2) operating non-destructively and with sub-minute time resolution, (3) not depending on external isotopes or other gases and (4) eliminating the need for non-fixing reference plants.

5. Summary and outlook

Analytical methods and instrumentation for diverse environmental applications were developed in this thesis. Exploiting the benefits of enhanced Raman gas spectroscopy, process monitoring solutions for gas leakage assessment, soil biodegradation, nitrogen fixation and fruit ripening were invented.

Successful postharvest fruit management requires continuous gas monitoring during conservation as well as forced ripening. We designed, built and characterized a fiber enhanced Raman gas spectroscopy setup as universal gas sensor for fruit storage and ripening applications. Due to the wide low-loss photonic bandgap, the sensor is capable of detecting relevant concentrations of O_2, CO_2, NH_3 and C_2H_4 at the same time. We demonstrated this feature by simulating and detecting typical gas atmospheres in conservation and ripening chambers. A robust calibration method was developed by accounting for physical parameters such as gas pressure, temperature and transmitted light intensity. Applied gas concentrations during laboratory test measurements were in good agreement with predicted data from the calibration routine. Further technical improvements of the optical part, e.g. the laser – fiber coupling efficiency or improvements in spectral background suppression, could be readily implemented without changes in the gas supply or detection parts of the sensor. Further, the present analytical methods could continue to apply for calibration and gas analysis purposes. The developed Raman setup indicates the potential to become a universally deployable on-site gas sensor for postharvest fruit applications.

An aspect of this thesis was not only to develop new analytical tools, where none yet exist with comparable potential, but also to find solutions to improve the quality of current methods. Mostly overlooked, but potentially significant, is the assessment of gas leakage in static environmental chambers. Leak gas fluxes might distort determined gas exchange rates, which leads to misinterpretations of contributing biogeochemical processes. Thus, we developed a general protocol for gas leakage assessment and correction, which is demonstrated with Raman gas spectroscopy, but can be easily transferred to any other sensing technique without loss of generality. Following the analytical protocol, 'effective' diffusivity ratios of SF_6 and the investigated gas species are determined and used to calculate gas leakage induced concentration changes during the experiment. This allows gas leakage correction parallel to the experiment, which improves the determined biogenic gas exchange rates especially in the case of small net gas fluxes or high concentration differences between the chamber headspace and the ambient atmosphere. We demonstrated that in model experiments, in which we quantified carbon dioxide exchange rates of a plant-soil ecosystem experiencing different light regimes. As the developed protocol also accounts for deviations between theoretically derived and experimentally observed diffusivity ratios, it might improve existing gas measurements in static environmental chambers and contribute to a better understanding of biochemical processes by including gas leakage as contributing mechanism into current experiments and eventually reducing gas flux data uncertainty.

A third focus of this thesis was the development of an analytical method to monitor short-term soil biodegradation processes non-invasively by quantifying the soil - gas exchange with high temporal resolution. For achieving this goal, we designed an environmental chamber experiment involving isotopic labelling, controlled exchange of headspace air and automatic, continuous gas monitoring by cavity enhanced Raman spectroscopy. To distinguish the enzymatic reaction dynamics during

contaminant degradation from common aerobic respiration, we used ^{13}C-labelled benzene as model contaminant. We programed an independent software algorithm, which keeps chamber conditions as natural as possible by regulating the internal CO_2 concentration. Finally, continuous gas monitoring of $^{13}C_6H_6$, CO_2, O_2 and $^{13}CO_2$ allows tracing the dynamics of respiration, metabolized substrates and biodegradation. We demonstrated the capability of this analytical approach in a model experiment with soils from Hainich natural park, central Germany. Using O_2 and CO_2 data from the CERS analyzer, we monitored the respiration quotient during the complete experiment. In doing so, we identified different activity phases, such as enhanced bacterial respiration immediately after the spiking or the change to benzene as metabolic substrate. Furthermore, simultaneous quantification of $^{13}CO_2$ and diffused benzene enabled us to estimate the fractions of diffused, biodegraded and retained benzene. The versatility and temporal resolution of the developed analytical method is to date unmatched and indicates the potential of Raman spectroscopy based gas analysis for short-term biodegradation monitoring.

In the last part of this thesis, an analytical method was developed, which allows direct quantification of biological N_2 fixation without any proxy, isotopic labelling or exchange of the natural atmosphere as it is common in standard methods. We introduce Raman spectroscopy as novel sensing technique for measuring N_2 uptake by legume - diazotroph symbioses under natural atmospheric conditions. We designed a continuous process monitoring setup encompassing an environmental chamber with the N_2 fixing ecosystem and the Raman gas analysis part. Using cavity enhanced Raman gas spectroscopy we monitored the concentrations of N_2, O_2 and CO_2 in the chamber headspace. To calculate the biological N_2 fixation rate, we determined an appropriate time interval first. We defined this interval by the CO_2 and O_2 content in the chamber, as a decrease in BNF was observed under reduced photosynthetic activity of the plant. Then, the slope of a linear regression onto N_2 dynamics of the chamber headspace yields the biological N_2 fixation rate, e.g. in µmol N_2 h^{-1}. Finally, the obtained rate was normalized to the nodule dry weight. In several replicate measurements, we measured a mean N_2 fixation rate of 78 ± 5 µmol N_2 (g dry weight nodule)$^{-1}$ h^{-1}, which agrees well with published data. To our best knowledge, this is the first report on successful biological N_2 fixation measurements with optical spectroscopy under natural atmospheric conditions. Given its simplicity and selectivity for N_2, O_2 and CO_2, the proposed method indicates the potential to open up a new avenue of nitrogen fixation research, e.g. physiological studies of N_2 fixation and photosynthesis, respiration or plant metabolism.

In dieser Arbeit wurden analytische Methoden und instrumentelle Techniken für unterschiedliche umweltwissenschaftliche Fragestellungen entwickelt. Die Vorteile der verstärkten Raman Gas Spektroskopie ausnutzend, kreierten wir Lösungen zur Prozessüberwachung von Gas Leckage, Biodegradation in Böden, Stickstoff-Fixierung von Pflanzen sowie kontrollierte Fruchtreife.

Erfolgreiches Nachernte-Management insbesondere von tropischen Früchten erfordert strikte Überwachung der eingesetzten Gasatmosphäre in Lagerungscontainern und Fruchtreifekammern. Da zurzeit eine Vielzahl unterschiedlicher Gassensoren dazu benötigt wird, lassen sich Messdaten untereinander nur bedingt vergleichen und es fallen hohe Anschaffungskosten und umfangreiche Nutzertrainings an. Daher haben wir ein faserverstärktes Raman Gas Spektroskopie System konzipiert, aufgebaut und charakterisiert, das als universeller Gassensor bestehende Technik zur Gasüberwachung im Fruchtmanagement ersetzen könnte. Aufgrund der großen photonischen Bandlücke der Faser können alle relevanten Prozessgase wie O_2, CO_2, NH_3 und C_2H_4 gleichzeitzeitig detektiert werden, was wir durch Messungen an simulierten Standard-Gasgemischen aus Fruchtlagerungscontainern und Reifekammern zeigen konnten. Um die Konzentrationen der individuellen Gasspezies exakt vorherzusagen, entwickelten wir eine umfangreiche Sensorkalibration, die auch Temperatur, Druck und transmittierte Laserleistung mit einschließt. Vom entwickelten Kalibrations-Algorithmus prognostizierte Konzentrationen stimmten gut mit Referenzwerten überein, was einen essentiellen Schritt in Richtung Verlässlichkeit und Genauigkeit des Sensors darstellt. Durch das modulare Sensordesign können zukünftige Verbesserungen des optischen Teils, z.B. die Effizienz der Laser – Faser Einkopplung oder der spektralen Untergrundunterdrückung, einfach integriert werden, ohne dass Änderungen der Detektions- oder Gaszuführeinheit nötig werden. Auch die entwickelte Kalibrationsroutine kann unverändert übernommen werden. Zusammengefasst hat der entwickelte Sensor das Potential als Universal-Gassensor im Nachernte-Fruchtmanagement eingesetzt zu werden.

Ein weiterer Schwerpunkt dieser Arbeit war die Entwicklung analytischer Methoden, die unterstützend zu Standard-Prozessüberwachungsmethoden eingesetzt werden, um deren Messdatenqualität zu erhöhen. Gasleckage-Flüsse in Klimakammern sind ein häufig unterschätztes Problem, das jedoch im Falle kleiner Netto Gasaustausch-Raten oder im Rahmen von Akkumulationsexperimenten an Bedeutung gewinnt. Diese Leckage-Flüsse können das biologische Signal überlagern und zu Fehlinterpretationen biogeochemischer Prozesse führen. Daher entwickelten wir ein generelles Protokoll zur online Abschätzung und Korrektur dieser Leckage-Flüsse. Wir demonstrierten das Protokoll mit Kavitäts-verstärkter Raman Gas Spektroskopie, es ist jedoch bewusst so allgemein konzipiert, dass es sich auch auf andere Techniken wie Absorptionsspektroskopie leicht übertragen lässt. Eine online Korrektur von Gasaustauschraten in Klimakammern ist durch die experimentelle Bestimmung von Diffusionsverhältnissen zwischen den gemessenen biogenen Gasen und dem Indikatorgas SF_6 möglich. Unser Protokoll beschreibt, wie solche Diffusionsverhältnisse bestimmt werden und erklärt die Berechnungen zur Korrektur der gemessenen Gasaustausch-Raten. Als Anwendungsbeispiel führten wir Messungen der CO_2 Austauschrate an einem Pflanze-Boden Modellsystem, genauer an *Mirabilis jalapa*, durch. Eine besondere Stärke des von uns vorgestellten analytischen Protokolls ist, dass die Abweichung zwischen theoretischen geschätzten und empirisch ermittelten Diffusionsverhältnissen bei Verwendung von SF_6, bereits fest eingebunden ist. Mit dem in dieser Arbeit entwickelten Ansatz ist es möglich, Gasleckage in Klimakammer-Experimenten besser zu berücksichtigen und damit zu einer Reduzierung der Ungenauigkeit von biogeochemischen Gasaustauschraten beitragen.

Ein dritter Schwerpunkt war die Entwicklung einer analytischen Methode zur nichtinvasiven Überwachung kurzfristiger Biodegradationsprozesse in Böden durch zeitlich hochaufgelöste Gasmessungen. Diese Prozesse treten beispielsweise nach der Verunreinigung von Böden mit Mineralölen, Benzen oder ähnlichen Stoffen durch Transportunfälle oder Unwetterschäden auf. Wir verfolgten einen kombinierten Ansatz aus isotopischer Stoffmarkierung, geregeltem Austausch der Klimakammeratmosphäre und kontinuierlicher Gasüberwachung mittels Kavitäts-verstärkter Raman Gas Spektroskopie. Isotopie-markiertes Benzen ermöglichte die Unterscheidung enzymatischer Biodegradations-Reaktionsdynamiken und aerober Bodenatmung. Um die Atmosphäre in der Klimakammer so natürlich wie möglich zu halten, programmierten wir eine Steuersoftware, die durch automatische Regelung der Zufuhr von CO_2-freier Luft den internen CO_2 Gehalt limitiert. Weiterhin konnten wir durch simultane Detektion von $^{13}C_6H_6$, CO_2, O_2 und $^{13}CO_2$ die zeitliche Dynamik von Bodenatmung, verstoffwechselten Substraten sowie der Biodegradation aufdecken. Das Potential unserer Methode demonstrierten wir in Modellexperimenten mit Böden aus der Nationalparkregion Hainich in Mitteldeutschland. Anhand gemessener O_2 und CO_2 Raten ermittelten wir die zeitliche Dynamik des Atmungskoeffizienten. So konnten wir verschiedene Aktvitätsphasen entschlüsseln, wie beispielsweise erhöhte Atmung unmittelbar nach Kontamination oder den genauen Zeitpunkt des Einsetzens der Biodegradation. Durch simultane Messung von isotopenmarkiertem $^{13}CO_2$ und evaporiertem Benzen konnten wir das Verhältnis von diffundierten, umgewandelten und zurückgehaltenen Schadstoffen ermitteln. Abschließend lässt sich sagen, dass die Vielseitigkeit und Geschwindigkeit unseres analytischen Ansatzes momentan unerreicht ist und daher Raman spektroskopische Methoden ein hohes Potential zur Überwachung von Bodenkontaminations- und Biodegradationsprozessen aufweisen.

Im letzten Teil dieser Arbeit wird eine analytische Methode vorgestellt, die es erstmals ermöglicht biologische Stickstoff-Fixierung direkt über die N_2 Aufnahme aus der Atmosphäre zu messen und dabei nicht, wie heutige Standardtechniken, auf Isotopie-Markierung, externe Indikatormoleküle oder künstliche Gasgemische als Umgebungsatmosphäre angewiesen ist. Dazu bauten wir ein Prozessüberwachungs-System aus Klimakammer mit Stickstoff-fixierender Leguminose und einer Gasanalyse-Einheit. Letztere besteht hauptsächlich aus dem Kavitäts-verstärkten Raman Gassensor und Hilfssensoren zur Überwachung von Druck, Temperatur und Luftfeuchtigkeit. Die Konzentrationen von N_2, O_2 und CO_2 in der Klimakammer wurden kontinuierlich gemessen und analysiert. Wir beobachteten, dass durch aktive Photosynthese die CO_2 Konzentration linear sank, was allerdings unterhalb eines bestimmten CO_2 Grenzwertes zu nachlassender N_2 Fixierung führte. Daher entwickelten wir eine CO_2 abhängige Methode zur Bestimmung der biologischen Stickstoff-Fixierungsrate. Hierbei wird durch lineare Regression an die N_2 Stoffmenge die Fixierungsrate bestimmt, allerdings ausschließlich solange, bis ein unterer CO_2 Grenzwert von 200 ppm erreicht wird. Die so ermittelte Stickstoff-Fixierungsrate wird auf das Trockengewicht der Wurzelknöllchen als Maß für die Menge an diazotrophen Bakterien normalisiert. Die in mehreren Wiederholungsmessungen ermittelte mittlere biologische N_2 Fixierungsrate von 78 ± 5 µmol N_2 (g Trockengewicht)$^{-1}$ h^{-1} stimmt gut mit Literaturwerten der verwendeten Luzerne Pflanze überein. Somit ist es zum ersten Mal gelungen, biologische Stickstoff-Fixierung direkt unter natürlichen Bedingungen mit optischer Spektroskopie zu messen. In Anbetracht der Einfachheit und Vielseitigkeit der verwendeten Analysetechnik besitzt sie das Potential neue Forschungsmöglichkeiten zur Stickstoff-Fixierung zu eröffnen, insbesondere Forschung zu physiologischen Zusammenhängen zwischen N_2 Fixierung und Photosynthese, aerober Atmung oder Stoffwechselvorgängen.

6. Publications

[1] All-in-one: a versatile gas sensor based on fiber enhanced Raman spectroscopy for monitoring postharvest fruit conservation and ripening

Tobias Jochum, Leila Rahal, Renè J. Suckert, Jürgen Popp, Torsten Frosch.

Analyst **2016,** *141* (6), 2023-9

[2] Multigas Leakage Correction in Static Environmental Chambers Using Sulfur Hexafluoride and Raman Spectroscopy

Tobias Jochum, Joseph C. von Fischer, Susan E. Trumbore, Jürgen Popp, Torsten Frosch.

Anal Chem **2015,** *87* (21), 11137-42

[3] Microbial respiration and natural attenuation of benzene contaminated soils investigated by cavity enhanced Raman multi-gas spectroscopy

Tobias Jochum, Beate Michalzik, Anne Bachmann, Jürgen Popp, Torsten Frosch.

Analyst **2015,** *140* (9), 3143-9

[4] Direct measurements of biological nitrogen (N_2) fixation under natural conditions: A novel analytical approach for studying nitrogenase activity

Tobias Jochum, Agnes Fastnacht, Susan E. Trumbore, Jürgen Popp, Torsten Frosch.

Anal Chem **2017**, 89 (2), 1117 - 1122

Erklärung zu Eigenanteilen

Für alle in dieser kumulativen Dissertation verwendeten Manuskripte liegen die notwendigen Genehmigungen der Verlage (‚reprint permissions') für die Zweitpublikation vor.

Die Koautoren der in dieser kumulativen Dissertation verwendeten Manuskripte sind sowohl über die Nutzung, als auch über die oben angegebenen Eigenanteile der weiteren Doktoranden/Doktorandinnen als Koautoren an den Publikationen und Zweitpublikationsrechten bei einer kumulativen Dissertation informiert du stimmen dem zu.

Jena,

Ich bin mit der Abfassung der Dissertation als publikationsbasiert, d.h. kumulativ, einverstanden und bestätige die vorstehenden Angaben. Eine entsprechend begründete Befürwortung mit Angabe des wissenschaftlichen Anteils des Doktoranden/der Doktorandin an den verwendeten Publikationen werde ich parallel an den Rat der Chemisch-Geowissenschaftlichen Fakultät richten.

Jena,

6.1 All-in-one: A versatile gas sensor based on fiber enhanced Raman spectroscopy for monitoring postharvest fruit conservation and ripening

Analyst **2016,** *141* (6), 2023-9

Tobias Jochum	concept development measurements and data evaluation discussion of concept and results manuscript preparation and discussion (proposed publication equivalents 1.0)
Leila Rahal	measurements and data evaluation
Renè J. Suckert	measurements and data evaluation
Jürgen Popp	manuscript preparation and discussion
Torsten Frosch	concept development discussion of concept and results manuscript preparation and discussion

Analyst

PAPER

View Article Online
View Journal | View Issue

Cite this: *Analyst*, 2016, **141**, 2023

All-in-one: a versatile gas sensor based on fiber enhanced Raman spectroscopy for monitoring postharvest fruit conservation and ripening†

Tobias Jochum,[a] Leila Rahal,[a] Renè J. Suckert,[a] Jürgen Popp[a,b] and Torsten Frosch*[a,b]

In today's fruit conservation rooms the ripening of harvested fruit is delayed by precise management of the interior oxygen (O_2) and carbon dioxide (CO_2) levels. Ethylene (C_2H_4), a natural plant hormone, is commonly used to trigger fruit ripening shortly before entering the market. Monitoring of these critical process gases, also of the increasingly favored cooling agent ammonia (NH_3), is a crucial task in modern postharvest fruit management. The goal of this work was to develop and characterize a gas sensor setup based on fiber enhanced Raman spectroscopy for fast (time resolution of a few minutes) and non-destructive process gas monitoring throughout the complete postharvest production chain encompassing storage and transport in fruit conservation chambers as well as commercial fruit ripening in industrial ripening rooms. Exploiting a micro-structured hollow-core photonic crystal fiber for analyte gas confinement and sensitivity enhancement, the sensor features simultaneous quantification of O_2, CO_2, NH_3 and C_2H_4 without cross-sensitivity in just one single measurement. Laboratory measurements of typical fruit conservation gas mixtures showed that the sensor is capable of quantifying O_2 and CO_2 concentration levels with accuracy of 3% or less with respect to reference concentrations. The sensor detected ammonia concentrations, relevant for chemical alarm purposes. Due to the high spectral resolution of the gas sensor, ethylene could be quantified simultaneously with O_2 and CO_2 in a multi-component mixture. These results indicate that fiber enhanced Raman sensors have a potential to become universally usable on-site gas sensors for controlled atmosphere applications in postharvest fruit management.

Received 14th October 2015,
Accepted 9th February 2016

DOI: 10.1039/c5an02120k

www.rsc.org/analyst

Introduction

Postharvest produce management encompassing storage and transport has become an important branch of modern logistics. Nowadays, more than half of the maritime transport of refrigerated products is represented by fruit transports.[1] Most of the imported fruit spends several days in transit between the country of production and the final market, where their ripening is typically performed by the wholesaler or retailer. Since consumers judge the quality of fruits by their appearance and sales increase if fresh, ready-to-eat produce are available,[2] postharvest technology and handling is a major challenge to successful fruit marketing. For all these reasons, thorough monitoring of fruit ripeness during the complete production chain is essential. To avoid fruit decay during transport and to optimize its quality on the market, most fruits are shipped in conservation chambers, which delay the ripening process.[3] In low-oxygen (LO) or ultra-low oxygen chambers (ULO), fruits are exposed to low temperatures around 0 °C, high humidity (90–95%), low oxygen (approx. 2–3% O_2 for LO, 1–1.5% O_2 for ULO) and high carbon dioxide levels (approx. 2–5% CO_2 for LO, 1–1.5% CO_2 for ULO).[4] The role of ethylene (C_2H_4) in fruit ripening is twofold: since low C_2H_4 concentrations are produced by the fruit itself during ripening, ethylene can act as a ripeness indicator; but it is also a natural plant hormone that triggers fruit ripening, as ethylene coordinates the expression of genes responsible for a variety of processes such as rise in respiration, autocatalytic ethylene production and changes in color, texture, flavor and aroma.[5,6] Depending on the fruit type, ethylene concentrations should thus be kept in low parts per million (ppm) or parts per billion (ppb) levels in conservation chambers to avoid early ripening and fruit losses;[7] whereas inside ripening rooms C_2H_4 concentrations of up to 1000 ppm are possible.[8] In food cooling systems such as LO's and ULO's, monitoring of ammonia (NH_3) is of particular interest because it becomes more and more the coolant of choice since substances with high ozone layer endangering potential are strictly regulated.

[a]Leibniz Institute of Photonic Technology, Jena, Germany
[b]Institute of Physical Chemistry and Abbe Center of Photonics, Friedrich Schiller University, Jena, Germany. E-mail: torsten.frosch@uni-jena.de, torsten.frosch@gmx.de
†Electronic supplementary information (ESI) available. See DOI: 10.1039/c5an02120k

In case of leakage, ammonia concentrations can rise easily to several hundred ppm or more, which demands safety actions for human protection.[9] Additionally, emergent ammonia could spoil stored fruit, *e.g.* by causing skin blackening.[10]

Commonly used fruit quality parameters such as firmness,[11] starch or sugar content[12] are not well suited for automated supervision, because they require unpacking or destructive sampling. Also, fruit color is often only weakly correlated to fruit ripeness.[13] Non-destructive methods to determine fruit ripeness by the level of soluble solids, ethylene concentration, chlorophyll or moisture content have been proposed, such as nuclear magnetic resonance[14] (NMR), proton magnetic resonance[15] (PMR), optical reflectance[16] or infrared absorption spectroscopy.[17–19] Recently, a variety of electronic nose (e-nose) approaches, widely utilizing chemoresistive gas sensors, attracted a lot of attention.[20–22] Here, mainly fruit-emitted aromatic volatiles or ethylene were measured to assess fruit ripening. Although most of these approaches are very sensitive, they rely upon expensive equipment[23] and/or are only suited to quantify a limited number of gases. Additionally, electrochemical sensors show gradual decrease in sensitivity which rapidly renders calibration data inapplicable.[24] Furthermore, chemoresistive metal oxide sensors for ethylene monitoring exhibit strong cross-interferences and are sensitive to humidity, which requires additional compensation methods.[25]

In this study, we present a gas sensor based on fiber enhanced Raman spectroscopy for on-site process gas monitoring throughout the complete postharvest production chain encompassing storage and transport in fruit conservation chambers as well as commercial fruit ripening in industrial ripening rooms. The gas sensor's capability was tested by obtaining and assessing a suitable sensor calibration for oxygen and carbon dioxide. Ammonia levels appropriate for chemical alarm purposes were established and successfully detected. Ethylene was measured down to a concentration of 100 ppm within a multi-gas mixture of O_2, CO_2, NH_3 and N_2 without any cross-sensitivity. The goal of the work presented here was to develop and demonstrate the use of a single sensor covering simultaneously non-destructive oxygen, carbon dioxide, ethylene and ammonia monitoring over a wide concentration range of ppm up to percent levels while maintaining short measurement times.

Materials and methods

Experimental setup – optical part

Raman gas spectroscopy offers simultaneous detection and quantification of multi-gas mixtures in a wide concentration range from ppm levels up to pure compounds.[26–33] Due to the gas molecule's small Raman cross-sections, typically in the order of 10^{-23} cm^2 sr^{-1},[34] Raman signals are intrinsically low and need to be enhanced. A novel approach is to use hollow-core photonic crystal fibers[35] (HC-PCF), which act as optical light guide as well as analyte container for the investigated processes gases.[36,37] The optical design of the Raman sensor is schematically depicted in Fig. 1. The laser beam from a frequency-doubled Nd:YAG laser (Laser Quantum, laser excitation wavelength $\lambda_{exc.}$ = 532 nm) is reflected by a dichroic beamsplitter (Semrock) into an objective (Olympus LUCPLFLN 20X), where it is focused in a 30 cm HC-PCF (NKT) with a bandgap suitable for low-attenuation guiding of Raman signals up to 3500 cm^{-1}. This length is a good compromise between low analyte–laser interaction times within shorter fibers resulting in a lower overall Raman intensity[38] and the increasing attenuation of guided light within longer fibers. The central transmission wavelength of the HC-PCF is 532 nm and the hollow core has a diameter of approx. 5 μm. Gases enter the HC-PCF *via* custom-made fiber adapters.[39] Adapters are installed at each end of the HC-PCF and provide reproducible laser coupling and scattered Raman light collection through optical windows as well as filling of the fiber with the analyte gases. The adapters can bear pressures up to 20 bar and have an internal dead volume of approx. 0.1 microliter. During measurements, the adapter's gas outlets were closed by mag-

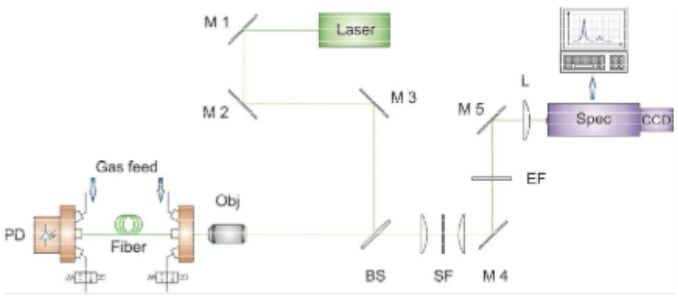

Fig. 1 Schematic sketch of the experimental setup. The 532 nm laser is guided by several mirrors (M1 to M3), a beamsplitter (BS) and an objective (Obj) into the hollow core photonic crystal fiber. The scattered Raman signal is coupled out in a backscattering geometry, passes the beamsplitter, a pinhole for spatial filtering (SF), an edge filter (EF) and a lens (L) and is eventually focused onto the spectrometer unit (Spec). Process gases are filled into the fiber *via* custom-made fiber adapters. A photodiode (PD) records the transmitted power during the gas measurements.

netic valves. After laser-molecule scattering, the redshifted Raman Stokes signal is coupled out of the fiber in a backscattering geometry, passing again the objective and the beamsplitter. Pinholes of 10 or 15 μm diameter (Thorlabs) were used for spatial filtering of the silica Raman signal originating from the fiber cladding and thus for reducing the spectral background.[40] After passing an edge filter to suppress the Rayleigh signal, the scattered light is focused on the slit of the spectrometer (Acton SP2500, Princeton Instruments). A grating with 1800 lines per mm was chosen for high resolution. The setup magnifies light from the hollow core at the fiber exit to an approximately 60 μm diameter spot with numerical aperture (NA) of 0.05 on the spectrometer entrance slit to achieve optimal etendue.

Gas feed and measurement

The gas feed line is schematically shown in Fig. 2. To simulate typical process gas compositions within the fruit ripening product chain, pure gases (purchased from Linde) were precisely mixed by mass flow controllers (Brooks Instrument) and subsequently injected. A gas mixing chamber provided homogeneous gas mixing and a stable gas flow, controlled by custom-made software based on LabView (National Instruments). Before each individual measurement, the fiber was automatically evacuated (inner pressure below 0.05 mbar) with a vacuum pump (Vacuubrand) to avoid cross-contamination. The gas mixture entered the HC-PCF from both ends with a pressure of approx. 2.0 bar by opening the magnetic valves 1 and 2 at the fiber adapters. During filling and measurement, magnetic valves 3 and 4 were shut. Given this pressure-driven filling procedure and the setup parameters, sub minute filling times for all gases were expected according to the model of Wynne *et al.*[41] In separate test measurements beforehand, we observed stable Raman intensities for several applied gas concentrations after a filling time of one minute. Thus, all reported gas measurements were initiated one minute after opening the fiber adapter's magnetic valves 1 and 2. During measurements, all magnetic valves were shut. After each individual measurement, all gas-containing components were evacuated again to avoid cross-contamination with subsequent measurements. Alternatively, measured gases originating from fruit conservation or ripening chambers could also be redirected into the chamber *via* the magnetic valves 3 and 4 without any manipulation of the gas composition, which facilitates process monitoring *in situ*. Due to the compact and airtight design of the gas feed line, contamination of the analyte gases with ambient air was not observed in the Raman spectra.

Obtained spectra were normalized by absolute pressure and temperature (both measured with a pressure sensor, Keller), as well as by transmitted power (power sensor, Thorlabs). A beforehand acquired spectrum of pure Argon was used for background correction. For each gas, the respective Raman band in the background corrected spectrum was integrated, yielding a peak area A, and normalized with the average pressure p (in bar), temperature T (in Kelvin) and transmitted power P (in Watt) during the spectrum acquisition according to

$$A_{\mathrm{norm}} = \frac{A \times T}{p \times P} \quad (1)$$

As not only macroscopic thermodynamic systems are temperature dependent, but also populations of molecular energy

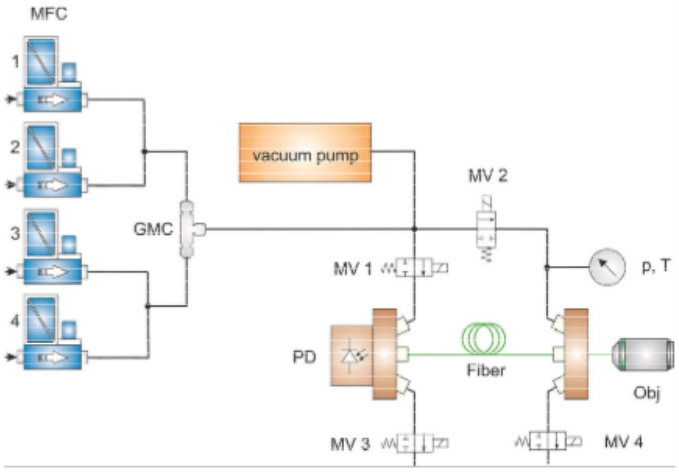

Fig. 2 Illustration of the gas feed line. After applying a vacuum, gases were injected by up to 4 mass flow controllers (MFC), additionally homogenized in a gas mixing chamber (GMC) and filled into the fiber *via* the magnetic valves 1 and 2. During measurements, the current pressure (p) and temperature (T) were monitored. In the end, measured gases were released by opening MV 3 and 4.

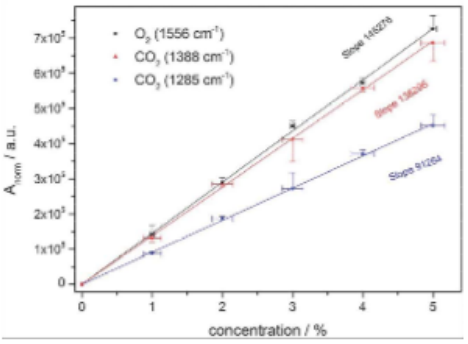

Fig. 3 Calibration data showing the linearity of the normalized Raman peak area *versus* the concentration (linear fits onto the measured data with coefficients of determination (R^2) larger than 0.999). The background corrected peak area was normalized by the current pressure (in bar), temperature (in Kelvin) and transmitted power (in Watt). Data points are mean normalized Raman peak areas, error bars represent standard errors.

levels and thus the Raman Stokes intensity, the used normalization formula applies only for moderate changes in temperature. The normalized peak area A_{norm} was referred to the applied gas concentrations in the sensor calibration (Fig. 3) and used in the subsequent measurements to quantify simulated process gas compositions.

Results and discussion

Monitoring of fruit conservation chamber gases

Sensor calibration to oxygen and carbon dioxide was performed with precisely mixed test gases of varying concentrations. A concentration range of 1 to 5 percent was chosen, since this reflects O_2 and CO_2 levels in fruit conservation chambers. After evacuation of the fiber, test gases containing equal levels of oxygen and carbon dioxide (remainder nitrogen) were filled in the fiber up to a pressure of approx. 2.0 bar. The temperature of gases entering the fiber was approx. 22 degree Celsius. Measurement time for one spectrum was 60 seconds (30 seconds exposure time and 2 accumulations). Thus, monitoring of O_2 and CO_2 concentration levels with suitable time resolution is feasible. Gas mixtures were measured in triplicate and averaged. After each single measurement, the HC-PCF and other gas-containing parts were evacuated. The vibrational band ν_0 at 1556 cm^{-1} of oxygen and the Fermi dyad of carbon dioxide (vibrational bands ν_1 at 1285 and $2\nu_2$ at 1388 cm^{-1}) were selected for concentration analysis. As sensor calibration for O_2 and CO_2 was done simultaneously in multi-gas mixtures containing O_2, CO_2 and N_2, the time needed to set the sensor up had been minimized.

The results (Fig. 3) show the linearity of the normalized Raman peak area *versus* the compound concentration, which can be used to quantify unknown gas compositions. Mean normalized peak areas along with the respective standard deviation were calculated based on triplicate measurements for every concentration value. In general, small standard deviations of the mean normalized Raman peak area of about 5 percent or lower were achieved for all established gas concentrations during the sensor calibration, only the mean peak area of the 3 percent CO_2 measurement shows standard deviations of approx. 13 percent. Most likely, this was caused by small deteriorations of the gas feed line and will be quantified and corrected by using inert gaseous tracers in future experiments. However, coefficients of determination (R^2) of more than 0.999 for all linear calibration functions indicate a stable sensor calibration. The standard deviation of the concentration was calculated according to the product specifications of the used mass flow controllers. Because of its higher Raman cross section, the calibration function of the CO_2 band at 1388 cm^{-1} provides a larger slope than the one from the band at 1285 cm^{-1}. Highest sensitivity was reached for oxygen.

Several gas mixtures common for fruit conservation chambers were established and quantified with the Raman sensor (Table 1). Since CO_2 concentrations of the applied gases were overdetermined by using both Raman bands of the Fermi dyad, the accuracy of the total carbon dioxide level in the gas samples can be further enhanced by combining their concentration values originating from individual calibration data. For all test gas concentrations, calculated concentration values are in good agreement with established ones, the average deviation is smaller than 1 percent with respect to the individual reference concentration.

Ammonia leakage in fruit conservation chambers can cause serious damage to humans and fruit. By evaluating the vibrational band of ammonia at 3334 cm^{-1},[42] the Raman sensor could be used to monitor ammonia levels continuously and to detect potential leakages, such that immediate response is possible. Ammonia concentrations of 750 ppm (remainder N_2) could be clearly detected (Fig. S2†). This concentration is suited for chemical alarm purposes,[43] since

Table 1 Quantification of several gas mixtures common for conservation chambers (ULO – ultra low oxygen, LO – low oxygen). Concentration values are given in percent

Gas mixture	O_2 conc. reference	O_2 conc. measured	CO_2 conc. reference	CO_2 conc. measured	Conservation chamber type
1	1.50	1.53	1.50	1.52	ULO
2	2.00	2.00	3.00	2.91	LO
3	3.00	3.02	5.00	5.01	LO

ammonia levels rise rapidly in case of leakage, and also higher concentrations up to percentage levels can be monitored without sensor re-calibration. Thus, all relevant process gases within standard ULO and LO fruit conservation chambers, namely O_2, CO_2 and NH_3, could be simultaneously monitored by the presented Raman sensor.

Fruit ripening monitoring

Oxygen and carbon dioxide are important gaseous indicators also beyond conservation chambers. Since many fruits such as peaches, bananas, apples *etc.* are climacteric, their ripening is accompanied by a dramatic increase in respiration.[44] Thus, monitoring O_2 and CO_2 levels (fruit respiration) with the Raman gas sensor (see Fig. 3 and Table 1) could assess fruit ripening performance in ripening chambers.[45] Here, measuring the respiratory quotient (RQ) could yield auxiliary information about the ripening process, indicating pre-climacteric, climacteric or post-climacteric stages.[46] For instance, CO_2 levels could rise approx. threefold during strawberry ripening under climacteric conditions.[47] Additionally, low carbon dioxide levels could indicate potential freeze damage, *e.g.* in oranges.[48]

However, ethylene plays the main role in fruit ripening as ripeness indicator and plant hormone as well. Thus, it is beneficial to monitor O_2, CO_2 and C_2H_4 concentrations simultaneously during forced fruit ripening. Fig. 4 displays a derived Raman spectrum of 20% O_2, 500 ppm CO_2 and 250 ppm C_2H_4, simulating a possible fruit chamber atmosphere. The gas composition was precisely mixed by mass flow controllers and the complete measurement time was

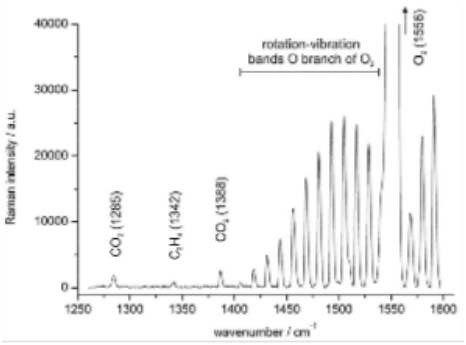

Fig. 4 Background corrected Raman spectrum of a simulated fruit chamber atmosphere containing 20% O_2, 500 ppm CO_2 and 250 ppm C_2H_4 (remainder N_2). Due to the high spectral resolution of the Raman sensor, carbon dioxide (1285 and 1388 cm^{-1}) and ethylene bands (1342 cm^{-1}) could be separated from the rotation–vibration bands of the O branch of the fundamental ν_0 vibration of oxygen (at wavenumbers approx. from 1405 to 1540 cm^{-1}) without any cross-sensitivity. The Q branch of O_2 (1556 cm^{-1}) was cut off for better visualization. Only Raman bands with assigned wavenumbers were needed for the analysis of the aforementioned gases.

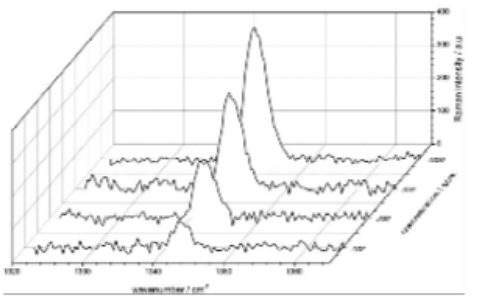

Fig. 5 Overview of the Raman signals of the vibrational band ν_3 of ethylene (1342 cm^{-1}) at 100, 250, 500 and 1000 ppm (front to rear). Ethylene was measured in a multi-gas mixture together with O_2, CO_2 and N_2.

10 minutes. Most prominent are the vibrational band ν_0 of oxygen (Q branch at 1556 cm^{-1}) and its rotation–vibration bands in the O branch (with rotational quantum number J = 25 at approx. 1405 cm^{-1} up to 1540 cm^{-1} for J = 1);[49] but due to the high spectral resolution of the Raman sensor, the carbon dioxide (Fermi dyad at 1285 and 1388 cm^{-1}) and ethylene signals (CH_2 scissoring vibration ν_3 at 1342 cm^{-1}) could be clearly distinguished from the stronger oxygen peaks within just a single measurement. For quantification of oxygen levels, only the mean normalized Raman peak area of the vibrational band (Q branch) is needed. The results additionally demonstrate the Raman sensor's high dynamic range of about 4 orders of magnitude.

To demonstrate the Raman sensor's sensitivity, several ethylene concentrations were established and measured. Fig. 5 displays the evolution of the vibrational band of ethylene at 1342 cm^{-1} from 100 ppm up to 1000 ppm (mixed with 20% O_2, 500 ppm CO_2 and remainder N_2). Plotted are the background corrected mean Raman spectra, exposure time was 10 minutes for each measurement. The signal-to-noise ratio for 100 ppm ethylene yielded 7.2. Thus, fiber enhanced Raman spectroscopy is a capable technique for simultaneously quantifying ethylene in a mixture together with the major atmospheric gases N_2, O_2 and CO_2.

Conclusion and outlook

A versatile gas sensor setup for on-site process gas monitoring throughout the complete postharvest fruit production chain was developed. Utilizing a hollow-core photonic crystal fiber for analyte gas confinement and sensitivity enhancement, simultaneous quantification of O_2, CO_2, NH_3 and C_2H_4 without cross-sensitivity was feasible in just one single measurement. Laboratory test measurements showed the reliability of the sensor calibration and were in good agreement with expected reference gas concentrations. Suitable ethylene concentrations

to assess fruit ripening were detected, preventing fruit to decline into senescence (typically over 100 ppm). Using one single sensor for all relevant process gases has many benefits; it reduces costs and facilitates user training, improves comparability of measured values and eliminates most systematic errors involved in the analysis or makes these errors constant. It is shown that fiber enhanced Raman spectroscopic sensors have a potential to become versatile applicable on-site gas sensors for controlled atmosphere applications in postharvest fruit management.

Acknowledgements

Funding of the research project by the Free State of Thuringia (Germany) and the European Union (EFRE) is highly acknowledged (FKZ: 2012 FGR 0013). We thank Di Yan for valuable support and advice during sensor build-up.

References

1 Y. Wild, R. Scharnow and M. Rühmann, *Container Handbook*, Gesamtverband der Deutschen Versicherungswirtschaft e.V. (GDV), Berlin, 2005.
2 A. A. Kader, *Acta Hortic.*, 1999, **485**, 203–208.
3 A. Kader, *Food Technol.*, 1980, **34**, 51–54.
4 J. Fonollosa, B. Halford, L. Fonseca, J. Santander, S. Udina, M. Moreno, J. Hildenbrand, J. Wollenstein and S. Marco, *Sens. Actuators, B*, 2009, **136**, 546–554.
5 S. Yang and J. Oetiker, *Postharvest Physiology of Fruits 398*, 1994, pp. 167–178.
6 M. Rhodes, *Biochemistry of fruits and their products*, Academic Press Inc., London, 1970.
7 A. Vergara, E. Llobet, J. L. Ramirez, P. Ivanov, L. Fonseca, S. Zampolli, A. Scorzoni, T. Becker, S. Marco and J. Woellenstein, *Sens. Actuators, B*, 2007, **127**, 143–149.
8 R. Jedermann, C. Behrens, D. Westphal and W. Lang, *Sens. Actuators, A*, 2006, **132**, 370–375.
9 A. Jerger, H. Kohler, F. Becker, H. B. Keller and R. Seifert, *Sens. Actuators, B*, 2002, **81**, 301–307.
10 G. B. Ramsey and L. Butler, *J. Agric. Res.*, 1928, **37**, 339–348.
11 B. D. Horton, *J. Am. Soc. Hortic. Sci.*, 1992, **117**, 784–787.
12 E. Vangdal, *Acta Agric. Scand.*, 1980, **30**, 445–448.
13 J. Brezmes, M. L. L. Fructuoso, E. Llobet, X. Vilanova, I. Recasens, J. Orts, G. Saiz and X. Correig, *IEEE Sens. J.*, 2005, **5**, 97–108.
14 M. Musse, S. Quellec, M. Cambert, M. F. Devaux, M. Lahaye and F. Mariette, *Postharvest Biol. Technol.*, 2009, **53**, 22–35.
15 W.-K. Wai, R. Stroshine and G. Krutz, *Trans. ASAE*, 1995, **38**, 849–855.
16 M. Li, D. C. Slaughter and J. F. Thompson, *Postharvest Biol. Technol.*, 1997, **12**, 273–283.
17 C. A. T. dos Santos, M. Lopo, R. N. M. J. Pascoa and J. A. Lopes, *Appl. Spectrosc.*, 2013, **67**, 1215–1233.
18 E. H. Wahl, S. M. Tan, S. Koulikov, B. Kharlamov, C. R. Rella, E. R. Crosson and D. Biswell, *Opt. Express*, 2006, **14**, 1673–1684.
19 R. Centeno, J. Mandon, S. M. Cristescu and F. J. M. Harren, *Sens. Actuators, B*, 2014, **203**, 311–319.
20 M. Peris and L. Escuder-Gilabert, *Anal. Chim. Acta*, 2009, **638**, 1–15.
21 E. Llobet, E. L. Hines, J. W. Gardner and S. Franco, *Meas Sci. Technol.*, 1999, **10**, 538–548.
22 B. Esser, J. M. Schnorr and T. M. Swager, *Angew. Chem., Int. Ed.*, 2012, **51**, 5752–5756.
23 M. Zude, M. Linke, B. Herold, R. Reisch and H. Ahlers, *Landtechnik*, 2002, **57**, 218–219.
24 SiraTechnology, *Gas Detector Selection and Calibration Guide*, Witherby, 2005.
25 A. Giberti, M. C. Carotta, V. Guidi, C. Malagu, G. Martinelli, M. Piga and B. Vendemiati, *Sens. Actuators, B*, 2004, **103**, 272–276.
26 T. Jochum, B. Michalzik, A. Bachmann, J. Popp and T. Frosch, *Analyst*, 2015, **140**, 3143–3149.
27 R. Keiner, T. Frosch, S. Hanf, A. Rusznyak, D. M. Akob, K. Kusel and J. Popp, *Anal. Chem.*, 2013, **85**, 8708–8714.
28 T. Frosch, R. Keiner, B. Michalzik, B. Fischer and J. Popp, *Anal. Chem.*, 2013, **85**, 1295–1299.
29 T. Jochum, J. C. von Fischer, S. Trumbore, J. Popp and T. Frosch, *Anal. Chem.*, 2015, **87**, 11137–11142.
30 R. Keiner, T. Frosch, T. Massad, S. Trumbore and J. Popp, *Analyst*, 2014, **139**, 3879–3884.
31 T. M. James, S. Rupp and H. H. Telle, *Anal. Methods*, 2015, **7**, 2568–2576.
32 J. Kiefer, T. Seeger, S. Steuer, S. Schorsch, M. C. Weikl and A. Leipertz, *Meas. Sci. Technol.*, 2008, **19**, 085408.
33 R. Salter, J. Chu and M. Hippler, *Analyst*, 2012, **137**, 4669–4676.
34 H. W. Schrötter and H. W. Klöckner, in *Raman Spectroscopy of Gases and Liquids*, ed. A. Weber, Springer, Berlin Heidelberg, 1979, vol. 11, ch. 4, pp. 123–166.
35 P. Russell, *Science*, 2003, **299**, 358–362.
36 S. Hanf, R. Keiner, D. Yan, J. Popp and T. Frosch, *Anal. Chem.*, 2014, **86**, 5278–5285.
37 M. P. Buric, K. P. Chen, J. Falk and S. D. Woodruff, *Appl. Opt.*, 2008, **47**, 4255–4261.
38 X. Yang, A. S. P. Chang, B. Chen, C. Gu and T. C. Bond, *Sens. Actuators, B*, 2013, **176**, 64–68.
39 T. Frosch, D. Yan and J. Popp, *Anal. Chem.*, 2013, **85**, 6264–6271.
40 S. Hanf, T. Bogozi, R. Keiner, T. Frosch and J. Popp, *Anal. Chem.*, 2015, **87**, 982–988.
41 R. M. Wynne, B. Barabadi, K. J. Creedon and A. Ortega, *J. Lightwave Technol.*, 2009, **27**, 1590–1596.
42 R. Dickinson, R. Dillon and F. Rasetti, *Phys. Rev.*, 1929, **34**, 582.
43 B. Timmer, W. Olthuis and A. van den Berg, *Sens. Actuators, B*, 2005, **107**, 666–677.

44 H. K. Pratt and J. Goeschl, *Annu. Rev. Plant Physiol.*, 1969, **20**, 541–584.
45 R. Jedermann, U. Praeger, M. Geyer and W. Lang, *Philos. Trans. R. Soc. London, Ser. A*, 2014, 372.
46 S. A. Sampaio, P. S. Bora, H. J. Holschuh and S. d. M. Silva, *Food Sci. Technol.*, 2007, **27**, 511–515.
47 P. P. M. Iannetta, L. J. Laarhoven, N. Medina-Escobar, E. K. James, M. T. McManus, H. V. Davies and F. J. M. Harren, *Physiol. Plant.*, 2006, **127**, 247–259.
48 E. S. Tan, D. C. Slaughter and J. F. Thompson, *Postharvest Biol. Technol.*, 2005, **35**, 177–182.
49 A. Weber and E. A. Mcginnis, *J. Mol. Spectrosc.*, 1960, **4**, 195–200.

Electronic Supplementary Material (ESI) for Analyst.

Supplementary Material

All-in-one: A versatile gas sensor based on fiber enhanced Raman spectroscopy for monitoring postharvest fruit conservation and ripening

Tobias Jochum[a], Leila Rahal[a], Renè J. Suckert[a], Jürgen Popp[a,b], Torsten Frosch[a,b,*]

[a] Leibniz Institute of Photonic Technology, Jena, Germany

[b] Institute of Physical Chemistry and Abbe Center of Photonics, Friedrich Schiller University, Jena, Germany, *torsten.frosch@uni-jena.de

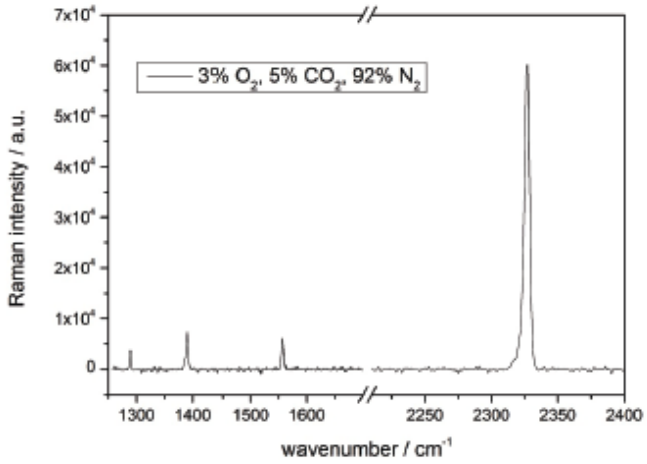

Figure S1: Exemplary Raman spectrum of a common low oxygen conservation chamber (LO) gas mixture of 3 % O_2, 5 % CO_2 and 92 % N_2. Observable are the Fermi dyad of carbon dioxide (1285 and 1388 cm^{-1}) and the vibrational bands of oxygen (1556 cm^{-1}) and nitrogen (2331 cm^{-1}).

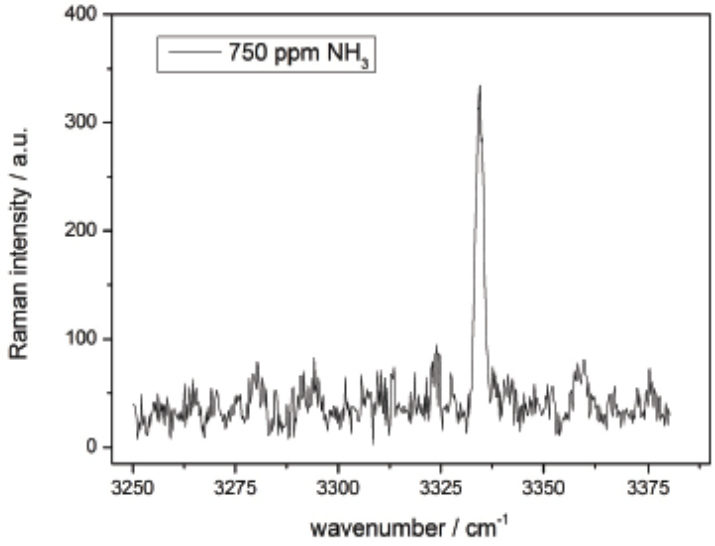

Figure S2: Baseline corrected Raman spectrum of 750 ppm NH_3 in N_2 with the vibrational band at 3334 cm^{-1}. This concentration range indicates possible ammonia leakage and is suited for chemical alarm purposes.

6.2 Multigas Leakage Correction in Static Environmental Chambers Using Sulfur Hexafluoride and Raman Spectroscopy

Anal Chem **2015,** *87* (21), 11137-42

Tobias Jochum	concept development measurements and data evaluation discussion of concept and results manuscript preparation and discussion (proposed publication equivalents 1.0)
Joseph C. von Fischer	discussion of concept and results manuscript preparation and discussion
Susan E. Trumbore	discussion of concept and results manuscript preparation and discussion
Jürgen Popp	manuscript preparation and discussion
Torsten Frosch	concept development discussion of concept and results manuscript preparation and discussion

analytical chemistry

Article

pubs.acs.org/ac

Multigas Leakage Correction in Static Environmental Chambers Using Sulfur Hexafluoride and Raman Spectroscopy

Tobias Jochum,[†] Joseph C. von Fischer,[‡] Susan Trumbore,[§] Jürgen Popp,[†,∥] and Torsten Frosch*[,†,∥]

[†]Leibniz Institute of Photonic Technology, Jena 07745, Germany

[‡]Department of Biology and Graduate Degree Program in Ecology, Colorado State University, Fort Collins, Colorado 80523, United States

[§]Max Planck Institute for Biogeochemistry, Jena 07745, Germany

[∥]Institute of Physical Chemistry and Abbe Center of Photonics, Friedrich Schiller University, Jena 07743, Germany

ABSTRACT: In static environmental chamber experiments, the precision of gas flux measurements can be significantly improved by a thorough gas leakage correction to avoid under- or overestimation of biological activity such as respiration or photosynthesis. Especially in the case of small biological net gas exchange rates or gas accumulation phases during long environmental monitoring experiments, gas leakage fluxes could distort the analysis of the biogenic gas kinetics. Here we propose and demonstrate a general protocol for online correction of diffusion-driven gas leakage in plant chambers by simultaneous quantification of the inert tracer sulfur hexafluoride (SF_6) and the investigated biogenic gases using enhanced Raman spectroscopy. By quantifying the leakage rates of carbon dioxide (CO_2), methane (CH_4), and hydrogen (H_2) simultaneously with SF_6 in the test chamber, their effective diffusivity ratios of approximately 1.60, 1.96, and 5.65 were determined, each related to SF_6. Because our experiments suggest that the effective diffusivity ratios are reproducible for an individual static environmental chamber, even under varying concentration gradients and slight changes of the chamber sealing, an experimental method to quantify gas leakage fluxes by using effective diffusivity ratios and SF_6 leakage fluxes is proposed. The method is demonstrated by quantifying the CO_2 net exchange rate of a plant−soil ecosystem (*Mirabilis jalapa*). By knowing the effective chamber diffusivity ratio CO_2/SF_6 and the measured SF_6 leakage rate during the experiment, the leakage contribution to the total CO_2 exchange rate could be calculated and the biological net CO_2 concentration change within the chamber atmosphere determined.

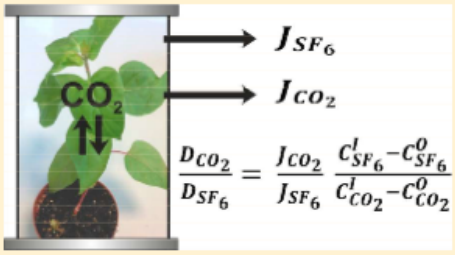

Accurately determining gas leakage rates is essential for reliably quantifying gas fluxes in controlled-environment chambers and hence for correcting measurements of, e.g., photosynthesis or respiration rates of plants or soils.[1] One way of estimating leakage rates of a closed or semiclosed chamber system is to determine leakage before or after an experiment using only the empty chamber, without any plants or soil. However, the gas concentrations outside the chamber can vary even within several hours. This in turn changes the concentration gradient between the chamber atmospheric concentration and the ambient air concentration for each gas and thus the leakage rates. Additionally, deterioration with time of chamber seals, septa, threads, etc. can alter the gas leakage rates. Therefore, tracer gases unaffected by the investigated biological processes are commonly used to estimate leakage rates in environmental research studies. Typical tracer gases include, e.g., carbon dioxide,[2] helium,[3] sulfur hexafluoride,[4] nitrous oxide,[5] or hydrogen,[6] but some of these gases are not biologically conservative and so their usefulness may be compromised. For example, carbon dioxide is utilized in many environmentally relevant processes such as photosynthesis and respiration or in various microbial metabolisms as energy or carbon source. Hydrogen is also known as microbial energy source, e.g., oxidized by the enzyme hydrogenase. Nitrous oxide, on the other hand, is a product of diverse nitrification and denitrification processes of aerobic soil microorganisms.[7] Thus, the dynamics of these biologically reactive gases are not well suited to determine solely gas leakage during complex environmental chamber experiments involving soil−plant−atmosphere ecosystems. Helium is a physiologically inert, but a very light molecule and has additionally a natural atmospheric background of approximately 5 ppm, which could be unfavorable under some experimental conditions.

Sulfur hexafluoride (SF_6) appears to be an ideal tracer for environmental gas flux experiments. SF_6 is purely anthropogenic and its natural background is extremely low, less than 1 ppb.[8] It is chemically stable, nontoxic, nonflammable, relatively

Received: August 28, 2015
Accepted: October 11, 2015
Published: October 22, 2015

DOI: 10.1021/acs.analchem.5b03312
Anal. Chem. 2015, 87, 11137−11142

inexpensive, and can be handled hazard-free. Sorption is only of importance in the presence of highly concentrated organic compounds of biological origin.[9] SF_6 has a very low aqueous solubility,[10] which makes it also a suitable tracer to delineate unsaturated zones in the subsurface.[11] On the other hand, the same properties that make SF_6 a useful tracer, e.g., long atmospheric lifetime, lack of biological reactivity combined with a strong ability to absorb in the infrared, make SF_6 a very potent greenhouse gas.[12] However, the amounts released by geochemical tracer experiments are very small compared to industrial sources. SF_6 is mainly used as an electrical insulator in high-voltage switchgear applications and as a blanket gas in magnesium metal production.[13] Its use in biogeochemistry is widespread and encompasses, for instance, monitoring and modeling of rivers[14] and groundwater flows,[15,16] measuring the rate of water−atmosphere gas exchange,[17] evaluation of methane emissions in natural gas facilities,[18] air flow monitoring during soil venting operations,[9] analyzing the properties of fractured rock aquifers,[19] investigation of gas migration in the unsaturated zone,[20] and modeling methanotroph activity in upland soils.[21] Tingey et al. used the decline of applied sulfur hexafluoride to estimate carbon dioxide leakage in terracosms.[22]

The standard technique to measure SF_6 is gas chromatography coupled to an electron capture detector.[23] This technique provides excellent sensitivity, typically down to very low (parts per trillion) levels.[24] However, because of the sample consumption during the measurements (typically about 0.1 mL per injection), these systems are not well suited to monitor continuously the atmospheric SF_6 dynamics in small (volume less than 1 L) closed experimental systems. Additionally, long analysis times for each gas sample of about 10 min[23] result in low time resolutions, which might conceal fast experimental gas exchange kinetics. Recently, cavity enhanced Raman gas spectroscopy (CERS) was presented as a powerful technique for simultaneous online monitoring of biogenic gases and isotopically labeled tracers in several environmental experiments.[25−27] In this study, the inert tracer sulfur hexafluoride is spectroscopically quantified using Raman, simultaneously with carbon dioxide (CO_2), methane (CH_4), and hydrogen (H_2), to provide an elegant way for fast online gas leakage correction. The benefit of making all measurements with the same device is that it eliminates or makes constant most systematic errors involved in the analysis. The relative rates of 4 different gases were simultaneously quantified and compared to theoretical diffusivity ratios based on the reduced masses of the pure compounds in background air. The repeatability of the rates was tested with multiple opening and closing of the chamber system to mimic the effect of putting a plant inside. The goal of the work presented here was to demonstrate the use of enhanced Raman multigas sensing to monitor and evaluate the effects of plant activity and leakage on concentrations of CO_2 and to provide a general protocol for simultaneous online correction of gas leakage for several biogenic gases during static environmental chamber experiments.

MATERIALS AND METHODS

Theoretical Models for Leakage. Previous approaches to estimate carbon dioxide leakage of dynamic environmental chambers by following tracer losses during an experiment assume an equal leak rate for CO_2 and the applied leakage tracer gas, independent of the individual molecular masses or diffusivities.[5,22,28] The measured gas leakage was treated as a bulk flow, mainly caused by air handlers that circulate air between large (volume $>10^3$ L) sun-lit outdoor chambers and cooling systems that regulate air temperatures. However, when operating environmental chambers in a static mode, i.e., without active pumping of chamber air, diffusion is more typically the major driver for leakage. The leakage diffusion flux J is expressed by Fick's first law of diffusion (one-dimensional, steady state):

$$J = -D\frac{\partial C}{\partial x} \tag{1}$$

where D is the gaseous diffusion coefficient in the chamber and $\partial C/\partial x$ the concentration gradient of the gas between the chamber and the ambient atmosphere. Considering an environmental chamber, the leakage rates J_A and J_B of the gases A and B relate as

$$\frac{J_A}{J_B} = \frac{D_A\,C_A^I - C_A^O}{D_B\,C_B^I - C_B^O} \tag{2}$$

with C_A^I and C_B^I being the concentrations of the gases A and B inside the chamber; C_A^O and C_B^O the ambient gas concentrations outside the chamber. Because gas diffusion is mass-dependent, Graham's law is often used to relate the leakage fluxes of two gases. It states that the effusion rates of two gases are inversely proportional to the square roots of their molecular weights, given the same temperature and pressure. But this is only true for diffusion in vacuo. If diffusion of a gas A through a gas B is considered, the reduced mass

$$\mu = \frac{M_A M_B}{M_A + M_B} \tag{3}$$

has to be used.[29] M_A and M_B denote the molecular weights of the gases A and B, respectively. Thus, the free-air diffusion coefficients of gas A and gas B are related according to[30]

$$\frac{D_A}{D_B} = \frac{\sqrt{\frac{M_{air}+M_A}{M_{air}M_A}}}{\sqrt{\frac{M_{air}+M_B}{M_{air}M_B}}} \tag{4}$$

with M_{air} as the average molecular weight of air being 28.9 g/mol. However, the dependence on the reduced mass is not regular and (binary) diffusion coefficients should be determined empirically.[31] The need for quantifying diffusion coefficients experimentally becomes obvious when comparing CH_4 (molecular weight M_{CH_4} = 16 g/mol), hydrogen (molecular weight M_{H_2} = 2 g/mol) or CO_2 (molecular weight M_{CO_2} = 44 g/mol) with SF_6 (molecular weight M_{SF_6} = 146 g/mol). The diffusivity ratios according to eq 4 and data from diffusion experiments[32−35] in free air as well as in nitrogen (N_2) are summarized in Table 1.

For each diffusivity ratio, theoretical calculations underestimate reported experimental values. Additionally, material permeability can vary from chamber to chamber and influence the diffusivity ratios. In general, possible temperature or pressure gradient changes between the environmental chamber and the ambient atmosphere are not included in the theoretical description of chamber leakage by diffusion. Thus, for environmental chamber experiments with diffusion-driven gas leakage and SF_6 as leakage tracer gas, experimentally derived "effective" diffusivity ratios of the gases at interest and SF_6 could improve chamber leakage assessment. Moreover, fast and

DOI: 10.1021/acs.analchem.5b03312
Anal. Chem. 2015, 87, 11137−11142

Table 1. Overview of the Diffusivity Ratios for CO_2, CH_4, and H_2, Each Compared to SF_6[a]

diffusivity ratio	diffusion theory	experimental data
D_{CO_2}/D_{SF_6}	1.18	1.5−1.6
D_{CH_4}/D_{SF_6}	1.53	1.9−2.1
D_{H_2}/D_{SF_6}	3.59	5.4−5.7

[a]Theoretical results according to eq 4 are displayed in the middle column, whereas the right-hand column shows ratios from calculations with reported experimental data.[32−35] Because published diffusion constants vary slightly and are not always measured at exact the same temperature or pressure, a range of expected diffusivity ratios is given here.

simultaneous quantification of all gases, including the tracer, allows online observation of possible temporary variations in leak tightness of the experimental setup and the chamber sealing, and offers the opportunity to correct these leaks in real-time.

Raman Gas Analysis. All gas concentrations and leakage rates were quantified with a single gas sensor based on cavity enhanced Raman spectroscopy (CERS).[36−38] A laser diode (50 mW at λ = 650 nm) is feedback coupled and passively frequency locked to a high finesse optical cavity. With this configuration, a power enhancement of up to 100 W can be achieved within the power build-up cavity (PBC, volume approximately 4 cm^3). The PBC supports a Gaussian beam and comprises an input coupler mirror and an end mirror, both with extremely low transmission. The spectral resolution is about 50 cm^{-1}. Membrane filters (Sigma-Aldrich) are used to prevent aerosols from entering the cavity. To avoid any degradation of the cavity mirrors and thus the sensor performance, reactive gases such as mononitrogen oxides or hydrogen sulfide were excluded. Full details of the optical setup will be published in a technical paper.

The Raman gas sensor can measure in a concentration range from approximately 100 ppm up to pure compounds and additional electronic sensors record the current temperature, absolute pressure and laser intensity. Investigated gases do not undergo any pretreatment and are not consumed during the measurement procedure, thus the CERS sensor can be operated in situ without manipulating the experimental gas composition. A robust sensor calibration is achieved by using pure reference gases of N_2, O_2, CO_2, CH_4, H_2, and SF_6. The measured Raman Stokes intensity

$$I_{Stokes} \sim N * I_0 * (\nu_S - \nu_L)^4 * |\alpha|^2 \quad (5)$$

scales with the number of gas molecules N, the laser intensity I_0, the difference of the scattered light frequency ν_S and the laser frequency ν_L, as well as with the polarizability of the gas molecule α. Thus, with (a) the given linearity of the Raman Stokes intensity versus the molecule concentration and (b) the individual gas calibration spectra, compound specific concentrations within a mixture of all investigated gases are obtained. For this, the measured spectra are least-squares fitted onto the spectra of the pure reference gases. Individual gas concentrations are quantified by solving an overdetermined linear equation system

$$\left|\sum_{k=1}^{m} I(\tilde{\nu}_{kl}^{ref}) * c_k = I(\tilde{\nu}_l^{mix})\right|_{l=1\ldots n} \quad (6)$$

with the number of reference gases m, the intensity at a specific relative wavenumber of a reference gas $I(\tilde{\nu}_{kl}^{ref})$ and the measured multigas mix $I(\tilde{\nu}_l^{mix})$, the concentration c_k and the number of CCD pixels n. The spectral underground was corrected by subtracting the spectrum of the Raman inactive noble gas Argon. Gas concentrations are expressed as mixing ratios and normalized to the sum of all measured concentrations.

Experimental Design. A custom-made cylindrical Plexiglas chamber (height 25 cm, volume 5.67 L) was used in all experiments. The complete gas volume was 5.7 L, including tubing (16 mL), pump (10 mL) and the Raman gas cell (4 mL). Leakage rates were determined with an empty chamber, without any plants or soils. Via a septum on top of the chamber, small volumes (several milliliters each) of pure CO_2, CH_4, H_2, and SF_6 were injected subsequently to create a concentration gradient between the chamber gases and the ambient atmosphere. A diaphragm pump established a constant flow of 120 mL/min through the environmental chamber and the gas sensor. To ensure a homogeneous gas composition in the chamber, leakage rate measurements began after a 30 min delay following the injection, allowing air to mix completely. However, because of sufficiently large interfaces between the individual components of the system, homogeneous gas mixing in less than 1 min after the injection was observed. Thus, abrupt changes in plant metabolism can be observed instantly with CERS. By continuously monitoring the concentration dynamics within the empty system, any gas concentration change can thus be attributed to leakage. The gas composition of the chamber was measured every 0.1 s and concentrations were averaged over 1 min. An average ambient carbon dioxide concentration of 390 ppm was measured directly before the leakage experiments. Because atmospheric methane, hydrogen, and sulfur hexafluoride concentrations lay below the sensitivity of the gas sensor, they were taken as zero. The system together with the Raman sensor is expected to have a nonzero leak rate, because of inherent open-ness.

Measurements were carried out using a plant (*Mirabilis jalapa*, height h = 15 cm) along with soil and roots (mass m = 250 g, soil surface area A = 75 cm^2) that was placed in the environmental chamber. Leakage was measured by following the change in concentration of injected SF_6 over time and using a plant-free chamber experiment to determine the effective leakage ratios of SF_6 and CO_2; the remaining changes in chamber headspace CO_2 then are attributed to plant photosynthesis and respiration.

RESULTS AND DISCUSSION

Quantification of Leakage Rates and Effective Diffusivity Ratios. Nitrogen, oxygen, carbon dioxide, methane, hydrogen, and sulfur hexafluoride were simultaneously monitored by the Raman gas sensor. Within the sensors spectral range of approximately 600−3200 cm^{-1}, the ro-vibrational Raman bands of N_2 and O_2 (O and S branches unresolved), the Fermi dyad of CO_2, the rotational band S_0 (J = 3) of H_2, the vibrational line ν_1 of CH_4 and the fundamental Q branch ν_1 of SF_6 could be observed (Figure 1).

Chamber leakage rates of carbon dioxide, methane, hydrogen and sulfur hexafluoride were measured simultaneously in a 3 h experiment with the Raman gas sensor and an empty chamber. The concentration dynamics after manual injection of small gas volumes (several milliliters) via a septum are displayed in Figure 2. Leakage rates were determined as the slope of a linear regression onto each gas concentration profile. The results are

DOI: 10.1021/acs.analchem.5b03312
Anal. Chem. 2015, 87, 11137−11142

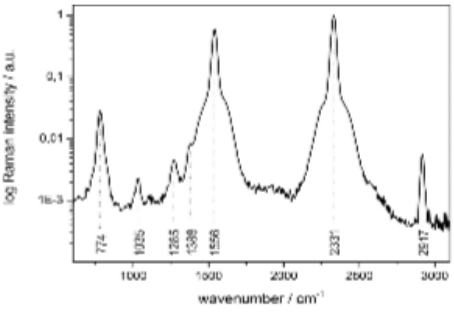

Figure 1. Example of an experimentally acquired multigas Raman spectrum during the leakage experiments. Tagged are the vibrational band ν_1 of methane at 2917 cm^{-1}, the ro-vibrational bands of nitrogen (around 2331 cm^{-1}) and oxygen (around 1556 cm^{-1}), the Fermi dyad of carbon dioxide (1285 and 1388 cm^{-1}), the rotational band S_0 (J = 3) of hydrogen (1035 cm^{-1}), and the fundamental band ν_1 of sulfur hexafluoride at 774 cm^{-1}. A logarithmic y-scale was used for better visibility of gases present across a range of concentrations.

summarized in Table 2. Following eq 2, the effective diffusivity ratios can be determined from the initial concentration gradients and the gas leakage rates. This yields 1.59 ± 0.16, 1.96 ± 0.20, and 5.65 ± 0.65 for the diffusivity ratios of CO_2, CH_4, and H_2, respectively, each compared to SF_6. These experimentally derived effective diffusivity ratios are in good agreement with previously reported diffusion ratios (see Table 1), demonstrating that the process responsible for chamber leakage could be approximated using diffusion. Because of the high permeability of CO_2 and H_2 for the installed polyvinyl chloride (PVC) tubing[39] and some small Teflon sealings[40] within the Raman gas sensor, our measured CO_2 and H_2 leakage rates might be slightly enhanced, whereas the CH_4 and SF_6 leakage rates would not be affected. This illustrates again that the experimentally derived effective diffusivity ratios can vary if changing the environmental chamber, the gas sensor or the ambient conditions and that diffusivity ratios need to be derived experimentally.

Table 2. Measured Gas Leakage Rates J^a

gas	$\partial C/\partial x$ (ppm)	J (μmol/h)
CO_2	1385	−0.60 ± 0.02
CH_4	2015	−1.08 ± 0.04
H_2	3520	−5.43 ± 0.27
SF_6	1315	−0.36 ± 0.02

[a]The initial concentration gradient $\partial C/\partial x$ specifies the concentration difference between the environmental chamber and the ambient atmosphere at the beginning of the experiment.

Quantification Repeatability. As the effective diffusivity ratios were determined before the actual plant experiment, and the chamber must be opened and sealed again to add the plant−soil ecosystem, we evaluated the reproducibility of the experimentally derived effective diffusivity ratios. A series of independent gas leakage experiments with the bare chamber was performed. After each experimental run, the chamber lid was opened and sealed again. Additionally, small manipulations were performed to mimic the effects of putting the plant into the chamber and reconnecting it to the instrumentation. Furthermore, the initial gas concentration gradients were varied to evaluate the applicability of the measured diffusivity ratios under changing chamber gas concentrations. In each leakage experiment, the gas leakage rates of CO_2 and SF_6, J_{CO_2} and J_{SF_6}, were quantified and the respective effective diffusivity ratios calculated (Table 3).

Under all conditions we tested, the measured effective diffusivity ratio of CO_2 to SF_6 was approximately 1.60. Thus, pre-experimental determination of effective diffusivity ratios seems to be stable and therefore expected to be representative for chamber leakage even for conditions with the plant introduced into the chamber.

Experimental Gas Leakage Quantification Method. On the basis of the need for an experimental quantification of effective diffusivity ratios and the robustness of the pre-experimental gas leakage measurements (see above), we propose the following method for online correction of gas

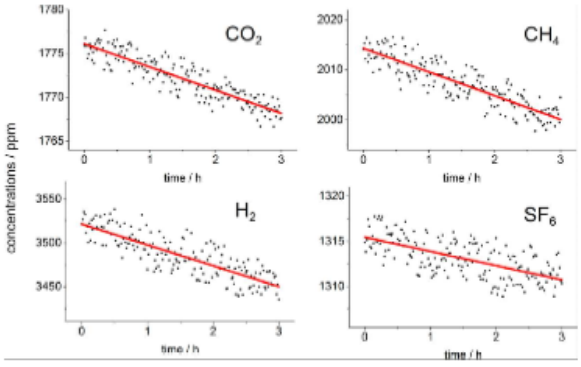

Figure 2. Overview of the concentration decrease of CO_2, CH_4, H_2, and SF_6 due to leakage into the ambient atmosphere. All concentrations are given in parts per million (ppm). The slope of a linear fit (red) onto the concentration dynamics was used to determine the leakage flux J of each compound.

DOI: 10.1021/acs.analchem.5b03312
Anal. Chem. 2015, 87, 11137−11142

Table 3. Results of Five Independent Gas Leakage Experiments with CO_2 and SF_6 under Varying Concentration Gradients $\partial C/\partial x$ (left-hand side, in ppm)[a]

$\partial C/\partial x$ (CO_2)	$\partial C/\partial x$ (SF_6)	J_{CO_2}	J_{SF_6}	D_{CO_2}/D_{SF_6}
2515	2430	−0.49 ± 0.01	−0.29 ± 0.01	1.60 ± 0.09
6910	9250	−1.83 ± 0.04	−1.49 ± 0.02	1.63 ± 0.06
8200	1535	−2.84 ± 0.09	−0.34 ± 0.02	1.58 ± 0.14
7390	7010	−1.77 ± 0.02	−1.05 ± 0.01	1.60 ± 0.03
4305	7670	−0.40 ± 0.02	−0.45 ± 0.02	1.60 ± 0.15

[a]The leakage fluxes for CO_2 and SF_6 (± statistical standard deviation) are displayed in the third and fourth column, respectively. The right-hand column shows the effective diffusivity ratios CO_2/SF_6 for each experiment.

leakage for static environmental chambers: (1) Injection of all relevant experimental gases together with SF_6 into the bare chamber and measurement of the experiment specific gas leakage rates. (2) Calculation of the effective diffusivity ratio of a gas A and SF_6 according to

$$\frac{D_A}{D_{SF_6}} = \frac{J_A}{J_{SF_6}} \frac{C^I_{SF_6} - C^O_{SF_6}}{C^I_A - C^O_A} \quad (7)$$

(3) Performing the environmental chamber experiment with SF_6 as leakage tracer gas. (4) Amendment of the gas exchange rates using the effective diffusivity ratios and the SF_6 leakage rate.

Here, $C^I_{SF_6}$ and $C^O_{SF_6}$ denote the sulfur hexafluoride concentration inside and outside the chamber, respectively.

Leakage during a Carbon Dioxide Exchange Rate Experiment. The SF_6-determined leakage rates were used to estimate the effect of CO_2 leakage on the concentrations observed in the headspace of the sealed chamber containing living plant and soil materials. The carbon dioxide exchange rate (of the chamber atmosphere) can be expressed as

$$CER = \Delta C + J_{CO_2} \quad (8)$$

where ΔC represents the net CO_2 concentration change due to biological processes, e.g., storage, fixation, photosynthesis, or respiration. CO_2 leakage fluxes will depend on the CO_2 concentration gradient with air outside the chamber and can potentially occur in either inward or outward direction. Leakage fluxes out of the chamber are assigned negative values, fluxes into the chamber positive ones.

The plant, together with its soil and root mass, was placed in the previously characterized environmental chamber and the top lid sealed in the same fashion as described above. Afterward, sulfur hexafluoride was manually injected into the chamber headspace, yielding an initial SF_6 concentration of 3115 ppm. The chamber was then exposed to various light regimes (Figure 3). Their effects on the CO_2 exchange rate could be investigated by quantifying the CO_2 and SF_6 concentration changes with time within the chamber using the Raman gas sensor.

Under the relatively low light conditions inside the laboratory, photosynthesis was less than respiration and CO_2 concentrations inside the chamber atmosphere increased from the initial 390 to 1640 ppm after 3 h (stage 1), yielding a net respiration rate of 81.5 μmol per hour. Meanwhile, the SF_6 concentration decreased at a constant rate of −0.54 μmol per hour throughout the experiment, indicating a stable gas leakage behavior. Considering a mean CO_2 concentration gradient of 1015 ppm and the previously determined effective diffusivity ratio CO_2/SF_6 of 1.60, the rate of loss of CO_2 by leakage $J^I_{CO_2}$

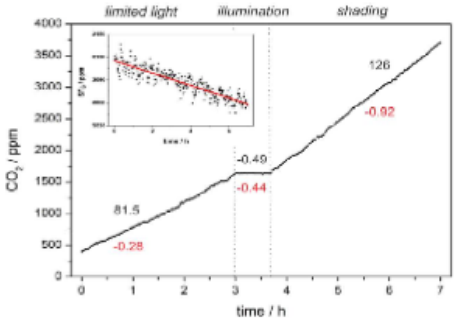

Figure 3. Overview of the chamber CO_2 concentration (black dots), the CER (black digits) and CO_2 leakage rates (red digits) for the three stages of the experiment: limited solar radiation, artificial lighting by plant growth lamps and shading (complete darkness). The rates are given in μmol per hour. The inset shows the constant sulfur hexafluoride leakage rate throughout the experiment; SF_6 concentration indicated by black dots, the linear fit by a red line.

averaged −0.28 μmol per hour in the first stage of the experiment. Following eq 8, the leakage corrected biological net CO_2 concentration change was 81.8 μmol per hour. Compared to the CER, the CO_2 leakage $J^I_{CO_2}$ thus played only a minor role in the first stage of the experiment.

In stage 2 of the experiment (Figure 3), the plant−soil ecosystem was illuminated with a commercial LED plant growth lamp for 45 min. The higher light-enhanced photosynthesis outpaced respiration and resulted in a net CO_2 loss of −0.49 μmol per hour. The CO_2 leakage in this stage with nearly constant CO_2 level (1600 ppm), amounted to −0.44 μmol per hour. Thus, the net CO_2 concentration change attributable to biological processes was only −0.05 μmol per hour, approximately a tenth of the value with no correction for loss of CO_2 by leakage. This demonstrates that quantifying gas leakage rates using SF_6 as tracer gas, which can be acquired by Raman gas spectroscopy, improves the analysis of environmental chamber experiments. Especially in cases with low net gas exchange rates, such as in continuous closed loop monitoring, the precision of the experimentally acquired values can be significantly increased.

In the last stage of the experiment (stage 3), the chamber was placed under shading, i.e., photosynthesis was zero. The CO_2 concentration in the chamber headspace increased at a rate equivalent to a combined flux of 126 μmol per hour (dark respiration). Assuming a mean CO_2 gradient of 3300 ppm between atmosphere and the chamber headspace for this stage

DOI: 10.1021/acs.analchem.5b03312
Anal. Chem. 2015, 87, 11137−11142

of the experiment, the leakage rate $J^3_{CO_2}$ was −0.92 μmol per hour. With this, the biological net CO_2 production can be calculated as 127 μmol per hour. Here, the CO_2 leakage of the chamber is again of minor influence for the determination of an appropriate biological CO_2 exchange rate. Regarding the small deviations of the individually measured diffusivity ratios of CO_2 and SF_6 (see Table 3) and the calculated high R^2 values of the measured gas exchange rates of 0.90 or larger, we assume the reported biological net CO_2 rates to be accurate and estimate the experimental error to be less than 5% of the given value.

CONCLUSION

This study demonstrates the capability of cavity enhanced Raman gas sensing in combination with sulfur hexafluoride for precise quantification of gas leakage in static environmental chamber experiments. By experimental determination of the effective diffusivity ratios of all relevant biogenic gases and the SF_6 tracer, an assessment of chamber gas leakage and its influence on the experimental data is possible. Independent measurements showed that the effective diffusivity ratios are stable under changing concentration gradients and chamber conditions. These effective diffusivity ratios differ significantly from what would be calculated theoretically. A general protocol was proposed for simultaneous online correction of gas leakage for several biogenic gases during static environmental chamber experiments. The high temporal resolution and selectivity of the Raman gas sensor enabled quantifying the CO_2 exchange rates of a *Mirabilis jalapa*−soil ecosystem under changing ambient conditions and amending these rates using the CO_2 leakage at that time, which was calculated by means of the measured SF_6 leakage rate. Even possible temporary changes in leak tightness during an experiment could be corrected online due to the continuous monitoring of all gases including the tracer SF_6. Especially if competing processes such as photosynthesis and respiration are present to a comparable extent, quantifying gas leakage using SF_6 as a tracer and Raman spectroscopy as the sensing technique could improve the analysis of the gas dynamics during environmental chamber experiments.

AUTHOR INFORMATION

Corresponding Author

*T. Frosch. E-mail: torsten.frosch@uni-jena.de, torsten.frosch@gmx.de.

Notes

The authors declare no competing financial interest.

ACKNOWLEDGMENTS

The authors kindly acknowledge the support by the Collaborative Research Center AquaDiva 1076, funded by the German Science Foundation (SFB 1076).

REFERENCES

(1) Flexas, J.; Diaz-Espejo, A.; Berry, J. A.; Cifre, J.; Galmes, J.; Kaldenhoff, R.; Medrano, H.; Ribas-Carbo, M. *J. Exp. Bot.* **2007**, *58*, 1533−1543.

(2) Ghazi, C. J.; Marshall, J. S. *Flow Meas. Instrum.* **2014**, *38*, 72−81.

(3) Cyr, R. R.; Watkins, D. W. *J. Vac. Sci. Technol.* **1975**, *12*, 419−422.

(4) Schmieder, P. J.; Ho, D. T.; Schlosser, P.; Clark, J. F.; Schladow, S. G. *Estuaries Coasts* **2008**, *31*, 1038−1051.

(5) Baker, J. T.; Kim, S. H.; Gitz, D. C.; Timlin, D.; Reddy, V. R. *Environ. Exp. Bot.* **2004**, *51*, 103−110.

(6) Reinders, M. E.; Schutten, J.; Kistemaker, J. *Appl. Sci. Res., Sect. B* **1952**, *2*, 66−70.

(7) Keiner, R.; Herrmann, M.; Kusel, K.; Popp, J.; Frosch, T. *Anal. Chim. Acta* **2015**, *864*, 39−47.

(8) Busenberg, E.; Plummer, L. N. *Geochem., Geophys., Geosyst.* **2010**, *11*, Q11001.

(9) Olschewski, A.; Fischer, U.; Hofer, M.; Schulin, R. *Environ. Sci. Technol.* **1995**, *29*, 264−266.

(10) Wilcock, R. J.; Battino, R.; Wilhelm, E. *J. Chem. Thermodyn.* **1977**, *9*, 111−115.

(11) Upstillgoddard, R. C.; Wilkins, C. S. *Water Res.* **1995**, *29*, 1065−1068.

(12) Dervos, C. T.; Vassiliou, P. *J. Air Waste Manage. Assoc.* **2000**, *50*, 137−141.

(13) Maiss, M.; Brenninkmeijer, C. A. M. *Environ. Sci. Technol.* **1998**, *32*, 3077−3086.

(14) Ho, D. T.; Schlosser, P.; Caplow, T. *Environ. Sci. Technol.* **2002**, *36*, 3234−3241.

(15) Zoellmann, K.; Kinzelbach, W.; Fulda, C. *J. Hydrol.* **2001**, *240*, 187−205.

(16) Wilson, R. D.; Mackay, D. M. *Groundwater* **1993**, *31*, 719−724.

(17) Tobias, C. R.; Bohlke, J. K.; Harvey, J. W.; Busenberg, E. *Limnol. Oceanogr.: Methods* **2009**, *7*, 185−195.

(18) Shorter, J. H.; Mcmanus, J. B.; Kolb, C. E.; Allwine, E. J.; Siverson, R.; Lamb, B. K.; Mosher, B. W.; Harriss, R. C.; Howard, T.; Lott, R. A. *Environ. Sci. Technol.* **1997**, *31*, 2012−2019.

(19) Shapiro, A. M.; Renken, R. A.; Harvey, R. W.; Zygnerski, M. R.; Metge, D. W. *Water Resour. Res.* **2008**, *44*, W08430.

(20) Walvoord, M. A.; Andraski, B. J.; Green, C. T.; Stonestrom, D. A.; Striegl, R. G. *Vadose Zone J.* **2014**, *13*, DOI: 10.2136/vzj2014.04.0045.

(21) von Fischer, J. C.; Butters, G.; Duchateau, P. C.; Thelwell, R. J.; Siller, R. *J. Geophys Res.* **2009**, *114*, DOI: 10.1029/2008JG000731.

(22) Tingey, D. T.; Waschmann, R. S.; Phillips, D. L.; Olszyk, D. M. *Environ. Exp. Bot.* **2000**, *43*, 101−110.

(23) Maiss, M.; Steele, L. P.; Francey, R. J.; Fraser, P. J.; Langenfelds, R. L.; Trivett, N. B. A.; Levin, I. *Atmos. Environ.* **1996**, *30*, 1621−1629.

(24) Upstill-Goddard, R. C.; Watson, A. J.; Liss, P. S.; Liddicoat, M. I. *Tellus, Ser. B* **1990**, *42*, 364−377.

(25) Frosch, T.; Keiner, R.; Michalzik, B.; Fischer, B.; Popp, J. *Anal. Chem.* **2013**, *85*, 1295−1299.

(26) Keiner, R.; Frosch, T.; Hanf, S.; Rusznyak, A.; Akob, D. M.; Kusel, K.; Popp, J. *Anal. Chem.* **2013**, *85*, 8708−8714.

(27) Hanf, S.; Fischer, S.; Hartmann, H.; Keiner, R.; Trumbore, S.; Popp, J.; Frosch, T. *Analyst* **2015**, *140*, 4473−4481.

(28) Baker, J. T.; Allen, L. H.; Boote, K. J.; Pickering, N. B. *Global Change Biol.* **2000**, *6*, 275−286.

(29) Zeebe, R. E.; Wolf-Gladrow, D. *CO_2 in Seawater: Equilibrium, Kinetics, Isotopes*; Elsevier Science: Amsterdam, 2001.

(30) Jost, W. *Diffusion in Solids, Liquids and Gases*; Academic Press: New York, 1952.

(31) Freney, J.; Simpson, J. R. *Gaseous Loss of Nitrogen from Plant-Soil Systems*; Springer: Dordrecht, 1983.

(32) Andrussow, L.; Schramm, B.; Schäfer, K. *Transportphänomene 1: (Viskosität und Diffusion)*; Springer: Berlin, 1969.

(33) Marrero, T. R.; Mason, E. A. *J. Phys. Chem. Ref. Data* **1972**, *1*, 3−118.

(34) Roberts, P. J.; Webster, D. R. *Turbulent diffusion*; ASCE Press: Reston, VA, 2002.

(35) Coward, H. F.; Georgeson, E. H. M. *J. Chem. Soc.* **1937**, 1085−1087.

(36) Jochum, T.; Michalzik, B.; Bachmann, A.; Popp, J.; Frosch, T. *Analyst* **2015**, *140*, 3143−3149.

(37) Keiner, R.; Frosch, T.; Massad, T.; Trumbore, S.; Popp, J. *Analyst* **2014**, *139*, 3879−3884.

(38) King, D. A.; Pittaro, R. J. *Opt. Lett.* **1998**, *23*, 774−776.

(39) Tiemblo, P.; Guzman, J.; Riande, E.; Mijangos, C.; Reinecke, H. *Macromolecules* **2002**, *35*, 420−424.

(40) Pinnau, I.; Toy, L. G. *J. Membr. Sci.* **1996**, *109*, 125−133.

DOI: 10.1021/acs.analchem.5b03312
Anal. Chem. 2015, 87, 11137−11142

6.3 Microbial respiration and natural attenuation of benzene contaminated soils investigated by cavity enhanced Raman multi-gas spectroscopy

Analyst **2015,** *140* (9), 3143-9

Tobias Jochum	concept development
	measurements and data evaluation
	discussion of concept and results
	manuscript preparation and discussion
	(proposed publication equivalents 1.0)
Beate Michalzik	discussion of concept and results
	manuscript preparation and discussion
Anne Bachmann	discussion of concept and results
	(proposed publication equivalents 0.5)
Jürgen Popp	manuscript preparation and discussion
Torsten Frosch	concept development
	discussion of concept and results
	manuscript preparation and discussion

Analyst

PAPER

View Article Online
View Journal | View Issue

Cite this: *Analyst*, 2015, **140**, 3143

Microbial respiration and natural attenuation of benzene contaminated soils investigated by cavity enhanced Raman multi-gas spectroscopy

Tobias Jochum,[a] Beate Michalzik,[b] Anne Bachmann,[a] Jürgen Popp[a,c,d] and Torsten Frosch*[a,c]

Soil and groundwater contamination with benzene can cause serious environmental damage. However, many soil microorganisms are capable to adapt and are known to strongly control the fate of organic contamination. Innovative cavity enhanced Raman multi-gas spectroscopy (CERS) was applied to investigate the short-term response of the soil micro-flora to sudden surface contamination with benzene regarding the temporal variations of gas products and their exchange rates with the adjacent atmosphere. ^{13}C-labeled benzene was spiked on a silty-loamy soil column in order to track and separate the changes in heterotrophic soil respiration – involving $^{12}CO_2$ and O_2 – from the natural attenuation process of benzene degradation to ultimately form $^{13}CO_2$. The respiratory quotient (RQ) decreased from a value 0.98 to 0.46 directly after the spiking and increased again within 33 hours to a value of 0.72. This coincided with the maximum $^{13}CO_2$ concentration rate (0.63 μmol m^{-2} s^{-1}), indicating the highest benzene degradation at 33 hours after the spiking event. The diffusion of benzene in the headspace and the biodegradation into $^{13}CO_2$ were simultaneously monitored and 12 days after the benzene spiking no measurable degradation was detected anymore. The RQ finally returned to a value of 0.96 demonstrating the reestablished aerobic respiration.

Received 15th January 2015,
Accepted 25th February 2015

DOI: 10.1039/c5an00091b

www.rsc.org/analyst

Introduction

Monitored natural attenuation refers "to the reliance on natural attenuation processes (within the context of a carefully controlled and monitored site cleanup approach) to achieve site-specific remediation objectives within a time frame that is reasonable compared to that offered by other more active methods", according to U.S. EPA.[1] Other terms associated with natural attenuation include for instance "intrinsic remediation or bioremediation", "passive bioremediation", "natural recovery", and "natural assimilation". These natural processes are used to reduce the concentration and amount of pollutants in contaminated soils and groundwater, encompassing microbial biodegradation, dispersion, dilution, volatilization and contaminant sorption onto soil solids. As a low cost means compared to thermal and other physico-chemical techniques, natural attenuation has become of widespread interest.[2–4] However, to test the effectiveness of natural attenuation processes and the underlying mechanisms under varying physico-chemical conditions and indigenous microflora, the contamination needs to be carefully monitored through the process.[5,6] Benzene, as an important component of gasoline and a widespread precursor in the chemical industry, is a major organic pollutant in soils and groundwater. Due to its toxicity as a carcinogenic and teratogenic agent, detailed characterization of possible benzene decontamination by microbial remediation processes is required in order to estimate the soil quality and the effectiveness of decontamination. One approach for elucidating the metabolic pathways of this degradation is the quantification of the gas exchange rates between the soil and the atmosphere.

The most commonly used sensing technique for environmental gas analysis is lab-based gas chromatography,[7] usually coupled with mass spectrometry[8] or flame ionization detection.[9] Although highly sensitive and selective, this technique is slow, sample consumptive and limited in terms of mobility. Infrared (IR) absorption spectroscopy methods[10–12] feature very high sensitivities for molecules with a permanent dipole moment, such as carbon dioxide or methane, down to the ppm and ppb range.[13] However, IR based techniques are not

[a]*Leibniz Institute of Photonic Technology, Jena, Germany.*
E-mail: torsten.frosch@uni-jena.de, torsten.frosch@gmx.de; Tel: +49 3641 206221
[b]*Friedrich Schiller University, Institute of Geography, Jena, Germany*
[c]*Friedrich Schiller University, Institute for Physical Chemistry, Jena, Germany*
[d]*Friedrich Schiller University, Abbe Center of Photonics, Jena, Germany*

suitable for the detection of crucial homonuclear atmospheric gases like N_2 or O_2. Particularly, quantifying dioxygen consumption rates is fundamental for calculating the respiratory quotient (RQ) and thus deducing the microbial activity.[14] Raman spectroscopy is an emerging technique,[15–18] based on molecular vibrations,[19–21] and offers the ability for simultaneous and selective multi-gas quantification. Almost all gases and volatiles, except for the noble gases, can be detected and quantified with only a single measurement.[22–24] As a fast, sensitive and non-consumptive technique, Raman spectroscopy promises great potential for onsite environmental gas analysis and process monitoring.[25,26]

Materials and methods

Soil characterization

The sampling of top soil material (0–10 cm depth) was conducted in May 2014 from a grassland plot close to Kammerforst, Hainich-Dün region in the western part of the federal state of Thuringia, central Germany. The climate exhibited an annual precipitation of 750–800 mm and an annual average air temperature of 6.8 °C (44.2 °F). The bedrock consists of Triassic shell limestone covered by a Pleistocene loess layer of variable thickness forming soils classified as Stagnosols and Luvisols.[27] For the determination of the organic carbon (C_{org}) and total nitrogen (TN) content and the soil pH, the air dried samples were sieved through a <2 mm sieve. Soil pH was measured in the supernatant of a 1 : 2.5 mixture of soil and deionized water using a glass electrode (WTW Multi 340i with SenTix41–3 electrode, Weilheim). Oven-dried subsamples for the elemental analysis were homogenized, ground and passed through a 40 μm sieve. The total carbon and nitrogen concentrations were determined by thermal oxidation (Trumac Elementaranalyzer, Leco). After removal of inorganic carbon by repeated washing with 10% hydrogen chloride (HCl), organic carbon was quantified with the same elemental analyzer. The soil texture was determined by laser diffraction particle size analysis (Laser Diffraction Particle Size Analyzer, Beckman Coulter). Table 1 summarizes the soil parameters.

Gas analysis

An innovative Raman gas sensor[28,29] was applied and adapted for the gas measurements reported here. It is based on a miniaturized laser diode ($\lambda_{excitation}$ = 650 nm, 50 mW), which is frequency locked and feedback-coupled to a power buildup cavity[30] to achieve a power enhancement of 5 orders of magnitude. This enhancement enables monitoring of gas concentrations down to approximately 50 ppm within one second. For a direct quantification of the different multi-gas compounds the pressure, temperature and laser intensity were monitored by additional sensors. The setup was calibrated with the relevant gases, namely nitrogen N_2, oxygen O_2, ^{13}C-labeled benzene $^{13}C_6H_6$, and the carbon dioxide isotopes $^{12}CO_2$ and $^{13}CO_2$. Here, pure $^{13}C_6H_6$ was cooled to 7 °C during the calibration to reduce its vapor pressure. By using the Clausius–Clapeyron relationship within the ideal gas approximation at low temperatures,

$$\ln\frac{p_2}{p_1} = \frac{L}{R}\left(\frac{1}{T_1} - \frac{1}{T_2}\right), \quad (1)$$

the gaseous benzene concentration could be directly linked to the Raman signal intensity and hence be calibrated. Here, the two sets p_1, T_1 and p_2, T_2 define the thermodynamic states 1 and 2 by their pressure and temperature, respectively. R is the universal gas constant and L the enthalpy of vaporization, which was assumed to be constant. A least squares fit of the experimental multi-gas spectrum was performed with the complete set of individually calibrated pure reference spectra in the wavenumber range from 500 to 3000 cm^{-1}. This fitting procedure reveals the concentrations of the particular gas components and is more precise than integrating only the specific peak areas. In addition, temperature induced wavenumber shifts were precisely corrected by a custom-made software routine.

Any difference between the measured spectrum and the convoluted calibration spectra also unveils the presence of unexpected, and not calibrated gases. These additional unexpected gases can also be quantified by adding their calibration spectra in the least square fit, which illustrates the versatility of the setup to address not only predetermined gases. All the above-mentioned gases can be distinguished without cross-sensitivity by their individual spectral shifts in the acquired Raman spectrum; an exemplary multi-gas spectrum is depicted in Fig. 1A. The two carbon dioxide isotopes, $^{12}CO_2$ and $^{13}CO_2$, can be distinguished and simultaneously be quantified due to their deviance in the Fermi dyad (Fig. 1B). The calibration data sets were proved in test measurements with defined gas compositions mixed by mass flow controllers. The obtained gas concentrations were normalized for a constant sum of all gas concentrations.

Experimental design

The field-fresh soil was acclimatized to 21 °C in a climate chamber one day before beginning the experiment. 200 g of the soil were filled in a custom-built Plexiglas column (V = 295 cm^3) and sealed airtight with a screw-in lid enclosing a septum (Fig. 2). In order to establish a reproducible gas composition, the soil headspace (V = 98 cm^3) was flushed with synthetic air (20% O_2, 80% N_2, Linde, Germany), precisely controlled by using a mass flow controller (MFC, Brooks Instrument, Germany). During flushing, the gases were quanti-

Table 1 Soil parameters. The top soil was sampled from a grassland plot in the Hainich-Dün region, Thuringia, Germany

Soil texture						
Clay (%)	Silt (%)	Sand (%)	pH (H_2O)	C_{org} (%)	TN (%)	C/N
18.1	81.3	0.6	4.87	2.35	0.221	10.65

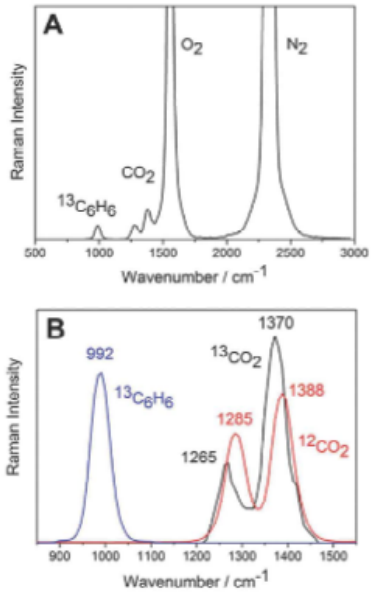

Fig. 1 (A) Example of an experimental multi-gas Raman spectrum ($\lambda_{excitation}$ = 650 nm) during the natural attenuation experiment. Most prominent are the rotation-vibrational bands of N_2 (2331 cm^{-1}) and O_2 (1556 cm^{-1}), both with unresolved O and S branches. The concentrations of the individual components were calculated by least-square fitting the multi-gas spectrum with the particular calibration spectra. (B) Due to their deviance in the Fermi dyad, the two carbon dioxide isotopes $^{12}CO_2$ (red) and $^{13}CO_2$ (black) can be distinguished. Also depicted is the $^{13}C_6H_6$ mode at 992 cm^{-1} (blue).

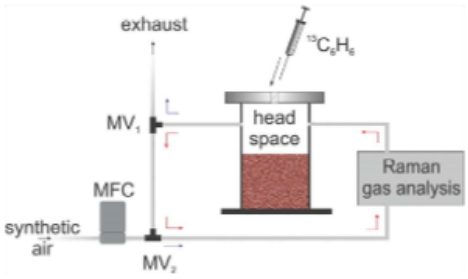

Fig. 2 Schematic diagram of the experimental setup, consisting of mass flow controller (MV), magnetic valves (MV_1 and MV_2), soil mesocosm, and Raman gas analyzer. The gas flow paths during rate measurement and flushing are indicated by red and blue arrows, respectively. All gas rates were determined within the closable inner cycle, comprising the soil column and the Raman gas sensor. Using a syringe, the soil was spiked once with ^{13}C-labeled benzene and the gas exchange was monitored afterwards.

fied and left as exhaust. After a selected time of 150 seconds, the magnetic valves (MV) were switched and the inner circuit with the soil column and the Raman gas sensor was closed. A custom-made LabView routine was used for automatic operation of the MVs, the MFCs, and the Raman gas spectrometer. The current headspace gas composition was permanently monitored by the Raman gas sensor. Due to the aerobic soil respiration (here the carbohydrate model)

$$C_6H_{12}O_6 + 6O_2 \rightarrow 6CO_2 + 6H_2O, \quad (2)$$

the $^{12}CO_2$ concentration in the headspace increased with time.

To avoid any inhibition of this natural process, for instance by back-diffusion into the soil, the $^{12}CO_2$ concentration had to be kept within an environmentally adequate concentration window. Therefore, by reaching a preset $^{12}CO_2$ concentration threshold of 600 ppm, the magnetic valves were switched automatically back to their former state for 150 seconds (feedback control), such that the headspace was flushed with synthetic air again. This eventually reduced the $^{12}CO_2$ concentration in the headspace to approximately 100 ppm and the gas dynamics could be monitored once more afterwards. Using the slope of a linear regression of an individual gas concentration with respect to the time, the respective gas exchange rates could be determined (Fig. 3). Here, each fit was only applied for the first 30 minutes of a period between two flushing events in order to stay within the linear flux regime.[31] The rates were normalized by the column surface area of 19.6 cm^2. The microbial respiratory behavior and the natural attenuation characteristics were confirmed in a follow-up experiment under the same conditions (data not shown).

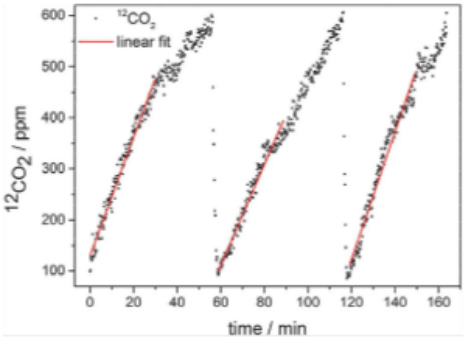

Fig. 3 Exemplary quantification of the $^{12}CO_2$ production rates. The change in concentration (black) with respect to time is linearly fitted (red). The linear regression is limited to the first 30 minutes of each cycle to stay within the linear regime. The slopes of the linear fits yielded the respective $^{12}CO_2$ gas exchange rates. Other gas rates were calculated accordingly. For better visualization, the time scale in this plot starts at zero-time, which does not match the experimental time scale in this case.

Results and discussion

Gas exchange rates

As mentioned above, the gas exchange rates of the bare, undisturbed soil were analyzed at first (indicated as negative time values in Fig. 4). The mean $^{12}CO_2$ concentration rate was 0.72 (±0.01) μmol m^{-2} s^{-1}, while the mean O_2 concentration rate amounted to −0.74 (±0.02) μmol m^{-2} s^{-1}. The respiratory quotient (RQ), defined as the molar ratio of the produced units of CO_2 per consumed unit of O_2, yielded 0.98 (±0.03) on average. This mirrors the case of aerobic soil respiration,[32] where the CO_2 evolution and the O_2 uptake are equimolar (eqn (2)). After measuring several gas exchange rates of the bare soil, the center of the soil surface was spiked with 0.1 ml pure labeled benzene $^{13}C_6H_6$ (Sigma-Aldrich, Germany) using a syringe penetrating the septum (Fig. 2). The syringe was immediately removed after the injection and the septum additionally sealed. Directly after surface spiking, exponential benzene diffusion in the gas phase was observed, different from other models assuming a subsurface contaminant injection.[33] Thus, the first post-spiking rates of CO_2 and O_2 in the gas phase were determined 30 minutes after spiking, such that abrupt non-equilibrium diffusion processes did not interfere with these acquired rates. Benzene was oxidized by the soil microorganisms to carbon dioxide and water *via*[34]

$$^{13}C_6H_6 + 7.5O_2 \rightarrow 6\ ^{13}CO_2 + 3H_2O. \quad (3)$$

Hence, for each mol of degraded benzene $^{13}C_6H_6$, 6 mol of $^{13}CO_2$ were produced. This enabled the calculation of the total amount of degraded benzene by measuring the headspace $^{13}CO_2$ concentration. Directly after the injection of benzene at time zero, a huge microbial response became apparent (Fig. 4). The $^{12}CO_2$ and O_2 concentration rates were remarkably increased up to 1.79 and −3.89 μmol m^{-2} s^{-1}, respectively. This strong response in microbial respiration is assumed to result from a phenomenon known as the "Birch effect"[35,36] describing a rapid release of carbon dioxide from the re-wetted soil material. The spiking resulted in an RQ of 0.46, which corresponds to the reported RQ values of about 0.4 after the addition of hexadecane to agricultural and forest soils.[37] On the one hand, this might be due to the metabolization of those deceased microorganisms,[38] which have been most directly exposed to the spiked benzene (caused by heterotrophic microflora); on the other hand, from microbial stress demanding more energy for cell repair mechanisms.[39] Within the first hours, the two rates dropped rapidly and the oxygen rate reached a minimum of −0.46 μmol m^{-2} s^{-1} 15 hours after

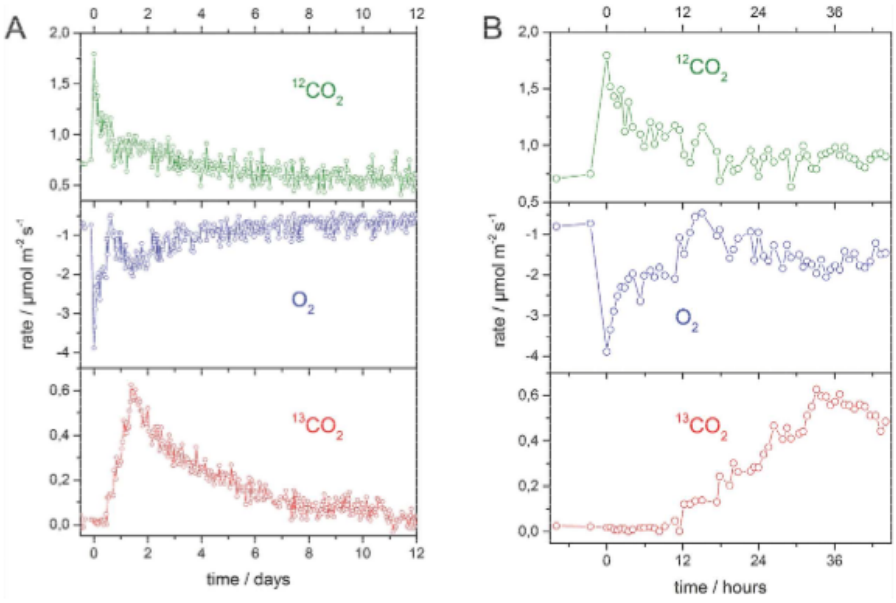

Fig. 4 (A) Evolution of the $^{12}CO_2$ (top), O_2 (center) and $^{13}CO_2$ (bottom) rates. Negative times correspond to the pre-spiking phase. (B) Detailed view onto the first 45 hours of the experiment after spiking.

spiking. During this decrease, both gas rates stabilized approximately from 3.5 to 11.5 hours after spiking; the $^{12}CO_2$ rate at 1.1 μmol m^{-2} s^{-1} and the O_2 rate at −2.0 μmol m^{-2} s^{-1}. However, the $^{13}CO_2$ rate remained unaffected within the first 12 hours, indicating that no measurable degradation of the labeled benzene took place. While the $^{12}CO_2$ rate decreased further after 15 hours, the O_2 rate increased again. This contrast behavior coincided with the emergence of the $^{13}CO_2$ production, demonstrating the initiated degradation of the labeled benzene, which accompanies an increased oxygen demand.

The maximum $^{13}CO_2$ rate of 0.63 μmol m^{-2} s^{-1} was reached 33 hours after spiking. This time corresponds with the reported time windows after application of D-glucose on soils[40] or benzene to pure cultures isolated from soils.[41] On the other hand, the observed 33 hours until maximum degradation was reached, differ from the reported – typically longer – times in cases when benzene[42] or hydrocarbons[43] were thoroughly mixed with the complete soil mass. After 34 hours – about the same time as the $^{13}CO_2$ production rate reached the maximum, – the O_2 consumption rate peaked at −2.06 μmol m^{-2} s^{-1} depicting again the correlation of $^{13}CO_2$ production and O_2 uptake. An RQ of 0.72 was measured at the time of highest $^{13}CO_2$ rates 33 hours after spiking, which is in good agreement with the theoretical RQ of 0.8 during benzene degradation, obtained by the stoichiometric eqn (3). The concentrations of all three gas rates – $^{12}CO_2$, O_2 and $^{13}CO_2$ – decreased continuously during the rest of the experiment. The $^{13}CO_2$ production disappeared 12 days after the spiking event. At the end of the experiment, the mean $^{12}CO_2$ rate amounted to 0.58 (±0.02) μmol m^{-2} s^{-1} and the mean O_2 rate was −0.63 (±0.03) μmol m^{-2} s^{-1}. These rates were slightly lower than the respective pre-spiking rates. This suggests that the microbes perished partly due to the lethal impact of benzene, which then resulted in a lowered overall microbial respiratory activity. A mean RQ of 0.96 (±0.04) was reached 12 days after the spiking event. Thus, the soil returned to the characteristic aerobic respiration following eqn (2).

Benzene fate

The benzene diffusion into the atmosphere was further investigated in order to quantify the degradation process. Utilizing the online multi-gas detection ability provided by the CERS sensor, the headspace concentration of the labeled benzene $^{13}C_6H_6$ was continuously monitored and analyzed. Due to its high vapor pressure (approximately 10.4 kPa at 21 °C)[44] and the direct surface application by the spiking, most of the benzene evaporated and diffused into the headspace. Diffused benzene was calculated by measuring the difference of initial and final concentrations during the flushing events, because of the observed non-linearity of the benzene flux. $^{13}C_6H_6$ diffusion dropped exponentially, which is in good agreement with theoretical calculations.[45] The total amount of diffused benzene is depicted in Fig. 5A. After 4 hours already half of the added benzene passed into the gaseous phase. The strong diffusion ended after almost 6.5 days. By then, 1025 μmol $^{13}C_6H_6$ diffused in total, which corresponds to 91.4% of the spiked mass. The total amount of degraded benzene was calculated by integration of the $^{13}CO_2$ production rates. Because 6 carbon dioxide molecules were produced per consumed benzene molecule, the total amount of degraded $^{13}C_6H_6$ could be directly evaluated (Fig. 5B). After a lag time of 12 hours, $^{13}CO_2$ was monitored in the column headspace, indicating the advent of the degradation process. Approximately 40 μmol $^{13}C_6H_6$ were degraded after 12 days, which was equivalent to 3.6% of the spiked benzene. Thus in total, 95% of the added $^{13}C_6H_6$ found its way into the headspace after 12 days, either by diffusion or degraded into $^{13}CO_2$. Several studies on transport and diffusion of organic compounds in unsaturated soil columns[46,47] suggest that the remainder most likely diffused into subjacent soil layers. These mechanisms will be studied in more detail (*e.g.* under varying benzene concentrations and soil pH) in further experiments.

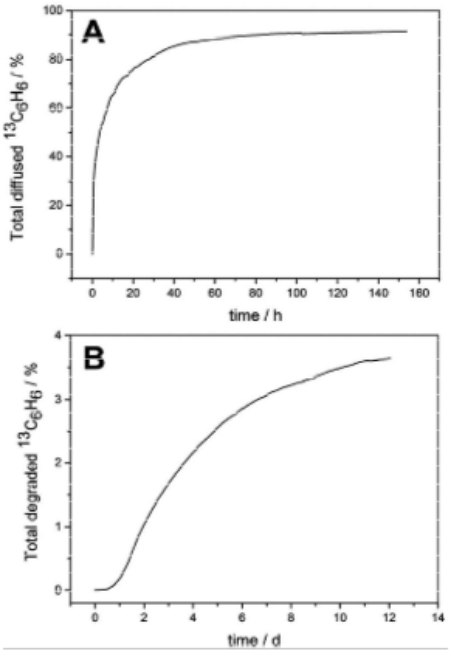

Fig. 5 (A) Diffusion of the spiked benzene from the soil surface into the headspace. (B) Biodegradation dynamics of benzene. The total amount of degraded benzene was calculated by integration of the $^{13}CO_2$ production rates.

Conclusion

In summary, cavity enhanced Raman gas sensing was demonstrated as a supremely versatile technique for online monitor-

ing of multi-gas compositions consisting of $^{12}CO_2$, $^{13}CO_2$, O_2, and $^{13}C_6H_6$ with just one single measurement. The application of CERS is non-consumptive, such that continuous and quantitative gas measurements are feasible, while preventing manipulations of the gas composition. The high temporal resolution and automated design of the Raman gas setup enabled the analysis of rapid gas dynamics and the elucidation of the accompanying chemical processes behind them. In this work, CERS was applied for the quantification of the natural attenuation of ^{13}C-labeled benzene after superficial application on a silty-loamy soil surface, representing sudden contamination events *e.g.* at petrol stations or industrial plants. The impact of benzene spiking on the microbial respiratory activity was investigated. The monitored RQ effectively indicated the subsequent microbial phases: first the aerobic pre-spiking respiration (RQ value of almost 1), the immediate response to the benzene application (with low RQ values and an increased oxygen demand), than the maximum degradation phase (with a RQ of 0.72 close to the theoretical value) and eventually the return to the aerobic respiration again. Considering the unique versatility and selectivity of cavity enhanced Raman gas sensing and its high potential for miniaturization, we foresee that CERS will develop into an important technique for the gas analysis of contaminated soils.

Acknowledgements

The authors kindly acknowledge the support by the Collaborative Research Centre AquaDiva, funded by the German Science Foundation (SFB 1076). We thank Robert Keiner for advice on Raman sensor operation.

Notes and references

1 U. S. EPA, Use of monitored natural attenuation at superfund, RCRA corrective action and underground storage tank sites, OSWER Directive Number 9200.4-17P, Office of Solid Waste and Emergency Response, Washington, DC, 1999.
2 H. Rugner, M. Finkel, A. Kaschl and M. Bittens, *Environ. Sci. Policy*, 2006, **9**, 568–576.
3 M. Tyagi, M. M. R. da Fonseca and C. C. C. R. de Carvalho, *Biodegradation*, 2011, **22**, 231–241.
4 M. Megharaj, B. Ramakrishnan, K. Venkateswarlu, N. Sethunathan and R. Naidu, *Environ. Int.*, 2011, **37**, 1362–1375.
5 C. N. Mulligan and R. N. Yong, *Environ. Int.*, 2004, **30**, 587–601.
6 E. Jindrova, M. Chocova, K. Demnerova and V. Brenner, *Folia Microbiol.*, 2002, **47**, 83–93.
7 B. Michalzik and B. Stadler, *Basic Appl. Ecol.*, 2000, **1**, 117–123.
8 J. F. Pankow, W. Luo, A. N. Melnychenko, K. C. Barsanti, L. M. Isabelle, C. Chen, A. B. Guenther and T. N. Rosenstiel, *Atmos. Meas. Tech.*, 2012, **5**, 345–361.
9 M. Deppe, K. H. Knorr, D. M. McKnight and C. Blodau, *Biogeochemistry*, 2010, **100**, 89–103.
10 O. Heinemeyer, H. Insam, E. A. Kaiser and G. Walenzik, *Plant Soil*, 1989, **116**, 191–195.
11 J. Iqbal, M. J. Castellano and T. B. Parkin, *Global Change Biol.*, 2013, **19**, 327–336.
12 S. Hashimoto, *Soil Biol. Biochem.*, 2002, **34**, 273–275.
13 E. R. Crosson, *Appl. Phys. B: Lasers Opt.*, 2008, **92**, 403–408.
14 A. J. Rixon and B. J. Bridge, *Nature*, 1968, **218**, 261–262.
15 R. A. Halvorson and P. J. Vikesland, *Environ. Sci. Technol.*, 2010, **44**, 7749–7755.
16 T. Frosch, D. Yan and J. Popp, *Anal. Chem.*, 2013, **85**, 6264–6271.
17 T. Frosch, S. Koncarevic, L. Zedler, M. Schmitt, K. Schenzel, K. Becker and J. Popp, *J. Phys. Chem. B*, 2007, **111**, 11047–11056.
18 T. Frosch, T. Meyer, M. Schmitt and J. Popp, *Anal. Chem.*, 2007, **79**, 6159–6166.
19 P. J. Hendra and C. J. Vear, *Analyst*, 1970, **95**, 321–342.
20 T. Frosch and J. Popp, *J. Mol. Struct.*, 2009, **924–926**, 301–308.
21 T. Frosch, S. Koncarevic, K. Becker and J. Popp, *Analyst*, 2009, **134**, 1126–1132.
22 R. Keiner, T. Frosch, S. Hanf, A. Rusznyak, D. M. Akob, K. Kusel and J. Popp, *Anal. Chem.*, 2013, **85**, 8708–8714.
23 S. Hanf, T. Bögözi, R. Keiner, T. Frosch and J. Popp, *Anal. Chem.*, 2015, **87**(2), 982–988.
24 T. Bögözi, J. Popp and T. Frosch, *Bioanalysis*, 2015, **7**(3), 281–284.
25 R. Keiner, M.-C. Gruselle, B. Michalzik, J. Popp and T. Frosch, *Anal. Bioanal. Chem.*, 2015, **407**, 1813–1817.
26 S. Hanf, R. Keiner, D. Yan, J. Popp and T. Frosch, *Anal. Chem.*, 2014, **86**, 5278–5285.
27 IUSS Working Group WRB, in World Soil Resources Reports No. 103, FAO, Rome, 2006.
28 R. Keiner, T. Frosch, T. Massad, S. Trumbore and J. Popp, *Analyst*, 2014, **139**(16), 3879–3884.
29 T. Frosch, R. Keiner, B. Michalzik, B. Fischer and J. Popp, *Anal. Chem.*, 2013, **85**, 1295–1299.
30 D. A. King and R. J. Pittaro, *Opt. Lett.*, 1998, **23**, 774–776.
31 T. Naganawa and K. Kyuma, *Soil Sci. Plant Nutr.*, 1991, **37**, 381–386.
32 F. Mavituna and B. Atkinson, *Biochemical engineering and biotechnology handbook*, Nature Press, New York, NY, 1983.
33 P. Du, M. Sagehashi, A. Terada, S. Zhou, F. S. Li and M. Hosomi, *Soil Sci. Soc. Am. J.*, 2011, **75**, 2147–2157.
34 T. H. Wiedemeier, J. T. Wilson, D. H. Kampbell, R. N. Miller and J. E. Hansen, *Technical Protocol for Implementing Intrinsic Remediation with Long-Term Monitoring for Natural Attenuation of Fuel Contamination Dissolved in Groundwater. Volume II*, DTIC Document, 1995.
35 H. F. Birch, *Nature*, 1958, **182**, 1172.
36 H. F. Birch, *Plant Soil*, 1959, **IX**, 262–286.
37 O. Dilly, S. Nii-Annang, G. Franke, T. Fischer, F. Buegger and A. Zyakun, *Soil Biol. Biochem.*, 2011, **43**, 1808–1811.

38 E. A. Steinhaus and J. M. Birkeland, *J. Bacteriol.*, 1939, **38**, 249–261.
39 F. Scheffer and P. Schachtschabel, *Lehrbuch der Bodenkunde*, Spektrum Akademischer Verlag, Heidelberg, 2010.
40 R. W. O'Dowd and D. W. Hopkins, *Soil Biol. Biochem.*, 1998, **30**, 2009–2016.
41 K. Haider, G. Jagnow, R. Kohnen and S. U. Lim, *Arch. Microbiol.*, 1974, **96**, 183–200.
42 W. X. Zhang and E. J. Bouwer, *Biodegradation*, 1997, **8**, 167–175.
43 E. Lamy, T. C. Tran, S. Mottelet, A. Pauss and O. Schoefs, *Int. Biodeterior. Biodegrad.*, 2013, **83**, 85–91.
44 P. D. Golding and W. D. Machin, *J. Chem. Soc., Faraday Trans. 1*, 1987, **83**, 2719–2726.
45 D. R. Shonnard and R. L. Bell, *Environ. Sci. Technol.*, 1993, **27**, 2909–2913.
46 E. A. Voudrias and C. Y. Li, *J. Hazard. Mater.*, 1993, **34**, 295–311.
47 R. Arands, T. Lam, I. Massry, D. H. Berler, F. J. Muzzio and D. S. Kosson, *Water Resour. Res.*, 1997, **33**, 599–609.

6.4 Direct Raman spectroscopic measurements of biological nitrogen fixation under natural conditions: an analytical approach for studying nitrogenase activity

Anal Chem **2017**, 89 (2), 1117 - 1122

Tobias Jochum	concept development measurements and data evaluation discussion of concept and results manuscript preparation and discussion (proposed publication equivalents 1.0)
Agnes Fastnacht	discussion of concept and results plant cultivation
Susan E. Trumbore	discussion of concept and results manuscript preparation and discussion
Jürgen Popp	manuscript preparation and discussion
Torsten Frosch	concept development discussion of concept and results manuscript preparation and discussion

Reprinted with permission from Jochum, T.; Fastnacht, A..; Trumbore, S. E.; Popp, J.; Frosch, T. Direct Raman spectroscopic measurements of biological nitrogen fixation under natural conditions: an analytical approach for studying nitrogenase activity. *Anal Chem* **2017**, 89 (2), 1117 – 1122.

analytical chemistry

Article

pubs.acs.org/ac

Direct Raman Spectroscopic Measurements of Biological Nitrogen Fixation under Natural Conditions: An Analytical Approach for Studying Nitrogenase Activity

Tobias Jochum,[†] Agnes Fastnacht,[‡] Susan E. Trumbore,[‡] Jürgen Popp,[†,§] and Torsten Frosch*[,†,§]

[†]Leibniz Institute of Photonic Technology, 07745 Jena, Germany

[‡]Max Planck Institute for Biogeochemistry, 07745 Jena, Germany

[§]Institute of Physical Chemistry and Abbe Center of Photonics, 07745 Jena, Germany

Supporting Information

ABSTRACT: Biological N_2 fixation is a major input of bioavailable nitrogen, which represents the most frequent factor limiting the agricultural production throughout the world. Especially, the symbiotic association between legumes and *Rhizobium* bacteria can provide substantial amounts of nitrogen (N) and reduce the need for industrial fertilizers. Despite its importance in the global N cycle, rates of biological nitrogen fixation have proven difficult to quantify. In this work, we propose and demonstrate a simple analytical approach to measure biological N_2 fixation rates directly without a proxy or isotopic labeling. We determined a mean N_2 fixation rate of 78 ± 5 μmol N_2 (g dry weight nodule)$^{-1}$ h^{-1} of a *Medicago sativa*−*Rhizobium* consortium by continuously analyzing the amount of atmospheric N_2 in static environmental chambers with Raman gas spectroscopy. By simultaneously analyzing the CO_2 uptake and photosynthetic plant activity, we think that a minimum CO_2 mixing ratio might be needed for natural N_2 fixation and only used the time interval above this minimum CO_2 mixing ratio for N_2 fixation rate calculations. The proposed approach relies only on noninvasive measurements of the gas phase and, given its simplicity, indicates the potential to estimate biological nitrogen fixation of legume symbioses not only in laboratory experiments. The same methods can presumably also be used to detect N_2 fluxes by denitrification from ecosystems to the atmosphere.

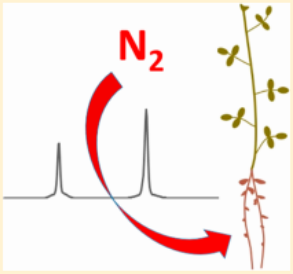

Nitrogen is an essential element for the synthesis of proteins and thus for sustaining life.[1] In the form of dinitrogen gas (N_2), it is abundantly available in the earth's atmosphere, but most organisms are unable to metabolize it.[2] Instead, N_2 needs to be converted to its hydrogenated product ammonia (NH_3) to become usable.[3] This process is known as nitrogen fixation[4] and represents a crucial step in the biogeochemical nitrogen cycle.[5] Only diazotrophs fix N_2 biologically[6] using a nitrogenase enzyme system,[7] which carries out the metabolically expensive reduction of N_2 to ammonia (NH_3) via

$$N_2 + 8e^- + 16ATP + 8H^+ \rightarrow 2NH_3 + H_2 + 16ADP + 16P_i \quad (1)$$

(P_i, inorganic phosphate). The nitrogenase activity is influenced by a variety of environmental factors including moisture, light level, temperature, trace metal availability, or the nitrogen to phosphorus ratio.[8] Despite its importance, environmental and physiological controls of biological nitrogen fixation (BNF) rates are not completely understood.[9] Quantification of N_2 fixation rates at the field level or in real time is difficult,[10] particularly because of the high natural background of N_2.[11] Further progress in technical instrumentation and analytical methods is needed to understand principal factors regulating N_2 fixation and to facilitate its management for the benefit of the environment or agricultural productivity. In this work, a novel analytical approach based on Raman gas spectroscopy is proposed, which enables the determination of biological nitrogen fixation rates without requiring a proxy or an exchange of the natural ecosystem atmosphere. Given its simplicity, the proposed method indicates the potential to open up a new avenue of nitrogen fixation research.

Existing direct methods for quantifying biological nitrogen fixation in plants and soils vary widely. For plants, the N difference method compares total N in N-fixing and non-N-fixing species. However, the N-fixing and the control plants may differ in their capacity to use soil nitrogen if their root morphology or rooting depths differ.[12] If soil mineral N has a different isotopic signature compared to atmospheric N, a mass balance approach can be used to estimate the fraction of plant N from each source (^{15}N natural abundance). This technique is reliable, but typically destructive, and integrates fluxes over long experimental times. Finally, another direct method to estimate BNF rates uses ^{15}N tracer, where N-fixing systems are

Received: August 9, 2016
Accepted: December 12, 2016
Published: December 22, 2016

DOI: 10.1021/acs.analchem.6b03101
Anal. Chem. 2017, 89, 1117−1122

incubated with isotopically enriched $^{15}N_2$ gas followed by the analysis of assimilated ^{15}N in plants or bacteria.[13] The ^{15}N incubation methodology is a highly sensitive and direct measure of nitrogen fixation, but destructive, integrates over time scales of hours (i.e., not real time), and is additionally limited to systems that can be enclosed in a ^{15}N atmosphere. This restricts the ^{15}N incubation method to small-scale laboratory experiments over short time frames.

Other methods to measure N_2 fixation rely on the detection of reaction intermediates or N_2 fixation inhibition. Nitrogenase activity can be measured indirectly by quantifying hydrogen evolution, because H_2 is an obligate byproduct of N_2 fixation (see eq 1), e.g., in legume nodules.[14] But H_2 represents only a portion of the total electron flux through nitrogenase. This necessitates the incubation of investigated nodules in a N_2-free atmosphere to measure the total nitrogenase activity,[15] which is not suitable for many field-based applications. Additionally, the hydrogen evolution technique cannot be applied if hydrogenase enzymes are active in the nodules, which scavenge H_2 produced by the nitrogenase.[16] Another indirect, frequently used method to assess BNF is the acetylene reduction assay (ARA),[17] as it is a simple, relatively inexpensive, and sensitive tool[18] for short-term monitoring of the nitrogenase activity.[19] Acetylene (C_2H_2) competitively inhibits N_2 fixation[20] and is converted to ethylene (C_2H_4) by the nitrogenase enzyme.[21] However, several difficulties arise when ARA is used in quantitative studies, e.g., for estimating the total N_2 fixation of a *Rhizobium*–Leguminosae symbiosis.[22] Acetylene could induce a decline in nitrogenase activity in some legume species as well as in respiration, if N_2 is replaced with argon or helium.[23] Further, the conversion ratio of reduced C_2H_2 to fixed N_2 is highly variable[24] and often differs from theoretical biochemical calculations.[25] This is especially the case when alternative vanadium- or iron-type nitrogenases are active besides the canonical molybdenum-type nitrogenase.[26]

In this work, we propose and demonstrate a novel approach for measuring biological nitrogen fixation by plant–diazotrophic bacteria symbioses. The nitrogenase activity is quantified by continuous spectral monitoring of the gaseous $^{14}N_2$ concentration in environmental chambers housing alfalfa plants (*Medicago sativa* L.). Here, the amount of N_2 in the chamber headspace is monitored by Raman gas spectroscopy.[27] This approach offers several benefits; it is sensitive, nonconsumptive, does not require nonfixing reference plants, additionally injected gases, or isotopic labeling, and allows for continuous detection of the nitrogen fixation dynamics at ambient N_2 levels. We report on the first biological nitrogen fixation rate estimates derived by optical spectroscopy of N_2 and discuss potential limitations and expansions of the presented method as a prelude to future investigations.

MATERIALS AND METHODS

Plant Growth. When it comes to agricultural nitrogen fixation inputs, most attention is directed toward legumes, because of their proven ability to fix N_2 symbiotically in tropical and temperate environments.[28] The plant we selected, the perennial legume *M. sativa*, takes a large fraction of its nitrogen from N_2 fixation (up to 100% when grown in a mixture with grasses).[29] *M. sativa* seed (Feldsaaten Freudenberger, Germany) was grown in plastic pots on N- and C-free quartz sand under controlled greenhouse conditions of 25/20 ± 1 °C (day/night, each 12 h). During cloudy or rainy days, natural sunlight was supplemented with sodium vapor lamps (400 W Gro-Lux, Osram Sylvania Ltd., U.S.A.) providing a minimum photosynthetic photon flux density (PPFD) of 400–500 μmol m^{-2} s^{-1}. Plants were inoculated with a commercial *Rhizobium* inoculant (RhizoFix, Feldsaaten Freudenberger, Germany) according to the manufacturers' instructions. The pots were fertilized weekly with a Hoagland solution[30] lacking ammonium nitrate (NH_4NO_3), forcing the plants to rely on symbiotic N_2 fixation as a source for nitrogen.[31] The inoculation led to effective nodulation, while noninoculated controls died due to N starvation. After the N_2 fixation measurements, nodules were detached and dried to a constant weight at 60 °C. Biological N_2 fixation rates were calculated on a nodule dry weight basis.

Experimental Design. N_2 fixation was measured in a laboratory chamber system with an internal volume of 3.0 L (Figure 1). The cylindrical plant chamber consists of acrylic glass and is connected to a pump and the Raman gas analyzer via polyurethane tubes. Different chamber volumes or geometries are also feasible, as long as they provide enough space for internal sensors and tube ports. Before the gas measurements, the quartz sand was carefully removed from the plants. In each measurement run (samples 1–5) several alfalfa plants were grouped and measured together. After introducing the undisturbed alfalfa plants including roots and nodules into the chamber, the headspace air was monitored continuously in a static mode. By using whole plants in just one compartment, the total gas exchange of the plant can be quantified. Elevated CO_2 levels are avoided because of the active leaf photosynthesis. Thus, a potential physiological influence of enhanced CO_2 levels on the specific nitrogenase activity of legume nodules,[32] which is still under discussion,[33,34] does not affect our measurements. However, significantly decreased CO_2 concentrations, and thus low photosynthetic activity, seem to have an effect on biological N_2 fixation. We considered this by incorporating a lower CO_2 threshold for BNF calculation; see the discussion in the following section.

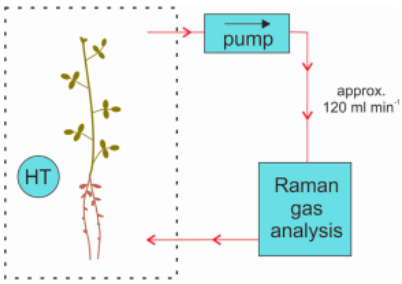

Figure 1. Schematic sketch of the experimental setup for continuous N_2 monitoring. Gases from the plant chamber are pumped to the Raman gas analyzer, measured, and returned to the chamber without change or consumption. The air humidity and temperature are recorded by an internal sensor (HT).

A diaphragm pump circulated air with a constant flow rate of ~120 mL min^{-1} from the plant compartment to the Raman gas analyzer and back. To measure the partial pressure of water vapor, a humidity and temperature sensor (model UFT75-AT, Sensor-Tec, Germany) was installed. As ambient air was used as initial plant atmosphere, no equilibration time for homogeneous gas mixing within the system is necessary and possible changes of the gas composition can be directly observed after

DOI: 10.1021/acs.analchem.6b03101
Anal. Chem. 2017, 89, 1117–1122

closing the chamber. Separate test measurements showed no detectable inherent N_2 leakage into the chamber system within typical experimental times of up to several hours. This illustrates on the one hand the airtight chamber design. On the other hand, N_2 leakage is additionally hindered by very low concentration gradients between the natural atmospheric background and the N_2 level inside the chamber system. The plant chamber was illuminated by a horticulture LED lamp (model M30, SANlight, Austria) providing a photosynthetic photon flux density of ~150 μmol m^{-2} s^{-1}. All experiments were performed in a controlled growth cabinet at ~25 °C.

For testing our method, we used five individual measurements. After introducing the complete plant with root and attached nodules, the chamber was closed and the headspace gases continuously analyzed by Raman gas spectroscopy. A spectrum was recorded every 10 s.

Raman Gas Analysis. Although gas chromatography (GC) coupled to various detector types is a very sensitive technique to quantify N_2,[35] it does not provide as high temporal resolution as Raman gas spectroscopy and also operates sample destructively. In most applications, N_2 exchange rates cannot be measured by GC techniques due to the high natural N_2 background concentration.[36] Thus, we applied Raman gas spectroscopy[37−39] for monitoring biological N_2 fixation. In Raman gas spectroscopy, the scattered light from gas molecules interacting with a laser contains information about their molecular structure and abundance.[40,41] Hence, analyzing this scattered light enables molecule identification and quantification.[42−45] The in-house built Raman gas analyzer (λ_{laser} = 650 nm, P_{laser} = 50 mW, spectral resolution ~50 cm^{-1}), which uses an optical cavity to enhance the laser intensity, has been described previously.[46−49] Briefly, mixing ratios are measured by analyzing the Raman light originating from gas molecules passing the optical cavity (volume ~4 cm^3) at atmospheric pressure. For the investigated gases, the instrument provides a measurement range from ~200 ppm (limit of detection, LOD) up to 100%. Investigated gases do not undergo any pretreatment and are not altered during the measurement procedure. Internal sensors record the current gas pressure and temperature in the cavity, which enables the calculation of partial pressures and absolute molecule numbers of the analyzed gases.

The instrument was calibrated with spectra of pure reference gases (N_2, O_2, and CO_2, Linde, Germany), which were measured individually and built the basis set for the data analysis. First, the spectral background was corrected by subtraction of a spectrum of the Raman-inactive noble gas argon. Second, the measured spectra were normalized by the current intracavity pressure and laser intensity. In the third step, a multiple linear regression was applied to predict weighting coefficients for N_2, O_2, and CO_2. Experimental spectra comprising a mixture of spectral features can then be expressed as a sum of the basis set spectra, where the weighting coefficients of each basis spectrum are proportional to the mixing ratios of that species (Figure S1). This strategy[50] allows for simultaneous quantification of several constituents in a gas mixture while minimizing cross interferences.[51] The robustness of this spectral data analysis was tested with reference gases comprising N_2, O_2, CO_2, and Ar at various mixing ratios close to experimental compositions. Reference gases were created using mass flow controllers (model GF80, Brooks Instrument, U.S.A.), which were calibrated using a primary standard air flow calibrator (model Gilibrator II, Sensidyne, U.S.A.). From these test measurements, a relative accuracy of about 1% was determined for the range of relevant N_2 mixing ratios (v/v), i.e., mixing ratios between (70 ± 0.7)% and (80 ± 0.8)% (Figure S2). The relative accuracy of O_2 was also 1% for mixing ratios (v/v) between 16% and 23%. Additional tests comparing measured CO_2 mixing ratios of prepared reference gases by the Raman instrument with a nondispersive infrared (NDIR) analyzer (model LI-840A, LI-COR Biosciences, U.S.A.) indicated a relative accuracy of the CO_2 mixing ratio of ~1% for CO_2 mixing ratios from 0 to 1500 ppm (v/v).

Water Vapor and Absolute Gas Quantity Calculation. In contrast to absorption spectroscopy techniques, water vapor yields only a weak Raman signal, which does not interfere with the main spectral features of N_2, O_2, and CO_2 (Q branches at 2331 and 1556 cm^{-1} for N_2 and O_2, respectively, as well as the Fermi dyad of CO_2 at 1388 and 1285 cm^{-1}). Thus, no water vapor correction was necessary, which was experimentally confirmed in separate tests. However, we monitored water vapor levels to avoid measurements under dry conditions, which might affect nitrogen fixation. The partial pressure of water vapor, p_{H_2O}, was quantified using the Antoine equation. The relative humidity ϕ in the environmental chamber is measured by the humidity sensor and converted to the water vapor partial pressure as

$$\log_{10} p_{H_2O}^{eq} = A - \frac{B}{C + T} \tag{2}$$

with temperature T in Celsius, $p_{H_2O}^{eq}$ the equilibrium water vapor pressure (mmHg) at that temperature, and the coefficients A = 8.05573, B = 1723.6425, and C = 233.08.[52] The current water vapor partial pressure p_{H_2O} is then given by the product of the relative humidity and the equilibrium water vapor pressure:

$$p_{H_2O} = \phi p_{H_2O}^{eq} \tag{3}$$

Determined p_{H_2O} values were validated in separate test measurements beforehand using the NDIR analyzer, indicating a relative accuracy for p_{H_2O} of ~1.8%.

The applied gas analysis strategy provides measurement data in units of the dimensionless volume mixing ratio χ_i (in 10^{-6} = ppm) of the corresponding gas species i. But for the calculation of release or consumption rates J_i (e.g., in mol g_{dw}^{-1} s^{-1} or g g_{dw}^{-1} s^{-1}), absolute quantities such as the amount of substance (in moles) or the mass (in grams) have to be used. Following ideal gas laws and Dalton's law, we determined the amount of substance n_i of the gas species i by

$$n_i = \frac{\chi_i PV}{RT} \tag{4}$$

with χ_i being the volume mixing ratio, P the total barometric pressure (hPa), V the system volume (m^3), R the universal gas constant (8.314 × 10^{-2} m^3 hPa K^{-1} mol^{-1}), and T the current air temperature (K) of the chamber headspace. By multiplication with the molar mass M_i (g mol^{-1}) of the corresponding gas species i (28.014 for N_2, 31.999 for O_2, and 44.010 for CO_2), the mass m_i was calculated as

$$m_i = n_i M_i \tag{5}$$

The calculated mixing ratios refer to humid air, as the total barometric pressure P includes water vapor. Using absolute quantities instead of volume mixing ratios was of particular importance, as varying water vapor levels during our experi-

DOI: 10.1021/acs.analchem.6b03101
Anal. Chem. 2017, 89, 1117−1122

ments caused a significant dilution of the other gases. Relative humidity levels of up to 85−95% were observed during the chamber measurements, which correspond to water vapor partial pressures of almost 30 hPa.

RESULTS AND DISCUSSION

For calculation of the N_2 fixation rates, we first determined what time interval was suitable, based on our monitoring of plant photosynthetic activity and CO_2 uptake. Then, a linear regression (ANOVA, analysis of variance) was performed onto the temporal evolution of n_{N2}, the amount of N_2 in the chamber. This is exemplarily illustrated in Figure 2, which

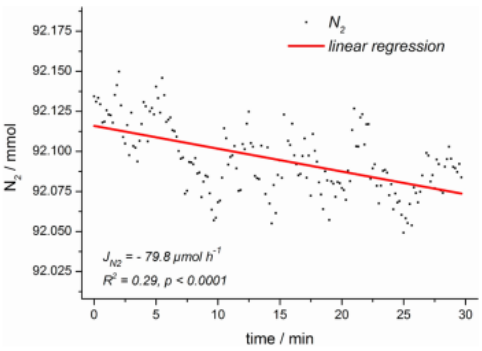

Figure 2. N_2 fixation rate calculation. The slope of a linear regression onto the amount of N_2 in the chamber atmosphere yields the N_2 fixation rate (μmol h^{-1}). The length of the respective time interval is defined by the CO_2 level. Data from sample 5 is depicted exemplarily for all alfalfa samples.

shows data from one of the analyzed *M. sativa* plants. The slope of the linear regression yields the biological N_2 fixation rate (here in micromoles of N_2 per hour). A negative rate means a decrease of N_2 in the chamber headspace, i.e., a biological uptake. The linear regression appears to be superimposed by a periodic fluctuation, which was most likely caused by a technical temperature feedback loop in the experimental setup. However, very low p values in each replicate measurement indicate a statistically significant correlation of the amount of N_2 in the headspace and time, i.e., biological N_2 fixation. Future technical improvements will help to decrease the temperature related fluctuations and, thus, the uncertainty of the linear approximation. Finally, the obtained rate was normalized to the nodule dry weight to account for differences between individual plants.

Photosynthetic Activity and CO_2 Uptake. N_2 fixation requires large amounts of energy (see eq 1), and thus rates of N_2 fixation may be affected by the rate of supply of C to mutualist bacteria by the plant. Although increasing leaf photosynthesis does not enhance the specific nitrogenase activity,[53] carbohydrate availability and especially bacterial carbon utilization within the nodule seem to play a role in regulating N_2 fixation.[54] Mobilization of reserve energy substrates by leguminous plants appears to have only a minor role, and readily available assimilates tend to be rapidly exhausted (within minutes).[55] Thus, when investigating N_2 fixation in legumes such as *M. sativa*, monitoring of the photosynthetic activity by analyzing current O_2 and CO_2 levels provides supplementary information about the relative effectiveness of biological N_2 fixation.

The five individual alfalfa plant replicates used in our experiments always showed net consumption of CO_2 and production of O_2, indicating that leaf net photosynthesis dominated root and nodule respiration fluxes (Table 1). The rate of net CO_2 consumption was initially generally constant (p values always less than 0.0001), until CO_2 mixing ratios had declined to ~200−150 ppm (v/v), see Figure 3. Once CO_2

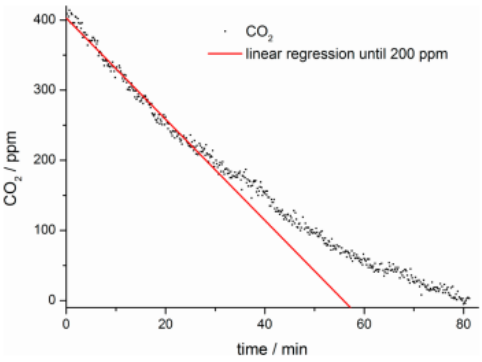

Figure 3. CO_2 uptake rate quantification. In general, CO_2 decreases linearly until a threshold of ~150−200 ppm (v/v). Below this threshold a slower CO_2 decrease along with a reduced N_2 fixation was observed. Thus, we defined the time until ~200 ppm (v/v) CO_2 is reached as the analysis time, the time interval for rate calculations of N_2, O_2, and CO_2. Data originates from sample 5.

levels dropped below ~150 ppm (v/v), the rate of decline in CO_2 levels generally slowed, suggesting a change in the balance of photosynthesis and respiration and/or nodule CO_2 fixation mechanisms. In that phase, the rate of N_2 fixation also declined,

Table 1. Overview of the Nodule Biomass, Analysis Time, Total Plant CO_2 Uptake, and O_2 Release of the Individual Alfalfa Samples[a]

sample	nodule biomass (g)	analysis time (min)	plant CO_2 uptake (μmol CO_2 h^{-1})	O_2 release (μmol O_2 h^{-1})
1	0.38	148	14.7 (0.1)	14.1 (1.8)
2	0.52	54	14.4 (0.5)	12.5 (3.9)
3	0.40	202	27.1 (0.1)	14.4 (1.0)
4	0.53	77	33.5 (0.5)	29.7 (3.8)
5	1.04	30	79.8 (9.2)	53.6 (8.8)

[a]Data in parentheses shows the respective standard deviation. The gas rates indicate a dominant photosynthesis but also a significant contribution of nodule CO_2 fixation.

DOI: 10.1021/acs.analchem.6b03101
Anal. Chem. 2017, 89, 1117−1122

in a few cases even ceasing at low CO_2 concentrations. Although this behavior needs to be investigated in much more detail in future experiments, it suggests that very low CO_2 levels could limit symbiotic N_2 fixation.

To improve the comparability of measured N_2 fixation rates, we thus defined a time period based on the interval when CO_2 data declined at a constant rate, and the reported N_2 fixation rates were determined only during this time interval. We selected the time window from closing the chamber (ambient CO_2 levels) until reaching a CO_2 mixing ratio of ~200 ppm (v/v) for the calculation of the CO_2 uptake, O_2 release, and N_2 fixation rate. The time until this CO_2 threshold was reached, defined here as the analysis time, depended on the biomass (leaves, stem, roots, and nodules) inside the chamber and varied between 30 min (sample 5) and almost 3.5 h (sample 3). Figure 3 illustrates the time window selection and CO_2 rate quantification, exemplarily for sample 1.

CO_2 uptake rates of the total plant are strongly correlated with O_2 release rates (correlation coefficient of 0.97). However, O_2 release rates are generally lower than CO_2 uptake rates, suggesting that nodule CO_2 fixation contributes significantly to the total CO_2 consumption of the plant. Nodule CO_2 fixation is known to be tightly coupled to N_2 fixation, e.g., shown by the concomitant expression of phosphoenolpyruvate carboxylase (PEPC) in nodules and emerging nitrogenase activity.[56]

Biological N_2 Fixation Rates of *M. sativa*. Measured N_2 fixation rates (Table 2), normalized to the nodule biomass, ranged from 70 to 85 μmol N_2 (g dry weight nodule)$^{-1}$ h^{-1}, which corresponds to 47–57 mg N (g dry weight nodule)$^{-1}$ day^{-1}. These rates show no trend when compared to the nodule biomass, which indicates that in each measurement the majority of the nodules were actively fixing N_2. Further, the N_2 fixation rates do not correlate with the analysis time (correlation coefficient of 0.14). All determined rates are statistically significant ($p < 0.0001$); also the shortest analysis time of approximately half an hour yielded statistically robust data (Figure 2). Thus, the proposed N_2 fixation rate quantification is applicable to short-term measurements from 30 min up to several hours without introducing artifacts due to the static environmental chamber design.

The mean N_2 fixation rate yields 78 ± 5 μmol N_2 (g dry weight nodule)$^{-1}$ h^{-1} or 52 ± 3 mg N (g dry weight nodule)$^{-1}$ day^{-1}. These rates are within the range of reported values from biological nitrogen fixation studies with alfalfa and other legumes using the $^{15}N_2$ incubation[57,58] or the H_2 evolution[59] technique. A direct comparison of measured N_2 fixation rates by the Raman analyzer and another technique is not feasible, as to our best knowledge, there is no comparable method capable of simultaneously quantifying N_2 dynamics and photosynthetic activity directly, with similar temporal resolution and in view of the high N_2 background.

It should be noted that the proposed analytical approach quantifies the net N_2 decrease within a chamber atmosphere. While this method also indicates the potential to be applied in the field, or for plants together with soil, other processes, including relevant denitrification processes, may affect the measured flux, e.g., by releasing N_2. Thus, careful experimental design is crucial when applying the proposed method. In this study, we ensured this by inoculation with selected *Rhizobium* strains and the absence of soil microorganisms, which could have had a potential denitrification capability. To improve its applicability, the reported approach might also be compared directly to common techniques such as ^{15}N isotopic methods, ARA, or H_2 evolution. For this, measured nitrogen fixation estimates from the mentioned techniques and the Raman gas analysis should be determined for the same ecosystem and, in the case of ARA and H_2 evolution, a conversion factor derived. We envisage these comparison measurements in future experiments.

Table 2. Raman Gas Spectroscopy Measurements of the N_2 Fixation of *M. sativa* Inoculated with Rhizobium[a]

	N_2 fixation	
sample	μmol N_2 g_{dw}^{-1} h^{-1}	mg N g_{dw}^{-1} day^{-1}
1	70 (15)	47 (10)
2	77 (16)	52 (11)
3	80 (9)	54 (6)
4	85 (18)	57 (12)
5	77 (9)	52 (6)
mean	78 (5)	52 (3)

[a]N_2 fixation rates are given in μmol N_2 (g dry weight nodule)$^{-1}$ h^{-1} (second column) and mg N (g dry weight nodule)$^{-1}$ day^{-1} (third column). Data in parentheses indicates the respective standard deviation.

CONCLUSION

The analytical approach presented in this study using Raman gas spectroscopy and the natural atmospheric gas composition provides accurate determinations of the N_2 fixation capability of alfalfa plants that are comparable to results obtained using other techniques. As cavity Raman gas analyzers get more popular and offer high potential for miniaturization and cost reduction,[60] we envisage a significant decrease in analysis costs compared to standard methods using gas chromatography or N_2 isotopes. The proposed method simplifies and develops biological nitrogen fixation measurements by (1) using ambient N_2 as a direct indicator for BNF, (2) operating non-consumptive, (3) depending on no external isotopes or other gases, and (4) eliminating the need for nonfixing reference plants. Moreover, Raman gas spectroscopy has also the capability to measure O_2 and CO_2 dynamics simultaneously. This may open new research avenues in nitrogen cycling processes, such as interactions of N_2 fixation and respiration, photosynthesis, or CO_2 fixation mechanisms. Application of this novel technique will assist with the determination of biological nitrogen fixation rates and nitrogenase activity in legume–diazotroph symbioses and potentially increase the knowledge of the physiology of nitrogen fixation.

ASSOCIATED CONTENT

Supporting Information

The Supporting Information is available free of charge on the ACS Publications website at DOI: 10.1021/acs.analchem.6b03101.

Decomposition of a measured multigas spectrum into its components, and comparison of the N_2 reference mixing ratios and predicted mixing ratios by the Raman analysis (PDF)

AUTHOR INFORMATION

Corresponding Author

*E-mail: torsten.frosch@uni-jena.de; torsten.frosch@gmx.de.

DOI: 10.1021/acs.analchem.6b03101
Anal. Chem. 2017, 89, 1117–1122

ORCID

Torsten Frosch: 0000-0003-3358-8878

Notes

The authors declare no competing financial interest.

■ ACKNOWLEDGMENTS

The work has been funded by the Deutsche Forschungsgemeinschaft (DFG) CRC 1076 "AquaDiva". We thank Gabriela Pereyra from the Max Planck Institute for Biogeochemistry for her helpful advice in plant cultivation.

■ REFERENCES

(1) Canfield, D. E.; Glazer, A. N.; Falkowski, P. G. *Science* **2010**, *330*, 192−196.
(2) Cheng, Q. *J. Integr. Plant Biol.* **2008**, *50*, 786−798.
(3) Jia, H.-P.; Quadrelli, E. A. *Chem. Soc. Rev.* **2014**, *43*, 547−564.
(4) Cleveland, C. C.; Townsend, A. R.; Schimel, D. S.; Fisher, H.; Howarth, R. W.; Hedin, L. O.; Perakis, S. S.; Latty, E. F.; Von Fischer, J. C.; Elseroad, A.; Wasson, M. F. *Global Biogeochem Cy* **1999**, *13*, 623−645.
(5) Gruber, N.; Galloway, J. N. *Nature* **2008**, *451*, 293−296.
(6) Raymond, J.; Siefert, J. L.; Staples, C. R.; Blankenship, R. E. *Mol. Biol. Evol.* **2004**, *21*, 541−554.
(7) Hoffman, B. M.; Lukoyanov, D.; Yang, Z. Y.; Dean, D. R.; Seefeldt, L. C. *Chem. Rev.* **2014**, *114*, 4041−4062.
(8) Vitousek, P. M.; Cassman, K.; Cleveland, C.; Crews, T.; Field, C. B.; Grimm, N. B.; Howarth, R. W.; Marino, R.; Martinelli, L.; Rastetter, E. B.; Sprent, J. I. *Biogeochemistry* **2002**, *57*, 1−45.
(9) Unkovich, M. *New Phytol.* **2013**, *198*, 643−646.
(10) Cassar, N.; Bellenger, J. P.; Jackson, R. B.; Karr, J.; Barnett, B. A. *Oecologia* **2012**, *168*, 335−342.
(11) Davidson, E. A.; Seitzinger, S. *Ecol Appl.* **2006**, *16*, 2057−2063.
(12) Chalk, P. M. *Aust. J. Agric. Res.* **1998**, *49*, 303−316.
(13) Warembourg, F. R.; Montange, D.; Bardin, R. *Physiol. Plant.* **1982**, *56*, 46−55.
(14) Schubert, K. R.; Evans, H. J. *Proc. Natl. Acad. Sci. U. S. A.* **1976**, *73*, 1207−1211.
(15) Hunt, S.; Layzell, D. B. *Annu. Rev. Plant Physiol. Plant Mol. Biol.* **1993**, *44*, 483−511.
(16) Robson, R. L.; Postgate, J. R. *Annu. Rev. Microbiol.* **1980**, *34*, 183−207.
(17) Pinto-Tomas, A. A.; Anderson, M. A.; Suen, G.; Stevenson, D. M.; Chu, F. S. T.; Cleland, W. W.; Weimer, P. J.; Currie, C. R. *Science* **2009**, *326*, 1120−1123.
(18) Anthraper, A.; DuBois, J. D. *Am. J. Bot.* **2003**, *90*, 683−692.
(19) Hara, S.; Hashidoko, Y.; Desyatkin, R. V.; Hatano, R.; Tahara, S. *Appl. Environ. Microb* **2009**, *75*, 2811−2819.
(20) Schöllhorn, R.; Burris, R. H. *Proc. Natl. Acad. Sci. U. S. A.* **1967**, *58*, 213−216.
(21) Hardy, R. W.; Holsten, R.; Jackson, E.; Burns, R. *Plant Physiol.* **1968**, *43*, 1185−1207.
(22) Mårtensson, A.; Ljunggren, H. *Plant Soil* **1984**, *81*, 177−184.
(23) Minchin, F. R.; Witty, J. F.; Sheehy, J. E.; Muller, M. *J. Exp. Bot.* **1983**, *34*, 641−649.
(24) Hardy, R. W. F.; Burns, R. C.; Holsten, R. D. *Soil Biol. Biochem.* **1973**, *5*, 47−81.
(25) Seitzinger, S. P.; Garber, J. H. *Mar. Ecol.: Prog. Ser.* **1987**, *37*, 65−73.
(26) Bellenger, J.; Xu, Y.; Zhang, X.; Morel, F.; Kraepiel, A. *Soil Biol. Biochem.* **2014**, *69*, 413−420.
(27) Weber, A. *Raman Spectroscopy of Gases and Liquids*; Springer Science and Business Media: Berlin, Heidelberg, Germany, 2012; Vol. *11*.
(28) Peoples, M.; Herridge, D.; Ladha, J. *Plant Soil* **1995**, *174*, 3−28.
(29) Carlsson, G.; Huss-Danell, K. *Plant Soil* **2003**, *253*, 353−372.
(30) Hoagland, D. R.; Arnon, D. I. *The Water-Culture Method for Growing Plants without Soil*: Agricultural Experiment Station: Berkley, CA, 1950; Vol. *347*.
(31) Pereyra, G.; Hartmann, H.; Michalzik, B.; Ziegler, W.; Trumbore, S. *Forests* **2015**, *6*, 3686−3703.
(32) Phillips, D. A.; Newell, K. D.; Hassell, S. A.; Felling, C. E. *Am. J. Bot.* **1976**, *63*, 356−362.
(33) Cabrerizo, P. M.; Gonzalez, E. M.; Aparicio-Tejo, P. M.; Arrese-Igor, C. *Physiol. Plant.* **2001**, *113*, 33−40.
(34) Fischinger, S. A.; Hristozkova, M.; Mainassara, Z. A.; Schulze, J. *J. Exp. Bot.* **2010**, *61*, 121−130.
(35) Cardenas, L. M.; Hawkins, J. M. B.; Chadwick, D.; Scholefield, D. *Soil Biol. Biochem.* **2003**, *35*, 867−870.
(36) Wang, R.; Willibald, G.; Feng, Q.; Zheng, X.; Liao, T.; Brüggemann, N.; Butterbach-Bahl, K. *Environ. Sci. Technol.* **2011**, *45*, 6066−6072.
(37) Jochum, T.; Michalzik, B.; Bachmann, A.; Popp, J.; Frosch, T. *Analyst* **2015**, *140*, 3143−3149.
(38) Keiner, R.; Herrmann, M.; Kuesel, K.; Popp, J.; Frosch, T. *Anal. Chim. Acta* **2015**, *864*, 39−47.
(39) Keiner, R.; Frosch, T.; Massad, T.; Trumbore, S.; Popp, J. *Analyst* **2014**, *139*, 3879−3884.
(40) Frosch, T.; Popp, J. *J. Mol. Struct.* **2009**, *924*−*926*, 301−308.
(41) Frosch, T.; Popp, J. *J. Biomed. Opt.* **2010**, *15*, 041516.
(42) Salter, R.; Chu, J.; Hippler, M. *Analyst* **2012**, *137*, 4669−4676.
(43) Kiefer, J.; Seeger, T.; Steuer, S.; Schorsch, S.; Weikl, M.; Leipertz, A. *Meas. Sci. Technol.* **2008**, *19*, 085408.
(44) Keiner, R.; Gruselle, M. C.; Michalzik, B.; Popp, J.; Frosch, T. *Anal. Bioanal. Chem.* **2015**, *407*, 1813−1817.
(45) Jochum, T.; Rahal, L.; Suckert, R. J.; Popp, J.; Frosch, T. *Analyst* **2016**, *141*, 2023−2029.
(46) Frosch, T.; Keiner, R.; Michalzik, B.; Fischer, B.; Popp, J. *Anal. Chem.* **2013**, *85*, 1295−1299.
(47) Jochum, T.; von Fischer, J. C.; Trumbore, S.; Popp, J.; Frosch, T. *Anal. Chem.* **2015**, *87*, 11137−11142.
(48) Keiner, R.; Frosch, T.; Hanf, S.; Rusznyak, A.; Akob, D. M.; Kusel, K.; Popp, J. *Anal. Chem.* **2013**, *85*, 8708−8714.
(49) King, D. A.; Pittaro, R. J. *Opt. Lett.* **1998**, *23*, 774−776.
(50) Beebe, K. R.; Pell, R. J.; Seasholtz, M. B. *Chemometrics: A Practical Guide*; Wiley-Interscience: New York, 1998; Vol. *4*.
(51) Le, L. D.; Tate, J. D.; Seasholtz, M. B.; Gupta, M.; Owano, T.; Baer, D.; Knittel, T.; Cowie, A.; Zhu, J. *Appl. Spectrosc.* **2008**, *62*, 59−65.
(52) Yaws, C. L. *The Yaws Handbook of Vapor Pressure: Antoine Coefficients*; Gulf Professional Publishing: Oxford, U.K., 2015.
(53) Vance, C. P.; Heichel, G. H. *Annu. Rev. Plant Physiol. Plant Mol. Biol.* **1991**, *42*, 373−392.
(54) Herridge, D. F.; Pate, J. S. *Plant Physiol.* **1977**, *60*, 759−764.
(55) Ryle, G. J. A.; Powell, C. E.; Gordon, A. J. *J. Exp. Bot.* **1985**, *36*, 634−643.
(56) Vance, C. P.; Stade, S.; Maxwell, C. A. *Plant Physiol.* **1983**, *72*, 469−473.
(57) Schulze, J. *J. Plant Nutr. Soil Sci.* **2004**, *167*, 125−137.
(58) Schulze, J.; Temple, G.; Temple, S. J.; Beschow, H.; Vance, C. P. *Ann. Bot.* **2006**, *98*, 731−740.
(59) Fischinger, S. A.; Schulze, J. *J. Exp. Bot.* **2010**, *61*, 2281−2291.
(60) Thorstensen, J.; Haugholt, K. H.; Ferber, A.; Bakke, K. A. H.; Tschudi, J. *J. Eur. Opt. Soc. - Rapid Publ.* **2014**, *9*, 14054.

DOI: 10.1021/acs.analchem.6b03101
Anal. Chem. 2017, 89, 1117−1122

Supplementary Information

Direct Raman spectroscopic measurements of biological nitrogen (N_2) fixation under natural conditions: An analytical approach for studying nitrogenase activity

Tobias Jochum,[a] Agnes Fastnacht,[b] Susan E. Trumbore,[b] Jürgen Popp[a,c] and Torsten Frosch[a,c,*]

[a] Leibniz Institute of Photonic Technology, 07745 Jena, Germany

[b] Max Planck Institute for Biogeochemistry, 07745 Jena, Germany

[c] Institute of Physical Chemistry and Abbe Center of Photonics, 07745 Jena, Germany

[*] torsten.frosch@uni-jena.de, torsten.frosch@gmx.de

Supplementary Information
Direct Raman spectroscopic measurements of biological nitrogen (N2) fixation under natural conditions: An analytical approach for studying nitrogenase activity

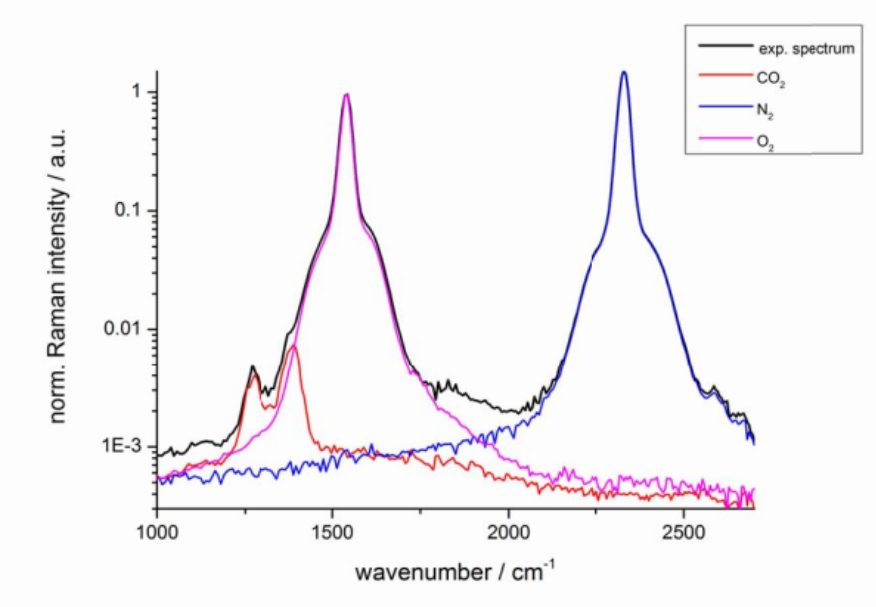

Figure S1: Decomposition of a measured multi-gas spectrum into its components N_2, O_2 and CO_2. Pure reference spectra of the individual components built the basis set of the multiple linear regression algorithm, which predicts component specific gas mixing ratios. In this figure, the normalized Raman intensity is scaled logarithmically for better visibility. However, computation of the mixing ratios is performed in a linear model.

Supplementary Information
Direct Raman spectroscopic measurements of biological nitrogen (N2) fixation under natural conditions: An analytical approach for studying nitrogenase activity

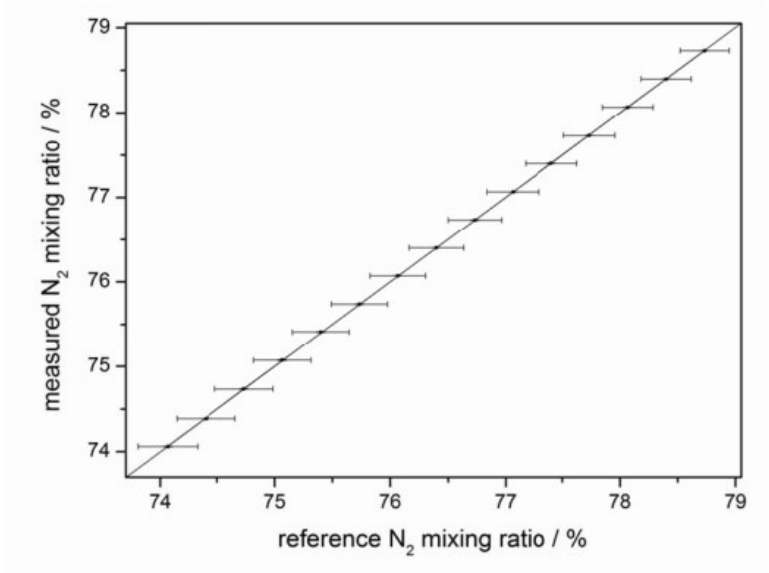

Figure S2: Comparison of the N_2 reference mixing ratios and predicted mixing ratios by the Raman analysis. Depicted values are mean values and error bars (x: given by relative precision of the used mass flow controllers for the reference flow; and y) indicate standard deviations of 3 individual measurements. The figure demonstrates the high accuracy of the spectral calibration and data analysis of the Raman analyzer.

References

(1) Zoback, M. L. *Grand challenges in earth and environmental sciences: Science, stewardship, and service for the twenty-first century*; GSA today, 2001, p 41-47.
(2) Schimel, D. S. *Global Change Biol* **1995**, *1*, 77-91.
(3) Vitousek, P. M.; Aber, J. D.; Howarth, R. W.; Likens, G. E.; Matson, P. A.; Schindler, D. W.; Schlesinger, W. H.; Tilman, D. G. *Ecol Appl* **1997**, *7*, 737-750.
(4) Running, S.; Baldocchi, D.; Turner, D.; Gower, S.; Bakwin, P.; Hibbard, K. *Remote Sens Environ* **1999**, *70*, 108-127.
(5) Richter, D. D.; Mobley, M. L. *Science* **2009**, *326*, 1067-1068.
(6) Baer, D.; Gupta, M.; Leen, J. B.; Berman, E. *Am Lab* **2012**, *44*.
(7) Canfield, D. E.; Glazer, A. N.; Falkowski, P. G. *Science* **2010**, *330*, 192-196.
(8) Angert, A.; Yakir, D.; Rodeghiero, M.; Preisler, Y.; Davidson, E. A.; Weiner, T. *Biogeosciences* **2015**, *12*, 2089-2099.
(9) Bond-Lamberty, B.; Thomson, A. *Nature* **2010**, *464*, 579-582.
(10) Randerson, J.; Masiello, C.; Still, C.; Rahn, T.; Poorter, H.; Field, C. *Global Change Biol* **2006**, *12*, 260-271.
(11) Hund, K.; Schenk, B. *Chemosphere* **1994**, *28*, 477-490.
(12) Flexas, J.; Diaz-Espejo, A.; Berry, J. A.; Cifre, J.; Galmes, J.; Kaidenhoff, R.; Medrano, H.; Ribas-Carbo, M. *J Exp Bot* **2007**, *58*, 1533-1543.
(13) Olschewski, A.; Fischer, U.; Hofer, M.; Schulin, R. *Environ Sci Technol* **1995**, *29*, 264-266.
(14) Wilcock, R. J.; Battino, R.; Wilhelm, E. *J Chem Thermodyn* **1977**, *9*, 111-115.
(15) Cheng, Q. *J Integr Plant Biol* **2008**, *50*, 786-798.
(16) Unkovich, M. *New Phytol* **2013**, *198*, 643-646.
(17) Cassar, N.; Bellenger, J. P.; Jackson, R. B.; Karr, J.; Barnett, B. A. *Oecologia* **2012**, *168*, 335-342.
(18) Davidson, E. A.; Seitzinger, S. *Ecol Appl* **2006**, *16*, 2057-2063.
(19) Petrucci, R. H.; Harwood, W. S.; Herring, F. G. *General chemistry: principles and modern applications*; Prentice Hall, 2002; Vol. 1.
(20) Behrendt, T.; Veres, P.; Ashuri, F.; Song, G.; Flanz, M.; Mamtimin, B.; Bruse, M.; Williams, J.; Meixner, F. *Biogeosciences* **2014**, *11*, 5463-5492.
(21) Wiegleb, G. *Gasmesstechnik in Theorie und Praxis: Messgeräte, Sensoren, Anwendungen*; Springer-Verlag, 2016.
(22) Jost, W. *Diffusion in Solids, Liquids and Gases*; Academic Press: New York, 1952.
(23) Freney, J.; Simpson, J. R. *Gaseous Loss of Nitrogen from Plant-Soil Systems*; Springer: Dordrecht, 1983.
(24) Andrussow, L.; Schramm, B.; Schäfer, K. *Transportphänomene 1: (Viskosität und Diffusion)*; Springer, 1969.
(25) Roberts, P. J.; Webster, D. R. *Turbulent diffusion*; ASCE Press, Reston, Virginia, 2002.
(26) Stephenson, R. M. *Handbook of the thermodynamics of organic compounds*; Springer Science & Business Media, 2012.
(27) Awang, Z. *Sensors & Transducers* **2014**, *168*, 61-75.
(28) Garzon, F. H.; Mukundan, R.; Brosha, E. L. *Solid State Ionics* **2000**, *136*, 633-638.
(29) Moseley, P. *Measurement Science and technology* **1997**, *8*, 223.
(30) Capone, S.; Forleo, A.; Francioso, L.; Rella, R.; Siciliano, P.; Spadavecchia, J.; Presicce, D. S.; Taurino, A. M. *J Optoelectron Adv M* **2003**, *5*, 1335-1348.
(31) Dubbe, A. *Sensors and Actuators B: Chemical* **2003**, *88*, 138-148.
(32) SiraTechnology. *Gas Detector Selection and Calibration Guide*; Witherby, 2005; Vol. 1.
(33) Giberti, A.; Carotta, M. C.; Guidi, V.; Malagu, C.; Martinelli, G.; Piga, M.; Vendemiati, B. *Sensor Actuat B-Chem* **2004**, *103*, 272-276.
(34) Gross, J. H. *Mass Spectrometry - A Textbook*, 2004.
(35) Brand, W. A. *J Mass Spectrom* **1996**, *31*, 225-235.

(36) Brand, W. A.; Coplen, T. B.; Aerts-Bijma, A. T.; Böhlke, J.; Gehre, M.; Geilmann, H.; Gröning, M.; Jansen, H. G.; Meijer, H. A.; Mroczkowski, S. J. *Rapid Commun Mass Sp* **2009**, *23*, 999-1019.
(37) Mariotti, A. *Nature* **1984**, *311*, 251.
(38) Michener, R.; Lajtha, K. *Stable isotopes in ecology and environmental science*; John Wiley & Sons, 2008.
(39) Wang, R.; Willibald, G.; Feng, Q.; Zheng, X.; Liao, T.; Brüggemann, N.; Butterbach-Bahl, K. *Environ Sci Technol* **2011**, *45*, 6066-6072.
(40) Ingle Jr, J. D.; Crouch, S. R. *Spectrochemical analysis*, 1988.
(41) Parson, W. W. *Modern optical spectroscopy*; Springer, 2007.
(42) Hodgkinson, J.; Tatam, R. P. *Measurement Science and Technology* **2012**, *24*, 012004.
(43) Smith, S.; Vass, A.; Karpushko, F.; Hardaway, H.; Crowder, J. *Philosophical Transactions of the Royal Society of London A: Mathematical, Physical and Engineering Sciences* **2001**, *359*, 621-634.
(44) Griffiths, P. R.; De Haseth, J. A. *Fourier transform infrared spectrometry*; John Wiley & Sons, 2007; Vol. 171.
(45) Levy, D.; Diken, E. G. *Ieee Sens J* **2010**, *10*, 564-571.
(46) O'Keefe, A.; Deacon, D. A. *Rev Sci Instrum* **1988**, *59*, 2544-2551.
(47) Baer, D. S.; Paul, J. B.; Gupta, J. B.; O'Keefe, A. *Appl Phys B-Lasers O* **2002**, *75*, 261-265.
(48) Sigrist, M.; Bartlome, R.; Marinov, D.; Rey, J.; Vogler, D.; Wächter, H. *Applied Physics B* **2008**, *90*, 289-300.
(49) Siebert, F.; Hildebrandt, P. *Vibrational Spectroscopy in Life Science* **2008**, 11-61.
(50) Demtröder, W. *Laser spectroscopy: basic concepts and instrumentation*; Springer Science & Business Media, 2013.
(51) Placzek, G. *Rayleigh-streuung und Raman-effekt*; Akad. Verlag-Ges., 1934; Vol. 2.
(52) Kukura, P.; Yoon, S.; Mathies, R. A. *Analytical chemistry* **2006**, *78*, 5952-5959.
(53) Hercher, M.; Mueller, W.; Klainer, S.; Adamowicz, R. F.; Meyers, R. E.; Schwartz, S. E. *Appl Spectrosc* **1978**, *32*, 298-302.
(54) King, D. A.; Pittaro, R. J. *Opt Lett* **1998**, *23*, 774-776.
(55) Salter, R.; Chu, J.; Hippler, M. *Analyst* **2012**, *137*, 4669-4676.
(56) Barnes, J.; Gough, T.; Stoer, M. *Rev Sci Instrum* **1999**, *70*, 3515-3518.
(57) Hippler, M.; Mohr, C.; Keen, K. A.; McNaghten, E. D. *The Journal of chemical physics* **2010**, *133*, 044308.
(58) Keiner, R. *Cavity-enhanced raman gas spectrometry of biogenic gases*. Friedrich-Schiller-Universität Jena, Diss.2015.
(59) Jochum, T.; von Fischer, J. C.; Trumbore, S.; Popp, J.; Frosch, T. *Anal Chem* **2015**, *87*, 11137-11142.
(60) Beebe, K. R.; Pell, R. J.; Seasholtz, M. B. *Chemometrics: a practical guide*; Wiley-Interscience, 1998; Vol. 4.
(61) Le, L. D.; Tate, J. D.; Seasholtz, M. B.; Gupta, M.; Owano, T.; Baer, D.; Knittel, T.; Cowie, A.; Zhu, J. *Appl Spectrosc* **2008**, *62*, 59-65.
(62) Kiefer, J.; Seeger, T.; Steuer, S.; Schorsch, S.; Weikl, M.; Leipertz, A. *Measurement Science and Technology* **2008**, *19*, 085408.
(63) Krafft, C.; Dietzek, B.; Schmitt, M.; Popp, J. *J Biomed Opt* **2012**, *17*.
(64) Russell, P. *Science* **2003**, *299*, 358-362.
(65) Ghenuche, P.; Rammler, S.; Joly, N. Y.; Scharrer, M.; Frosz, M.; Wenger, J.; Russell, P. S.; Rigneault, H. *Opt Lett* **2012**, *37*, 4371-4373.
(66) Benabid, F.; Roberts, P.; Couny, F.; Light, P. S. *J Eur Opt Soc-Rapid* **2009**, *4*.
(67) Johnson, S. G.; Joannopoulos, J. D. *Photonic Crystal Tutorial* **2003**, 1-16.
(68) Wynne, R. M.; Barabadi, B.; Creedon, K. J.; Ortega, A. *J Lightwave Technol* **2009**, *27*, 1590-1596.
(69) Jerger, A.; Kohler, H.; Becker, F.; Keller, H. B.; Seifert, R. *Sensor Actuat B-Chem* **2002**, *81*, 301-307.
(70) Ramsey, G. B.; Butler, L. *J. Agric. Res* **1928**, *37*, 339-348.
(71) Frosch, T.; Yan, D.; Popp, J. *Analytical Chemistry* **2013**, *85*, 6264-6271.
(72) Jochum, T.; Rahal, L.; Suckert, R. J.; Popp, J.; Frosch, T. *Analyst* **2016**, *141*, 2023-2029.

(73) Fonollosa, J.; Halford, B.; Fonseca, L.; Santander, J.; Udina, S.; Moreno, M.; Hildenbrand, J.; Wollenstein, J.; Marco, S. *Sensor Actuat B-Chem* **2009**, *136*, 546-554.
(74) Rhodes, M. *Biochemistry of fruits and their products*; Academic Press Inc.: London, 1970; Vol. 1.
(75) Busenberg, E.; Plummer, L. N. *Geochem Geophy Geosy* **2010**, *11*.
(76) Maiss, M.; Steele, L. P.; Francey, R. J.; Fraser, P. J.; Langenfelds, R. L.; Trivett, N. B. A.; Levin, I. *Atmos Environ* **1996**, *30*, 1621-1629.
(77) Koukkou, A.-I. *Microbial Bioremediation of Non-metals: Current Research*; Horizon Scientific Press, 2011.
(78) Rugner, H.; Finkel, M.; Kaschl, A.; Bittens, M. *Environ Sci Policy* **2006**, *9*, 568-576.
(79) Mulligan, C. N.; Yong, R. N. *Environ Int* **2004**, *30*, 587-601.
(80) Cappello, S.; Caruso, G.; Zampino, D.; Monticelli, L. S.; Maimone, G.; Denaro, R.; Tripodo, B.; Troussellier, M.; Yakimov, M.; Giuliano, L. *J Appl Microbiol* **2007**, *102*, 184-194.
(81) Peoples, M.; Herridge, D.; Ladha, J. *Plant and soil* **1995**, *174*, 3-28.
(82) Cardenas, L. M.; Hawkins, J. M. B.; Chadwick, D.; Scholefield, D. *Soil Biol Biochem* **2003**, *35*, 867-870.
(83) Herridge, D. F.; Pate, J. S. *Plant Physiol* **1977**, *60*, 759-764.
(84) Ryle, G. J. A.; Powell, C. E.; Gordon, A. J. *J Exp Bot* **1985**, *36*, 634-643.
(85) Schulze, J. *Journal of Plant Nutrition and Soil Science* **2004**, *167*, 125-137.
(86) Schulze, J.; Temple, G.; Temple, S. J.; Beschow, H.; Vance, C. P. *Ann Bot-London* **2006**, *98*, 731-740.
(87) Fischinger, S. A.; Schulze, J. *J Exp Bot* **2010**, *61*, 2281-2291.
(88) Jochum, T.; Michalzik, B.; Bachmann, A.; Popp, J.; Frosch, T. *Analyst* **2015**, *140*, 3143-3149.

Index of abbreviations

ANOVA	analysis of variance
BNF	biological nitrogen fixation
CCD	charge-coupled device
CER	carbon dioxide exchange rate
CERS	cavity enhanced Raman spectroscopy
FERS	fiber enhanced Raman spectroscopy
FTIR	Fourier transform infrared
GRIN	gradient-index
HC-PCF	hollow-core photonic crystal fibers
IR	infrared
IRMS	isotope ratio mass spectrometry
LOD	limit of detection
NDIR	non-dispersive infrared
PBC	power build-up cavity
PBG	photonic band gap
ppb	parts per billion (10^{-9})
ppm	parts per million (10^{-6})
RQ	respiration quotient
SNR	signal to noise ratio
TDLAS	tunable diode laser absorption spectroscopy

Conference contributions

Talks *(secondary authorships not included)*

Enhanced Raman spectroscopy for biogeochemical process monitoring
T. Jochum, J. Popp, T. Frosch
Seminar Department of Biology, Colorado State University, Fort Collins, USA, May 24, 2016

Soil microbial response to benzene contamination: new onsite gas analysis technique reveals respiration and biodegradation kinetics
T. Jochum, J. Popp, T. Frosch
Geological Society of America (GSA) Annual Meeting, Baltimore, USA, November 1-4, 2015

Raman gas spectroscopy meets Environmental Science: Potentials and selected applications
T. Jochum, J. Popp, T. Frosch
Bio-Geo-Colloquium, Jena, Germany, October 27, 2015

Poster presentations *(secondary authorships not included)*

Using ^{13}C-labeled benzene and Raman gas spectroscopy to investigate respiration and biodegradation kinetics following soil contamination
T. Jochum, J. Popp, T. Frosch
European Geosciences Union (EGU) Annual Meeting, Vienna, Austria, April 17-22, 2016

Benzene biodegradation kinetics and soil microbial respiration characterized by Raman gas spectroscopy
T. Jochum, B. Michalzik, A. Bachmann, J. Popp, T. Frosch
EuroAnalysis, Bordeaux, France, September 6-10, 2015

Monitoring soil microflora gas exchange with cavity enhanced Raman multi-gas spectroscopy
T. Jochum, B. Michalzik, A. Bachmann, J. Popp, T. Frosch
Deutsches BioSensor Symposium, Munich, Germany, March 11-14, 2015

Simultaneous biogenic multi-gas analysis of climate relevant soil ecosystems by cavity enhanced Raman gas spectroscopy
T. Jochum, R. Keiner, B. Michalzik, J. Popp, T. Frosch
International Congress on Raman Spectroscopy (ICORS), Jena, Germany, August 10-15, 2014

Acknowledgements

This part is dedicated to all who facilitated my interdisciplinary research.

First, I thank Prof. Jürgen Popp for the unique opportunity to do research in his department, his trust and constructive feedback.

I am indebted to Dr. Torsten Frosch for great supervision and helpful advice in any part of my work. The almost unlimited freedom in my research activities is something I will surely miss. Further, I had also the opportunity to visit several renowned international conferences to present my work. Many thanks, Torsten, for making all of this possible.

I want to thank my PhD advisory committee from the Collaborative Research Center AquaDiva, namely Prof. Susan E. Trumbore, Prof. Jürgen Popp, Prof. Joseph C. von Fischer, Dr. Torsten Frosch, Dr. Anna Späthe and Dr. Christine Hess. All of you greatly supported me in keeping track of my studies and asking the right scientific questions.

Within the AquaDiva graduate program, I spent three months at the Colorado State University in Fort Collins visiting the group of Joseph C. von Fischer. Thank you, Joe, for this outstanding experience and the always friendly and welcoming atmosphere. Many thanks also to the group members Samuel Dunn, Emily Stuchiner, Paul Brewer, Samuel Chamberlain and Charlotte Alster for great discussions and shared ideas. I thank Dan Kotter for introducing me to his study sites in Yellowstone National Park. Sincere thanks to Prof. Jill Baron, Daniel Bowker and Bella Oleksy for doing research and wonderful hiking trips in Loch Vale, Rocky Mountain National Park.

My interdisciplinary research would have been impossible without the help of many distinguished collaborators. I thank Prof. Beate Michalzik for support, advice and sampling in the context of the microbial biodegradation study. For continuous support and great ideas within the projects on chamber leakage assessment and biological nitrogen fixation, I thank Prof. Susan E. Trumbore. Further, my gratitude goes to Agnes Fastnacht and Gabriela Pereyra for invaluable help in plant cultivation.

I want to thank all my colleagues for their excellent support and the pleasant atmosphere, during and after work: Anne Sieburg, Leila Rahal, Sebastian Schneider, Andreas Knebl, Annika Düver, Sebastian Wolf, Rene Suckert, Theresa Schott, Di Yan, Sebastian Stemplewitz, Björn Lorenz, Christian Domes, Elisabeth Wyrwich, Timea Bögözi, Robert Domes and Tycho Kirchner.

Last but not least, many thanks to my family for their unlimited support and trust.

Curriculum Vitae

Academic training

2017	PhD	Physical Chemistry, Friedrich Schiller University, Jena Leibniz Institute of Photonic Technology, Jena "Development and application of analytical methods based on enhanced Raman gas spectroscopy for biogeochemical process monitoring"
2013	Master of Science	Physics, Ludwig Maximilian University, Munich "Investigation of photoswitchable azobenzene molecules by surface enhanced Raman spectroscopy"
2011	Bachelor of Science	Physics, Ludwig Maximilian University, Munich "Imaging with a femtosecond stimulated Raman microscope"

Professional experience

May – August 2016	Visiting researcher, Department of Biology, Colorado State University, Fort Collins, CO, USA
2014 – 2016	Participant AquaDiva International Graduate School
2015 – 2016	Advisor Bachelor and Master students
2014 – 2016	Teaching assistant, Institute of Physical Chemistry, Friedrich Schiller University, Jena
2012 – 2013	Teaching assistant, Faculty of Physics, Ludwig Maximilian University, Munich

Declaration of originality

Ich erkläre, dass ich die vorliegende Arbeit selbstständig und unter Verwendung der angegebenen Hilfsmittel, persönlichen Mitteilungen und Quellen angefertigt habe.

Jena, 29.08.2017

Tobias Jochum